An Interoperability Concept for Inductive Charging Systems

Marius E. Haßler

Lehrstuhl für Datenverarbeitung
Technische Universität München

An Interoperability Concept for Inductive Charging Systems

Marius E. Haßler

Vollständiger Abdruck der von der Fakultät für Elektrotechnik und Informationstechnik der Technischen Universität München zur Erlangung des akademischen Grades eines

Doktor-Ingenieurs (Dr.-Ing.)

genehmigten Dissertation.

Vorsitzende: Prof. Dr.-Ing. Sandra Hirche

Prüfer der Dissertation:

1. Prof. Dr.-Ing. Klaus Diepold
2. Prof. Dr.-Ing. Hans-Georg Herzog

Die Dissertation wurde am 22. Januar 2020 bei der Technischen Universität München eingereicht und durch die Fakultät für Elektrotechnik und Informationstechnik am 04. November 2020 angenommen.

Marius E. Haßler. *An Interoperability Concept for Inductive Charging Systems.* Dissertation, Technische Universität München, Munich, Germany, 2021.

Chair of Data Processing, Technische Universität München, 80290 München, Germany, http://www.ldv.ei.tum.de/.

Acknowledgement

My special thanks goes to my supervisor Professor Diepold for supporting me with helpful advice whenever I was asking.

Second I want to thank Josef Krammer for his support, his patience and that he always found the time for technical discussions.

Further thanks goes to my colleagues at BMW and LDV chair for constructive exchange, an open ear and their help. Especially, Florian Niedermeier, Johannes Birkendahl, Daniel Weida, Jakob Pfeiffer, Martin Knopp and Veronika Gamper.

I also want to thank Morris Kesler and Daniel Kürschner for their support and expertise.

And last I want to thank my family for their support during the last years, especially my love.

Zusammenfassung

Um den Wandel hin zur Elektromobilität erfolgreich zu beschreiten, ist es wichtig die größten Hindernisse aus Kundensicht aufzugreifen und für diese technische Lösungen zu entwickeln. Hierzu zählen vorrangig Reichweite und Ladeinfrastruktur.

Induktives Laden ist eine Komfort Ladefunktion und kann bei der Lösung beider Probleme unterstützen. Indem in den langen Standzeiten, wie über Nacht oder während der Arbeit, problemfrei und automatisch aufgeladen wird, steht stets die volle elektrische Reichweite zur Verfügung. Damit kann die Notwendigkeit des aktiven Aufladevorgangs durch den Nutzer, bei dem er selbst das Ladekabel mit dem Fahrzeug verbindet, auf Langstreckenfahrten mit kurzen Stehzeiten reduziert werden. Um die Kompatibilität von Ladeinfrastruktur und Fahrzeug beim induktiven Laden sicherzustellen, beschäftigt sich die vorliegende Dissertation mit einer Beschreibungsmethodik des herstellerübergreifenden kompatiblen Energietransfers. Hierzu wird ein induktives Ladesystem bezüglich seiner Systemparameter analysiert. Aus den daraus gewonnenen Erkenntnissen wird ein Konzept entwickelt, das die sogenannte Interoperabilität, also eine Herstellerübergreifende Kompatibilität zwischen Fahrzeug und Infrastruktur, beschreibt. Zusätzlich zu dem Beschreibungskonzept wird ein Testkonzept erarbeitet und vorgestellt. Das Beschreibungskonzept etabliert neue, auf Impedanz basierte Schnittstellen. Zur Interoperabilitätsprüfung ist eine Messung der Impedanz an der Schnittstelle im laufenden Betrieb der Primär- oder Sekundärseite nötig. Im Rahmen dieser Dissertation wird das Testkonzept in einem Prüfstandsaufbau am Beispiel der Primärseite gezeigt. Herausfordernd hierbei ist, dass es für die Impedanzmessung keine praktische Testmethodik und kein kommerziell erhältliches Messgerät gibt, das die Impedanz präzise ermitteln kann. Deshalb wird für die Bestimmung der Impedanz ein spezielles Impedanz-Anpassungsnetzwerk entwickelt, das an mehreren Positionen einen Abgriff für Spannungsmessungen vorsieht. Auf diese Weise kann die Impedanz um eine Vielzahl genauer bestimmt werden als dies bei bisherigen direkten Impedanzmessungen möglich ist.

In dieser Arbeit wird ein theoretisches Beschreibungskonzept für interoperable induktive Ladeeinheiten vorgestellt und dessen Machbarkeitsnachweis erbracht. Zusätzlich werden die Resultate eines analytischen und simulativen Analyseverfahrens mit den Ergebnissen der Impedanzmessung verglichen. Die Ergebnisse aus dieser Arbeit sind zudem bereits in die induktive Ladestandards der Society of Automotive Engineers (SAE) *J2954* und International Electrotechnical Commission (IEC) *61980–3* eingebracht und darin aufgenommen worden.

Summary

To support the change towards electromobility, it is essential to develop technical solutions for the biggest obstacles from customer's perspective. These include range and charging infrastructure.

Inductive charging is a convenient, wireless charging solution that can support solving both problems. By using long idle times as overnight or during work, an automatic hassle-free charging function not only ensures to have a recharged vehicle battery. It also spares customers the necessity to manually connect vehicle and charging infrastructure with a charging cable. Therewith, a real recharging experience is only needed when traveling long distances.

This dissertation presents a description methodology of manufacturer independent and compatible wireless power transfer. For this reason, I analyzed an inductive charging system with regard to its system parameters. The findings are used to develop an interoperability concept, which describes compatibility between vehicle and infrastructure beyond manufacturer. In addition, a test concept will be developed and presented. The interoperability concept establishes new impedance based interfaces that require an impedance measurement at the ground or vehicle coil terminals during operation. For this reason, the test stand concept was realized in context of this dissertation. The main challenge was that there exist no practical test method or commercially available measurement devices suitable for a precise impedance measurement. Therefore, I developed a special impedance matching network with multiple voltage measurement ports. This way, it becomes possible to determine the impedance much more precisely than with state-of-the-art direct impedance measurement method.

In this thesis, an interoperability concept for inductive charging systems is presented and a proof of its practical feasibility is provided. Furthermore, an analytical and a simulative analysis method are introduced and the results are compared with data from the impedance measurements. The interoperability concept presented within this thesis has already entered and been accepted by the inductive charging standards Society of Automotive Engineers (SAE) *J2954* and International Electrotechnical Commission (IEC) *61980–3*.

Contents

List of appended papers

This cumulative thesis is presenting the comprehensive research results. The detailed results were presented in the following scientific journals and conferences:

1 M. Hassler, F. Niedermeier, J. Krammer, and K. Diepold, “A Method for Interoperable Interface Description of Inductive Power Transfer Systems,” in *2018 IEEE PELS Workshop on Emerging Technologies: Wireless Power Transfer (Wow)*, IEEE, 2018, pp. 1–5.

2 F. Niedermeier, M. Hassler, J. Krammer, and B. Schmuelling, “The Effect of Rotatory Coil Misalignment on Transfer Parameters of Inductive Power Transfer Systems,” *Wireless Power Transfer*, vol. 6, no. 2, pp. 77–84, 2019.

3 M. Hassler, O. Atasoy, M. Kesler, K. Twelker, T. Achatz, M. Jetz, and J. Krammer, “Impedance Measurement on Inductive Power Transfer Systems,” in *2019 IEEE PELS Workshop on Emerging Technologies: Wireless Power Transfer (Wow)*, IEEE, 2019, pp. 39–44.

4 M. Hassler, O. Atasoy, M. Kesler, K. Twelker, J. Birkendahl, J. Krammer, “A Comparison on Simulated, Analytic and Measured Impedance Values for an Inductive Power Transfer System,” *Wireless Power Transfer*, vol. 7, no. 1, pp. 51–59, 2020.

List of Acronyms

A4WP Alliance for Wireless Power

CCS Combined Charging System

ICEV Internal Combustion Engine Vehicle

IEC International Electrotechnical Commission

ISO International Organization for Standardization

EIS Electrochemical Impedance Spectroscopy

EMC Electromagnetic Compatibility

EV Electric Vehicle

FEM Finite Element Method

GA Ground Assembly

PMA Power Matter Alliance

PWM Pulse Width Modulation

RMS Root Mean Square

RP Recommended Practice

RQ Research Question

SAE Society of Automotive Engineers

TIR Technical Information Report

IPTS Inductive Power Transfer System

VA Vehicle Assembly

VNA Vector Network Analyzer

WPC Wireless Power Consortium

WPT3 Wireless Power Transfer Class 3

1 Introduction

1.1 Motivation

With the ongoing trend to megacities, more and more people are moving into steadily growing cities. Air pollution and its consequences are becoming a matter of public health [1, 2, 3]. To avoid banning vehicles from cities, governments are looking for alternative solutions.

One possibility - seen by many experts as a key technology to a climate-friendlier mobility - is electromobility. Especially in use with renewable energies life cycle carbon dioxide emissions can be reduced [4, 5]. Direct emissions, as health-damaging nitrogen oxides and other smog-forming pollutants produced by fuel combustion in conventional vehicles, do no longer occur in electric vehicles. Therefore, the air quality in cities can be improved by substituting Internal Combustion Engine Vehicles (ICEVs) with Electric Vehicles (EVs) [6]. These health and climate aspects are a reason for governments to support the change towards electromobility and help to address its challenges.

One challenge towards electromobility is to improve the poor customer acceptance for electric vehicles [7]. Besides widely discussed cost and range issues more elaborate charging infrastructure and charging experience are decisive [8, 9].

Wireless charging, a comfort charging solution, faces the inconvenience that comes along with recharging the battery of EVs. Conductive charging solutions require the customer to connect and disconnect the heavy, unwieldy charging cable with vehicle and grid much more frequently than customers are used from refueling their vehicles and thus negatively affects their EV experience. In contrast to conductive charging and to increase the EV customer acceptance, wireless charging is not only removing the pain point of the charging cable - instead it is supposed to even make charging easier than refueling. With an automatic charging function that provides the regular needed power when the vehicle is parked above the ground charging system. Hence, it can almost avoid cable based charging events, where the customer himself needs to connect the charging cable and could leave the recharging experience to DC fast charging on highways, when traveling long distances.

Electromobility requires a change of thinking. Refueling an ICEV and recharging an EV does not have to follow the same routine. Unlike a gas station - electricity is

EV charging ranges [km]

Use Cases		charging en route			intermediate charging		charging at work		charging over night
Charging time		10 min	20 min	30 min	1 h	2 h	4 h	6 h	8 h
AC-charging (private)	1 kW	0.8	1.7	2.5	5	10	20	30	40
	2.3 kW	1.9	3.8	5.8	12	23	46	69	92
	3.7 kW	3.1	6.2	9.3	19	37	74	111	148
	7.4 kW[1]	6.2	12.3	18.5	37	74	148	222	296
	11 kW[2]	9.2	18.3	27.5	55	110	220	330	440
	22 kW	18.3	36.7	55.0	110	220	440	660	880
DC-charging (public)	50 kW	41.7	83.3	125.0	250	500	1000	1500	2000
	150 kW	125.0	250.0	375.0	750	1500	3000	4500	6000
	350 kW	291.7	583.3	875.0	1750	3500	7000	10500	14000
	500 kW	416.7	833.3	1250.0	2500	5000	10000	15000	20000

[1] 1ph 32A 240V (US) [2] 3ph 16A 230V (ECE)
inductive charging regime; DC charging regime
charging rate [km/h]
available EV ranges (battery limit ≤ 100 kWh)
limit of household sockets (US/GER) ↔ fixed installation

Table 1.1: Electric vehicle ranges for different charging powers and charging times taking a consumption rate of $20\,\mathrm{kWh}$ per $100\,\mathrm{km}$.

widespread and can be made available almost everywhere. So, there is no need to drive EVs like ICEVs, until the gas light warning flashes—instead each parking time could be used for recharging the vehicle's battery. This way, a charged electric vehicle is available for use at anytime. Since high AC charging rates are not sufficient to recharge an empty battery in under 10 minutes (cf. Table 1.1) and high DC fast charging stations are still rare[1], it should be recharged in shorter intervals, also referred to as *snack charging*[2], whenever the vehicle is unused. An interoperable inductive charging[3] unit with an integrated automatic charging function makes this possible and for customers very comfortable in use.

In near future, the designated applications of inductive charging are in particular domestic, at work or in public spaces, where long parking times prevail and the available power is rather small (cf. Table 1.1). Inductive charging units with a charging power of up to $22\,\mathrm{kW}$ are sufficiently suited for the average user as it can be seen in Table 1.1.

For example, a German commuter travels in average only $\sim 34\,\mathrm{km}$ a day [10].

[1] Digital Charging Solutions GmbH, "ChargeNow Map," [Online]. Available: https://chargenow.com/web/chargenow-de/map. [Accessed 08-March-2019].

[2] Forbes, "How Wireless Charging Will Make Life Simpler (And Greener)," [Online]. Available: https://www.forbes.com/sites/davidferris/2012/07/24/how-wireless-charging-will-make-life-simpler-and-greener/#82004c63c35e. [Accessed 08-March-2019].

[3] The term inductive charging is often used instead of wireless charging to emphasis that the physical effect of electromagnetic induction is used to transfer energy wirelessly.

Taking a consumption rate of $20\,\mathrm{kWh}$ per $100\,\mathrm{km}$ yields an energy consumption of $6.8\,\mathrm{kWh/day}$, which can easily be recharged over night in 8 hours with a reduced charging power of $\sim 1\,\mathrm{kW}$. One consider another example: drawing $10\,\mathrm{A}$ single phase of the $230\,\mathrm{V}$ grid from an ordinary socket gives $2.3\,\mathrm{kW}$. Taking the same consumption rate, allows a commuter to travel $92\,\mathrm{km}$ every day when only recharging for 8 hours over night at home. Therewith, the majority of the everyday users can recharge daily needed power over night with a charging rate of only a few kW. And for greater ranges, also conductive chargers with $22\,\mathrm{kW}$ or the discussed AC level 3 chargers with powers up to $96\,\mathrm{kW}$ are not sufficient to recharge EVs within minutes [11]. The benefit of the trend to higher and higher AC power levels should be critically scrutinized. The associated additional weight for the respective charging unit in the vehicle and thus higher consumption rate are counterproductive.

Also the vision of autonomous driving vehicles that can find a parking slot on their own are in need of an automatic interoperable charging solution when their powertrain is electrified and their passenger is not present to connect the charging cable [12]. And disruptive business models involving shared, autonomous taxi fleets prefer EVs due to lower operational costs, tax and registration incentives and thus share the same requirement for an automatic interoperable charging function [13, 14, 15].

In the long term, also dynamic charging[4], where the vehicle battery is recharged while driving, is seen as an interesting application by many researchers [16, 17, 18, 19, 20, 21, 22]. There, an electrified road can supply the vehicle with electric power for driving or even recharging. With a well-developed infrastructure, large battery capacities would become obsolete, which is especially interesting for buses and trucks[5] [23]. Such an infrastructure could also ensure that plug-in hybrids are sufficiently charged when entering urban environment to drive purely electrified with zero emissions. Some researchers think that in opposition to high infrastructure investment costs, are savings from smaller battery packages [16] and longer battery lifetime [24], which surprisingly could be more cost-effective than conventional vehicles [25].

There also exist considerations to integrate the possibly large number of electric vehicles into the grid and use them as energy storage systems to buffer peak demands or peak supplies especially with integration of renewable energies [26, 27, 28]. However, resulting capacity losses and the range anxiety must be solved and attractive customer reward models be found.

[4] Dynamic charging is no part of this thesis. To transfer the herein presented interoperability concept onto dynamic charging could be part of a new dissertation.

[5] Scania AB, “Scania tests fast wireless charging in urban traffic,” [Online]. Available: https://www.scania.com/group/en/scania-tests-fast-wireless-charging-in-urban-traffic/. [Accessed 08-March-2019].

For high customer acceptance, it is essential that inductive charging works interoperable without any problem. Charging errors that prolong or abort the recharging process may not happen as customers expect charging to work without failures and power restrictions. Therefor, a lot of engineering challenges have to be mastered. Movable mechanical components should be avoided to prolong the lifetime. Power losses in the form of heat must be dissipated to protect the components from damage by overheating. The system must work robust with different vehicle underfloor heights over different positions. Essentially, every inductive charging infrastructure must be usable by any customer independent of its vehicle manufacturer, as customers are used from refueling their vehicles or recharging their phones with USB plugs. Therefor an interoperability concept for inductive charging systems has to be developed and to become part of an international standard for charging EVs.

1.2 State of the art

In this section the state of the art of interoperable power transfer of inductive charging systems will be described. First, the meaning of the word “interoperability” in context of this thesis is provided. Then, geometric and electric understandings of interoperability will be presented. Existing standards at the time of the thesis preparation will be given and it will be shown how these standards cope with the challenge of interoperability.

In the context of inductive power transfer, interoperability is the ability of the ground and vehicle systems to exchange information and to transfer power. For the exchange of information the *ISO 15118* standard already existed and was extended to meet the new requirements for inductive charging. However, the transfer of power between ground and vehicle systems was a blind spot at the beginning of this thesis. Therefore, this thesis put emphasis on interoperability requirements for the power transfer.

In the classical mechanic context, the understanding of interoperability can be illustrated using the example of a male and female connector both defined by their geometric dimensions. Male and female connectors can only be connected when both interacting component parts are built according to their specification and the component tolerances are fulfilled. If one part of a component, e.g. a pin size, does not comply with the allowed tolerance, a proper connection cannot be ensured. For this reason, all components are specified with tolerances as depicted in Fig. 1.1. When both interacting components comply with their respective tolerances, mechanical compatibility is certain.

Electrical connectors have in addition to the mechanical requirements, also elec-

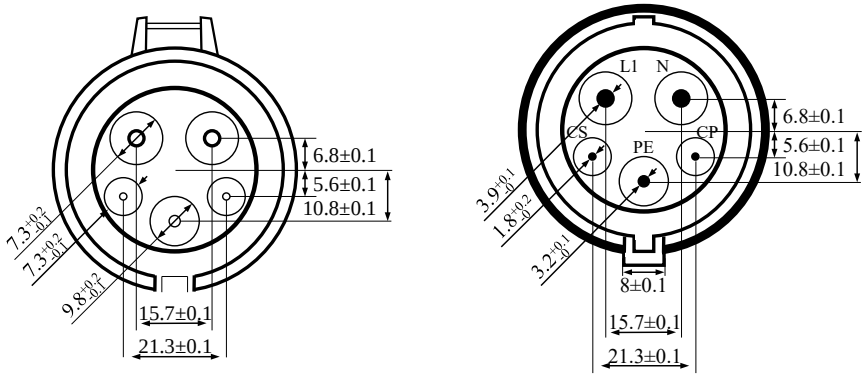

(a) Vehicle inlet. **(b)** Vehicle connector.

Figure 1.1: Mechanical tolerance specifications for AC connector and inlet from [11]. All components are defined with tolerances to ensure mechanical compatibility.

tric requirements that need to be fulfilled to achieve interoperability. For example, additional signals that communicate the maximum current rating between wallbox and vehicle maximum current and voltage ratings or maximum allowed connector resistance between inlet and connector that may not be exceeded. Taking the control pilot signal depicted in Fig. 1.2, which is used in conductive charging for the secure communication between vehicle and wallbox. The voltage level generated and measured at the supply equipment can be changed by the vehicle, indicating its status. Thus, different signal levels have to be clearly distinguishable. The signal tolerance consists of $\pm 0.6\,\mathrm{V}$ for the generation and $< \pm 0.5\,\mathrm{V}$ for the measurement that need to be met for the specified temperature ranges [11, 30]. This can only be ensured when all circuit components comply with their specified tolerances. In consequence, interoperability of male and female component requires both to fulfill the mechanical and the electrical requirements.

For inductive charging systems interoperability becomes more complicated. The physical connection between male and female connector for power transfer is broken up and ground and vehicle system are connected when an alternating current inside the coils generate an electromagnetic field. The field depends on ground and vehicle system components and the environment, the applied materials and their respective position, cf. Fig. 1.3. Hence, position and material affect the self inductance of ground and vehicle coil and their mutual coupling. It effects the electrical behavior of the complete system and makes interoperability a difficult challenge. Since the magnetic field is difficult to measure and the mutual influence of ground and vehicle coil on the self inductances is therewith not detectable, a new interface needed to be established. Although ground and vehicle system are physically

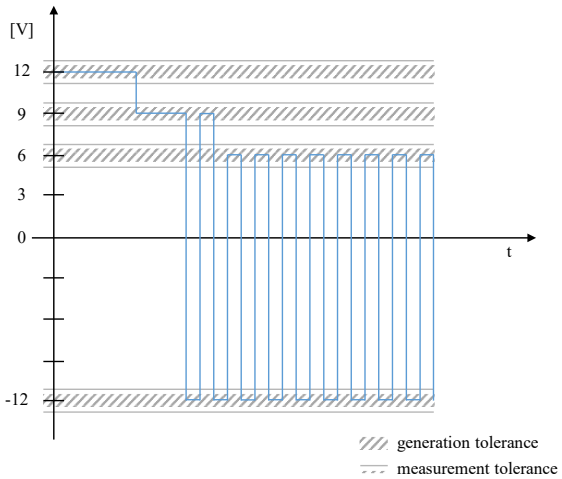

Figure 1.2: Electrical tolerance specification of the control pilot signal according to SAE J1772 for conductive charging. The voltage level indicates the vehicle status. Its tolerance is divided into generation and measurement tolerance to ensure electrical compatibility of supply equipment with vehicle including the connecting cable. The duty cycle indicates the maximum available current.

separated, their mutual dependence requires them to be described together as a system. A pragmatic approach is to establish an interface on each coil terminal of the magnetic transformer. These interfaces use impedance to characterize systems. In this way, changes in the magnetic field as well as changes in the self inductances can be described.

In context of this thesis, this approach was theoretically elaborated and verified. Initial doubts about the technical feasibility of an impedance measurement at the interface among technical experts within the standardization working groups, were dissolved and approved by experimental verification of the proposed test setup. Up to now, this is the only known way to characterize these systems completely.

Standardization bodies At the time of the preparation of this thesis, there existed several standardization bodies with the goal to define acceptable criteria for inductive charging of electric vehicles. The three leading bodies are summarized in Table 1.2. Additional information on other bodies can be found in [31].

Interoperability in Consumer Electronic Standardization The commercial success of inductive charging started with low power applications for the consumer electronics. In November 2008, the *Wireless Power Consortium* (WPC) was estab-

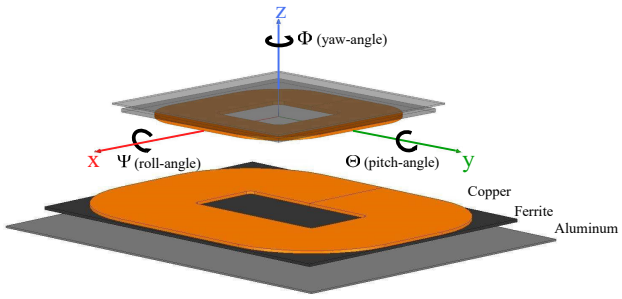

Figure 1.3: Simplified simulation model of an inductive charging system with indicated (x, y, z) offset and rotation axes (Ψ, Θ, Φ). With no mechanical connection but mutually interdependent magnetic properties, the interface was proposed at the coil terminals with electrical requirements including tolerances to ensure interoperability.

Organization	Issue	Content	Releases
IEC	61980	General Requirements for Infrastructure, Control and Positioning	Drafts published 04/19
ISO	19363	General requirements for Vehicles	To be published
	15118	Communication	Published 04/19
SAE	J2954	Comprehensive, leading Standard	TIR 2016 [32] RP 2017 [33]

Table 1.2: Leading standardization bodies.

lished to develop a standard wireless charging interface that is compatible beyond manufacturers [34]. In 2012, other consortia like *Power Matter Alliance* (PMA) and *Alliance for Wireless Power* (A4WP) followed and formed—as a counterbalance to the more and more importance gaining "Qi" standard of the WPC—the AirFuel Alliance[6] in 2015 [35].

The Qi standard requires new products to be tested for compliance with the latest Qi specification by an authorized test lab. However, to ensure interoperability, further tests in so called "interoperability testing centers" are mandatory. There, the new product is tested with some previously certified Qi products[7], which are currently

[6] AirFuel Alliance, "Charging is Changing," [Online]. Available: https://www.airfuel.org/about/. [Accessed 19-April-2019].

[7] Eurofins GSC Lux SARL, "Qi Testing & Pre-Testing Services," [Online]. Available: https://www.eurofins-digitaltesting.com/test-solutions/consumer-device-testing/qi-testing-pre-testing-services/. [Accessed 19-March-2019].

over 5300 certified products[8]. The test criteria are only available for WPC members. However, the recommended minimum system efficiencies from [36] suggest that power has to be transferred with a certain minimum system efficiency to reference devices. In cases of error or lower efficiency than expected, there remains the open question about the error cause.

This kind of test procedure, where a new product is tested with all existing products on the market ($n_1 \cdot n_2$ variants, where n_1 = number of primary systems and n_2 = number of secondary systems), represents the alternative method to test for interoperability judged by the system efficiency. However, this procedure is very time consuming and cannot test for all environmental influences. In this case it would be over 3 million test variants ($n_1 = 4713$, $n_2 = 647$), which is not feasible.

The AirFuel Alliance also requires new products to conduct a certification procedure that tests compliance with the "Conformance Test Specification" and "Interoperability Test Specification" at an authorized test laboratory[9]. The test documents are reserved for members and not publicly accessible. However, the stated magnetic transformer efficiencies also suggest that a certain power transfer efficiency for the system measurements needs to be achieved with a reference. It can be seen from the currently available "Baseline System Specification" [37] that it evolved from the former available A4WP specification [38] and adopted one part of the interface description methodology from [33]. However, in case of error or lower efficiency than expected, there also remains the open question what part of the system does not behave as specified.

Interoperability in EV standardization At the beginning of this thesis, the understanding of interoperability was only existent on a macroscopic scale. It was only possible to formulate a statement like, it is possible to transfer power from the ground system to the vehicle system with a certain efficiency that does or does not exceed the lower efficiency limit. But there existed no way of describing how the complex interaction between magnetic and electric properties behaves on a system component level. However, this was desperately needed for the independent development of infrastructure and vehicle system, referred to as Ground Assembly (GA) and Vehicle Assembly (VA), respectively. Note, it is also common to refer to the infrastructure as ground or primary and to the vehicle system as secondary. GA and VA are both in need of a counterpart with an interface describing the requirements. We proposed to use the impedance at the coil terminals on both sides of

[8] Wireless Power Consortium, "Product Database," [Online]. Available: https://www.wirelesspowerconsortium.com/products. [Accessed 16-November-2019].

[9] AirFuel Alliance,"AirFuel Certification," [Online]. Available: https://www.airfuel.org/build-with-airfuel/get-airfuel-certified/. [Accessed 19-April-2019].

the magnetic transformer, in order to incorporate the mutual dependence of the self inductances. Therewith the multidimensional state space can be reduced from a seven dimensional problem to a two dimensional problem for a fixed frequency. It was also desirable to have an interface that can be tested for conformance. Therefor we developed a testing concept that is likewise applicable for qualifying product designs, testing interoperability cirteria together with quality assurance testing. The concepts entered into the SAE *J2954 Annex G* and IEC *61980–3 Annex E* [33, 39].

Impedance measurements Impedance measurements are conducted in a variety of fields and so different methods specialized to the respective requirements evolved. In the field of electrochemestry, the system response e.g. of a fuel cell or of batteries to a small excitation signal is measured to calculate the resistance and capacitance material properties of such systems for different frequencies. This experimental method is called impedance spectroscopy or Electrochemical Impedance Spectroscopy (EIS) [40] and can be used to examine inner cell phenomena in fuel cells or state of health in batteries [41, 42, 43]. Besides spectroscopic investigations across different frequencies, impedance measurements are also performed for precise measurement of standard resistances, where typically manual or auto-balancing bridge networks are applied [44]. Commercially available LCR-meters or Vector Network Analyzers (VNAs) apply standard resistances and auto-balancing networks for impedance measurements.

However, the previous mentioned methods are unsuited for impedance measurements of inductive charging systems, where the impedance of the GA or VA during operation is of interest. A pragmatic approach is the direct measurement of voltage, current and their phase difference, sometimes referred to as the I-V method in literature [44]. However, the name is misleading as the phase difference between voltage and current is of interest. Therefor it will be referred to it as UI method. According to Steigerwald's fundamental mode approximation [51], the majority of the energy transfer is occurring in the fundamental frequency. This is further promoted by the design of the resonant transformer with high quality factors to comply with Electromagnetic Compatibility (EMC) requirements [33]. Therefore, only the impedance at fundamental frequency is considered.

But with prevailing close to 90° phase angles, an accurate impedance measurement cannot be achieved by means of the UI method. This motivates the research for a device which is capable to measure the impedance more precisely than the direct method.

In addition, the test setup shall also take the following requirements into account:

- Impedance can be measured at the coil terminals.
- Different power levels, battery voltages, frequencies and positions (x, y, z) can be tested.

- Device under test (DUT) can be treated as a black box. No internal measurements are required.
- Uncertainty in impedance measurement shall be reduced as much as possible.

An overview of different impedance measurement techniques can be found in [44]. It is also worth to mention that [45] are investigating the implementation of an impedance measurement sensor that shall be applied for power transfer efficiency maximization.

1.3 Scope of the thesis

In this thesis interoperability among Inductive Power Transfer Systems (IPTSs) was studied with the goal to develop an interoperability concept.

Previously, the power transfer between IPTSs was a blind spot that only considered the system efficiency as criterion. However, efficiency does not give insights into error causes and cannot differentiate between vehicle and ground side. Both are necessary aspects for the independent development of ground and vehicle systems as well as a missing, not yet sufficiently described interface.
First of all, an interoperability concept requires a suitable description methodology, which is able to characterize the systems comprehensively. The methodology needs to be capable of comprising magnetic as well as electric properties of the system to enable the independent development of infrastructure and vehicle systems.
Therefore, the first, elementary Research Question (RQ) is

RQ 1: How can interoperability be described and how can it be tested?

After an appropriate description methodology was found, existing systems were analyzed with it and the second part of the question was addressed to establish a testing concept based on the new interface description. Because a theoretical characterization alone is not very helpful when it cannot be put into practice.

The description uses the electric transfer parameters to describe the magnetic behavior of the two coils. Their offset dependency is well known, however, vehicle and infrastructure are not always perfectly aligned and in addition to translational offset, also rotatory offsets are possible. This raised the question

RQ 2: What effect has rotation on the transfer parameters?

To answer this question, a SAE reference system was analyzed by means of a FEM simulation for its three rotational degrees of freedom at each translational offset position.

After the presentation of the interoperability concept we received feedback from the technical experts within the standardization bodies that showed their sceptisism about the technical feasibility of an impedance measurement during power transfer at the exemplary parameter values shown in Table 1.3. Because there exist no

$U_{\mathrm{GA}}\,[\mathrm{V}]$	$I_{\mathrm{GA}}\,[\mathrm{A}]$	$\varphi\,[^\circ]$	$f\,[\mathrm{kHz}]$	$P\,[\mathrm{kW}]$
1500	75	88	85	11

Table 1.3: Exemplary Parameter Values.

commercial available systems capable of measuring the impedance with acceptable uncertainty at similar conditions. This led to the question

> **RQ 3**: Is it possible to measure the impedance during power transfer? And how much safety tolerance must be foreseen due to the measurement uncertainty?

To find out the answer and proof or disproof the concept, real measurements with a special device were performed. The results validate the theoretical interoperability concept as well as the proposed testing concept and raise the question

> **RQ 4**: Do analytic and simulation results agree with the impedance measurement data?

Answers to these fundamental questions will be presented in this thesis. The next section presents the approach and structure of this thesis.

1.4 Scientific Approach and Thesis Structure

This section outlines the approach and the thesis structure. First, the used nomenclature will be introduced shortly. Then, the methodological procedure to answer the research questions from section 1.3 is given.

System Overview and Nomenclature Within this thesis, the applied nomenclature is based on SAE *J2954* definitions [32]. As ground and vehicle assembly are composed of many components, it is common to use the abbreviation GA or VA for better understanding. The definitions are illustrated in Fig. 1.4. The GA comprises all infrastructure components from grid connection to the GA coil and the VA all components on the vehicle except the battery.

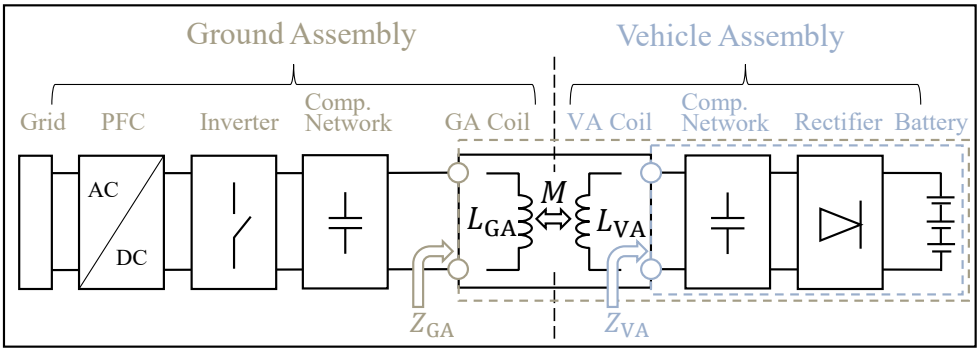

Figure 1.4: System overview illustrating ground and vehicle nomenclature.

Approach At the beginning of this thesis, an inductive charging system was analyzed for system parameters that influence its behavior. The found necessary parameters affecting the system behavior are:

- Power P
- Frequency f
- Battery Voltage U_{Bat}
- Offset Dependent Transfer Parameters $(L_{\mathrm{GA}}, L_{\mathrm{VA}}, k)\,(x, y, z, \Psi, \Theta, \Phi)$
- Active Components

These system parameters span a multi dimensional state space that is difficult to describe. To reduce complexity, the variables can be summarized in a two dimensional impedance space. Then, the impedance characterizes the system reaction to

applied current or voltages. This idea was the starting point to develop an interoperability concept - presented in the first paper. The concept is connected very closely to the standard and based on the idea to use reference systems as development foundation that new proposals should comply with. With describing the magnetic behavior by the offset dependent variables $(L_{\mathrm{GA}}, L_{\mathrm{VA}}, k)$ - instead of magnetic fluxes, it was possible to abstract the electromagnetic problem into an electric problem. The electric parameters $(L_{\mathrm{GA}}, L_{\mathrm{VA}}, k)$ can either be retrieved simulatively by Finite Element Method (FEM) simulations [46, 47] or metrologically via measurements [48, 49, 50]. In the second paper, Finite Element Method was applied to study the effect of rotatory offsets in over 7000 positions, which is only practical by simulative methods. Prior, the FEM model was empirically validated [47]. To test the interoperability concept, I employed analytical calculations based on the Steigerwald approximation [51] and circuit simulation tools like *LTspice* and *Simulink*[10]. However, the question concerning the feasibility of an impedance measurement - discussed in the third paper - required empirical data acquisition and statistical evaluation. Finally, the fourth paper concludes this thesis with a comparison between analytical, simulative and empirical results.

Thesis Structure Chapter 1 of this thesis motivates with short- and long-term goals for inductive charging the necessity of having interoperability between ground and vehicle charging system.

In section 1.2 the current state of the art is presented. First, the understanding of interoperability is elucidated with mechanical and electrical examples. Afterwards, it is shown how recent standards cope with the challenge of interoperability and to which standards this thesis already contributed. Section 1.3 introduces the research questions. And section 1.4 presents the approach and the thesis structure.

Chapter 2 presents summaries of the appended papers - each provides answers to one research question - followed by my individual contribution to each paper.

In chapter 3 the research questions will be answered and starting points to further research will be offered. The thesis structure with respective content is depicted in Fig. 1.5 at a glance.

[10] Simscape Power Systems Specialized Technology.

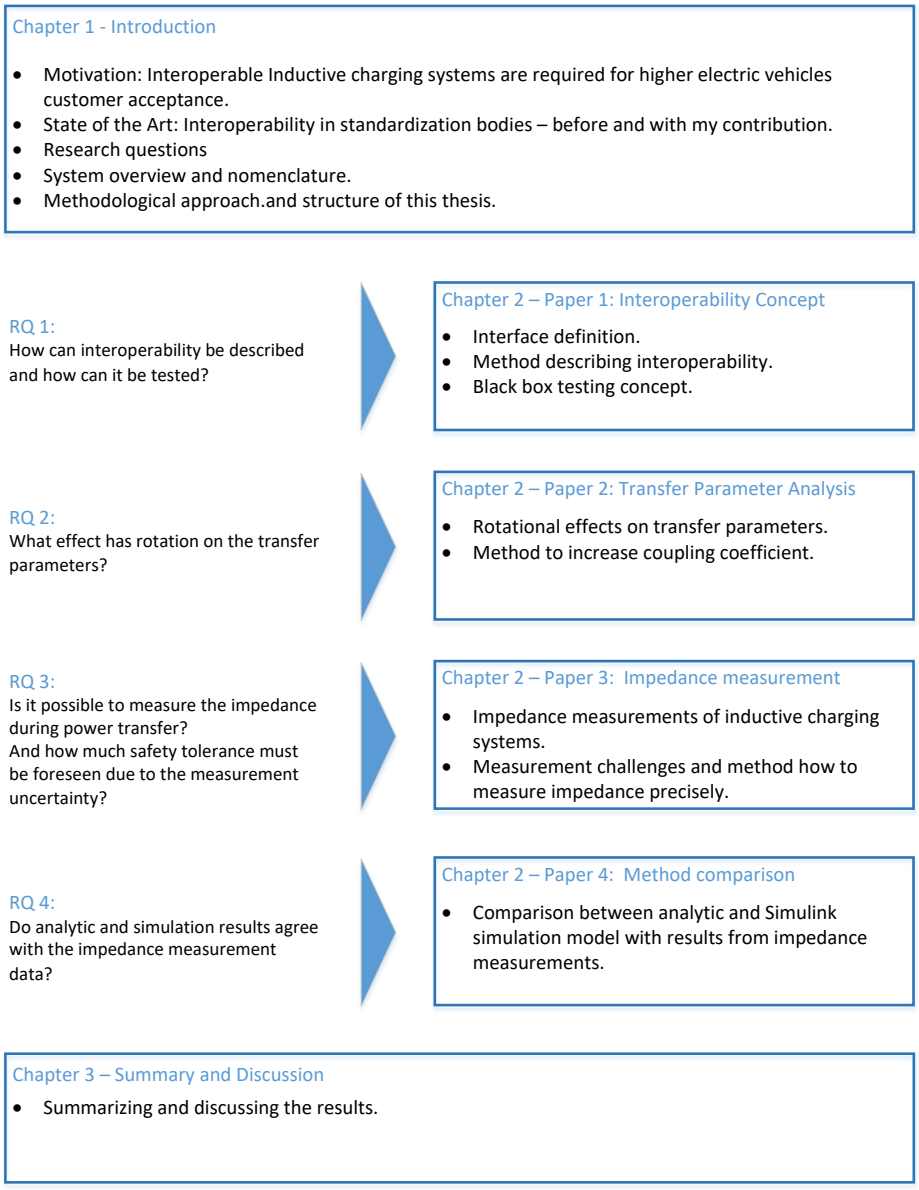

Figure 1.5: Thesis structure.

2 Paper Summaries

2.1 Paper 1: Interoperability Concept

Paper title: **A method for Interoperable Interface Description of Inductive Power Transfer Systems**.

The paper proposes answers to the fundamental Research Question (RQ) **RQ 1**: “How can interoperability be described and how can it be tested?”. In addition, it also answers the question “How to cope with the multidimensional state space, which is created by magnetics and electronics as a function of offset position and vehicle operation points?”.

It proposes a method that suggests how to describe interoperability between Inductive Power Transfer Systems (IPTSs). It therefor introduces new interfaces at the VA and GA coil terminals depicted in Figure 2.1. The interface is based on impedance. The establishment of these interfaces enable the independent development of VA and GA while preserving flexibility in electronic and magnetic design by not imposing specific electrical circuits or coil topologies. A typical representation is to plot its real part against its imaginary part, which is shown using the example of a reference proposal. That reduces the dimensionality of the state space from seven $(f, P, U_{\mathrm{Bat}}, (x, y, z),$ poss. active component$)$ to two $(\mathrm{Re}(Z_{x\mathrm{A}}), \mathrm{Im}(Z_{x\mathrm{A}}))$ for a fixed frequency. Frequency variation adds one dimension. The paper also

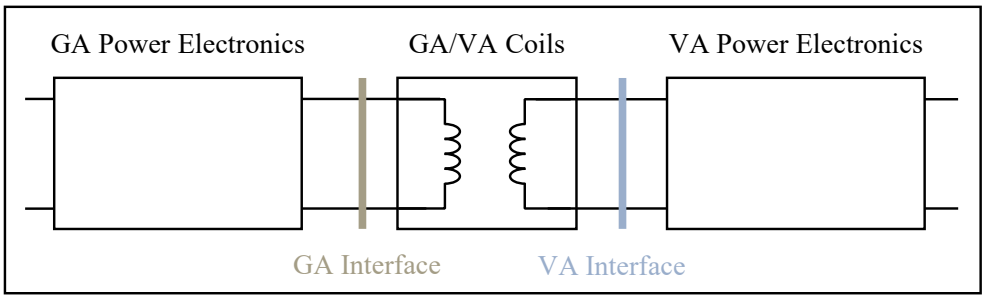

Figure 2.1: Interfaces defined between power electronics and coils [52].

introduces the theoretical framework and shows how an impedance zone can be derived by using the example of an existing IPTS. It further suggests how a practical applicable test for product GAs and product VAs can look like. In this way, interop-

erability between product GAs and VAs can be assured for all possible operation points in the field.

Author Contribution: I developed the idea to use impedance for the characterization into a concept for interoperability of IPTSs. Based on this, I developed together with Josef Krammer a practical testing concept presented in this study. Shown simulation results also use FEM simulation results from Florian Niedermeier. Professor Diepold supported the concept development with helpful advice from his experiences with standardization.

2.2 Paper 2: Transfer Parameter Analysis

Paper title: **The Effect of Rotatory Coil Misalignment on Transfer Parameters of Inductive Power Transfer Systems**.

The paper presents answers to the research question **RQ 2**: "What effect has rotation on the transfer parameters?".

Rotational effects are studied by the use of FEM simulation. Therefor the SAE *J2954* reference coil system from [32] was modeled in *ANSYS Maxwell*. The FEM simulation model was verified with real measurement data for 7626 translational offsets. The investigated parameter range is

$$\begin{aligned} -6^\circ \leq \Psi \leq 6^\circ\,, \\ -6^\circ \leq \Theta \leq 6^\circ\,, \\ 0^\circ \leq \Phi \leq 90^\circ\,, \end{aligned}$$

with Ψ, Θ resolution in steps of 2° and Φ in steps of 15°. The angles are defined as rotation around the respective (x, y, z)-axis as depicted in Fig. 2.2. It uses the

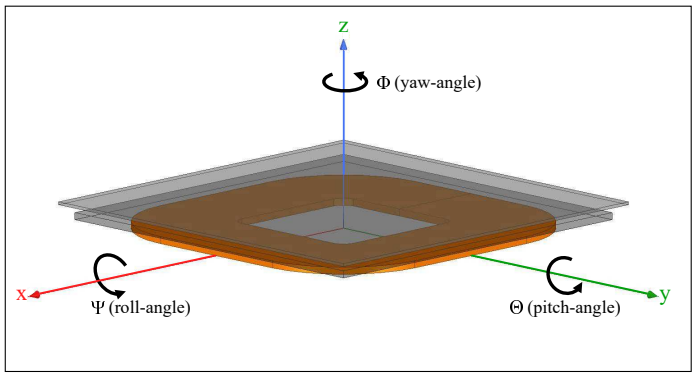

Figure 2.2: Simulation model of VA coil with definition of rotation angles [53].

percentage change of the coupling coefficient Δk with respect to zero rotation to describe improvements or deteriorations that come with rotations. The results show that the change of coupling factor for single rotation around the z-axis can be neglected, which means that power could still be transferred to a vehicle parked with rotatory offset in Φ. This approximation can also be made for rotations including both other axes. Consequently, the influence of the z-axis rotation is neglected. The two remaining rotation axes effect the transfer parameters and were identified as new control parameters to improve transfer efficiency. E.g., this could be realized by controlled air suspensions in EVs and would permit to increase the allowed offset (parking) range by 44% while maintaining the same functionality and component

dimensions. On the other side, this could also be used to decrease the component dimensions while maintaining the same offset range. However, if the rotation parameters come as a random variable determined by the parking behavior or the infrastructure characteristics and cannot be controlled—they can also negatively affect the transfer parameters. For this reason, the influence of small rotatory offsets must be foreseen in the tolerances and incorporated in the system design process.

Author Contribution: This was a 50/50 shared work. I was interested in the effect of rotation on the transfer parameters and approached Florian Niedermeier who setup the FEM simulation. We shared measurement analysis and writing tasks.

2.3 Paper 3: Impedance Measurement

Paper title: **Impedance Measurement on Inductive Power Transfer Systems**.

The paper provides answers to the research question **RQ 3**: “Is it possible to measure the impedance during power transfer? And how much safety tolerance must be foreseen due to the measurement uncertainty?”.

It uses the interface proposed by the first paper [52] to characterize the vehicle system. Therefor the presented impedance of the VA at the GA interface is of interest and needs to be measured. Until now, there exist no commercially available systems capable of measuring the impedance precisely while power transfer. For this reason, this paper introduces a special power matching network with measurement ports that can be used to measure the impedance more precisely than possible by the direct measurement of voltage, current and their phase difference, referred to as UI method. The main idea is to decrease the phase angle from close to 90° to lower values to decrease the measurement uncertainty. With the proposed setup also decreasing voltage or current RMS values follow and contribute to additional uncertainty reduction. Decreasing the measurement uncertainty is important because the GA must be designed to support the full range of presented impedances including tolerances from measurement uncertainties.

Besides the direct method, seven different methods of expressing the impedance Z_{GA} at the GA interface are presented with theoretical derivation. The different methods are compared using uncertainty propagation and the result is stated as weighted mean to include all measurements in the result. Systematic measurement errors are compensated by a set of correction factors that minimize the deviation between the different methods. The improvement factor upon the direct UI method varies between 6 to 34 depending on the measured parameters. In average the proposed method is 16 times better than the direct method with a mean real part uncertainty $\overline{\Delta\,\mathrm{Re}(Z_{\mathrm{GA}})}$ of $0.125\,\Omega$. The smaller needed tolerance margin is depicted in Fig. 2.3. The results demonstrate the technical feasibility of an impedance measurement during power transfer and show that the setup can be used for qualifying VA designs, for quality assurance tests as well as interoperability conformance tests.

Author Contribution: I worked from the measurement idea to its realization. Designed together with Josef Krammer the test bench and approached WiTricity to design an impedance matching network that connects the Wireless Power Transfer Class 3 (WPT3)[1] reference GA and our lab inverter. Together with Zollner colleagues, we performed the measurements. The scientific data analyzation, the

[1] Defined as $11.1\,\mathrm{kVA}$ input power [32].

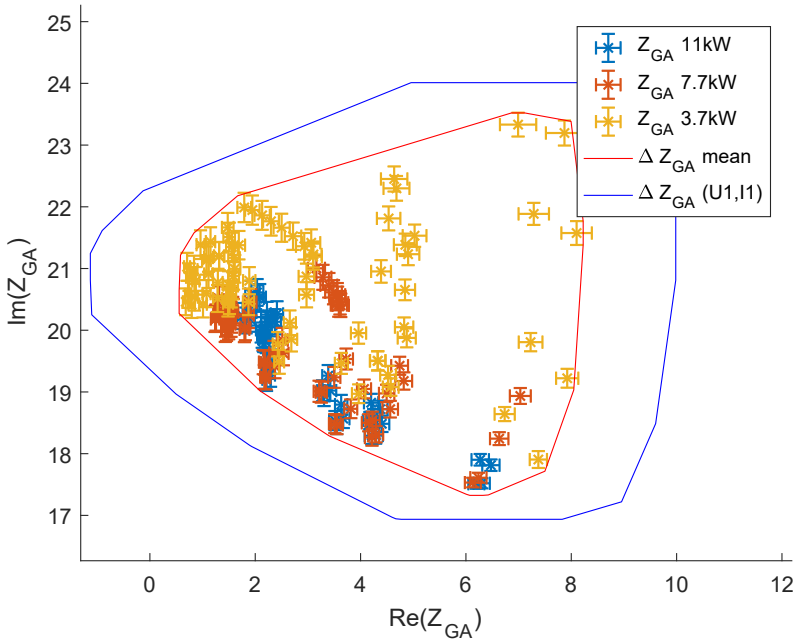

Figure 2.3: Measured impedances for different power levels P_{in}, different battery voltages U_{bat} and offset positions (x, y, z) with required uncertainty tolerances for the UI-method $\Delta Z_{\mathrm{GA}}(U_1, I_1)$ (blue) and the proposed method ΔZ_{GA} mean (red) [54].

underlying theory and the writing of this research was my work.

2.4 Paper 4: Method comparison

Paper title: **A comparison on simulated, analytic and measured impedance values for an inductive power transfer system**.

The paper provides answers to the research question **RQ 4**: “Do analytic and simulation results agree with the impedance measurement data?”.

This paper builds upon the interoperability concept proposed by the first paper [52] and the measurement results obtained with the method proposed by the third paper [54]. It introduces an analytical model that describes the VA electronics in terms of its VA impedance. The applied VA can be considered as a more developed version and therefor holds a challenge when determining its transfer parameters that will be encountered more often when having actual prototypes for vehicles. There, the transfer parameters can no longer be measured by means of a VNA measurement when the capacitors are within the compound and thus are no longer detachable. Hence, we measured the transfer parameters before the final assembly, however, measuring not at the exact same spots that were used in the measurement introduces additional uncertainty that could manifest in a shift between measured and calculated/simulated impedance. This was compensated by means of a fit within the assumed uncertainty ranges of the transfer parameters that cancels out systematic errors. In addition to the analytical model, we also presented a Simulink model. Both models are compared with the measured impedance. We found that the analytical model shows better accordance with the measured values. In mean it deviates by $0.190\,\Omega$ from the measured values and shows good agreement for higher powers. Fig. 2.4 shows the results for $11\,\mathrm{kW}$ with the test system and the calculated capability of the respective WPT3 ground system in purple. All impedances within the purple envelope can be driven by the respective WPT3 GA. This shows how the compatibility of VA and GA can be simulated, calculated and tested.

Author Contribution: I performed the analytical and simulative analysis and compared those results with the measurement results.

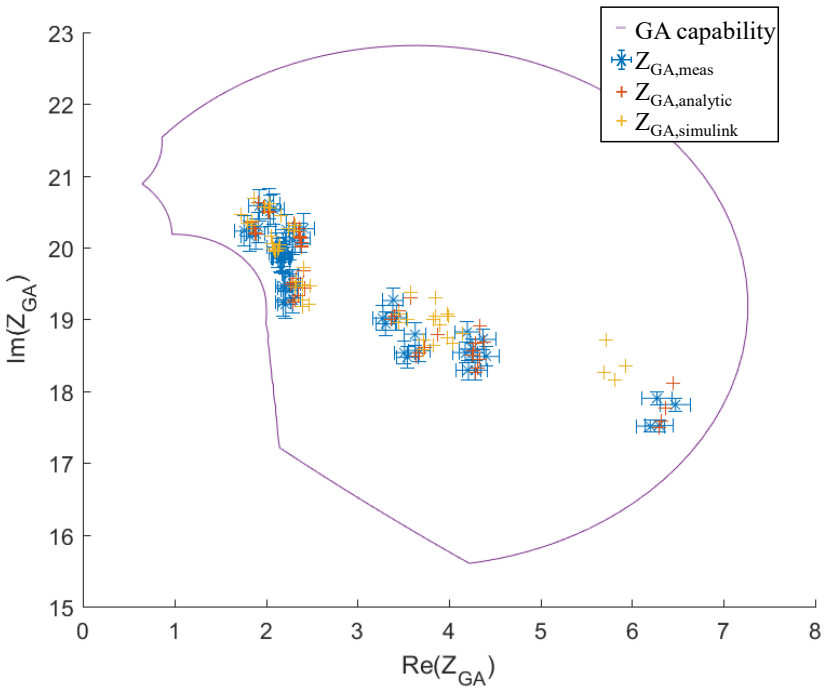

Figure 2.4: Calculated, simulated and measured impedance Z_{GA} with WPT3 reference GA electronics capability from [33]. All impedances within the purple envelope correspond to different EV operation points that can be powered with $11\,\mathrm{kW}$ [55].

3 Summary of Results and Conclusion

In this chapter, answers to the initially raised research questions from section 1.3 are consolidated and ideas that could be used as starting point to further research presented.

The overreaching research goal of this dissertation was to find a way to describe interoperability of wireless charging systems. More precise, this thesis focused on the energy transfer aspect of interoperability.

The first research question asks the fundamental question, how interoperability can be described and how it can be tested.

For the first part of the question, I developed an interoperability concept that on the one hand incorporates already existing systems from standardization and on the other provides the maximum possible freedom for new product development by not imposing the use of specific circuit topologies, components or geometries. Instead, the interoperability concept introduced two new impedance based interfaces at the GA and VA coil terminals. The idea is to use the GA interface to characterize product VAs, and the VA interface to characterize product GAs, respectively. Therewith the problem of the mutual coil inductance dependencies can be resolved.

Based on the proposed description methodology, I developed for the second part of the question two testing concepts - one for product VAs and one for product GAs. The test setup for product GAs uses the reference VA coil(s) and an adjustable load that is capable to set a certain impedance, which will be defined by standardization. The test is successful when the required set of impedances can be powered. The test setup for product VAs uses the reference GA coil(s) and measures the impedance at the GA coil terminals. The test is passed, if the measured impedance at the primary coil terminals is within an impedance zone that also will be defined by standardization.

The second research question asks what transfer parameters really need to be considered for this test and generally looks into rotational displacement between GA and VA coil. To answer, we analyzed a SAE reference system by means of FEM simulation and verified the simulation results by LCR measurements. We found out that a single rotation around the z-axis can be neglected. If three dimensional rotation could be controlled, it holds opportunities to increase the possible parking range or decrease the system size. However, when 3D rotational offset is random,

it can also negatively affect the transfer parameters. In consequence, small three dimensional rotations must be foreseen in the design process and incorporated in the tolerance factors. As the three system parameter dimensions are very impractical for testing, we did not consider them in the impedance measurements.

The third research question looks into the feasibility of the impedance measurement and the uncertainty of this measurement technique, which needs to be considered in the tolerance factor. At first, I reviewed the existing literature for existing solutions that could be applied to wireless EV charging and spoke with many technical experts in the measurement instrument industry. After no company was yet capable to do such kind of measurement, we decided to realize our own product VA test bench proposal and manufactured an impedance measurement device on our own. The device was designed to connect a powerful lab inverter with the WPT3 reference GA coil, to support many different product VAs and to provide measurement ports for the impedance measurement. Besides the physical challenge to measure the real part of the impedance, which is proportional to the cosine of the phase difference between voltage and current and close to $90°$ phase angle, we also faced the challenge that there are no calibrated measurement probes at our nominal frequency of $85000\,\mathrm{Hz}$. In consequence their uncertainty is not well known. In addition, the phases of voltage and current need to be measured with preserved phase relation. The main idea to overcome these challenges was to decrease the phase angle values and therewith reduce the measurement uncertainty. Besides using several measurement positions to calculate the impedance Z_{GA} in different ways. Then, systematic measurement errors can be compensated by means of an error minimization. In this way, the proposed method of the third paper improves upon the direct impedance measurement in average by factor 16 less uncertainty for the real part of the impedance and the mean uncertainty becomes $\overline{\Delta\,\mathrm{Re}(Z_{\mathrm{GA}})} = 0.125\,\Omega$.

This shows the technical feasibility of an impedance measurement during power transfer and the average uncertainty of this measurement technique that needs to be taken into account when defining the impedance zones with tolerance factors.

The fourth research question concludes this work by asking for the agreement between analytic and simulation model results with the impedance measurement data. To answer this question, I present an analytic model and a *Simulink* model in the fourth paper, which can be very helpful to other researchers. The models characterize the VA that was used in the impedance measurement in terms of its VA impedance. Its GA impedance is then calculated with transfer parameters that were measured by means of a VNA. For both models I found that the results share a similar structure with the measured impedances, however, a slight offset to the measured impedance values can also be identified. The offset was introduced because the transfer parameters needed to be measured before the final assembly

stage. This deviation could be overcome by an offset dependent correction factor. The results from the fourth paper show that the analytic model yields a better accordance with the measured values than the *Simulink* model. For this reason, we suggest to use the analytic model to support the design development process. Due to the transfer parameter sensitivity and the challenge to measure them when encountering more sophisticated prototypes that e.g. have capacitors integrated into the compound—impedance measurements are essential as they result in the lowest known additional uncertainty. Additional uncertainty is generally undesired because it entails higher demands to the power electronics and thus higher costs.

Further Research Suggestions During this thesis, I came across many interesting questions that could serve as a starting point for future research. Some of them are given in the outlook sections of the appended papers, others that can help to reduce costs shall be mentioned in this section.

In the SAE *J2954* an allowed offset range of $\pm 75\,\mathrm{mm}$ in x-direction (driving direction) and of $\pm 100\,\mathrm{mm}$ in y-direction is given. All systems are designed to achieve efficiency requirements over the whole offset range. There, the question of how do customers park their vehicles would be a very interesting topic to address. Having the results from such a study could help to reduce unnecessary requirements, increase the efficiency at parking positions with high parking probability and to save costs.

Another interesting topic for further research could be to investigate how the uncertainty of the impedance measurement could be further reduced. One promising path would be to study how different available current and voltage probes perform and which deliver the best results. Also very appealing and helpful would be to have a method that can be applied to calibrate their phase differences.

Further interesting research topics that shall be mentioned are loss models that help to improve simulation accuracy and investigations into the effects of vehicle integration on the inductances.

A Method for Interoperable Interface Description of Inductive Power Transfer Systems

Marius Hassler
BMW Group
80788 Munich, Germany
Marius.Hassler@bmw.de

Florian Niedermeier
BMW Group
80788 Munich, Germany

Josef Krammer
BMW Group
80788 Munich, Germany

Klaus Diepold
Technical University of Munich
80333 Munich, Germany

***Abstract*—In this paper we propose a method for inductive power transfer systems (IPTS) that uses an impedance-based approach for the interface description between vehicle and infrastructure. Thus, interoperability between vehicle and infrastructure can be described and both subsystems can be developed independently. The method preserves flexibility in electronic and magnetic design by not imposing specific electrical circuits or coil topologies. We show how an impedance zone can be derived by using the example of an existing IPTS. We then present a test bench that can be applied to verify the requirements for conformance. In this way, interoperability in the field can be assured, with any Vehicle Assembly (VA) being able to receive power from any Ground Assembly (GA) for all possible operation points.**

***Index Terms*—inductive power transfer, wireless charging, interoperability, SAE J2954**

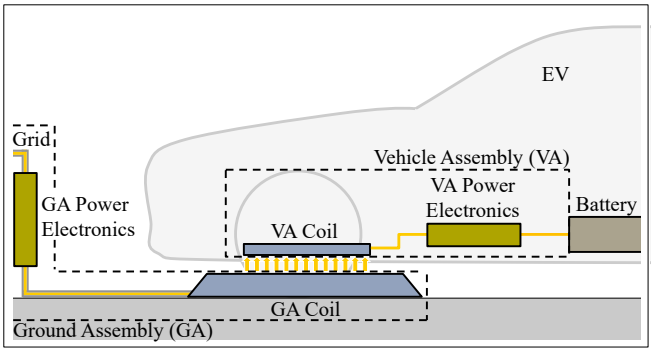

Fig. 1. Schematic of inductive charging EVs.

I. Introduction

The recent demand for electrical vehicles (EVs) also calls for a more convenient way of charging vehicles and overcoming additional efforts result from the use of a charging cable. Therefore, many experts see inductive charging as one of the key technologies that will help electromobility in its breakthrough.

Since its beginnings, inductive charging has grown to a $1.3 billion market in 2015 and is expected to continue its growth to a $17.9 billion market by 2024 [1], starting with low power applications for the consumer electronics (CE) and spreading out to other applications such as wireless vehicle charging. The reason for this is clear: inductive charging allows customers to stick to their habits, since no charging cable has to be connected every time the battery needs to be recharged. In addition, it even removes the efforts of refueling. Interoperability of inductive charging systems is mandatory for high customer acceptance and appreciation. Interoperability means that any vehicle is able to charge with any infrastructure, regardless of manufacturer.

A glimpse at the development of mobile charging reveals the need for interoperability. At first, manufacturers had proprietary charging devices that could only recharge one specific device. Then, manufacturers tried to establish interoperability within their own products, but this was still disappointing from the customers perspective. Afterwards, USB-charging cables superseded the proprietary charging plugs, which led to much higher customer satisfaction. A European Commission initiated standard for a common power supply was published in 2011 [2]. Interoperability is vital in order to live up to today's customer expectations. For this reason, we intensively address the complex topic of interoperability in this paper. We propose answers to fundamental questions such as: "How can interoperability be described?", "How to cope with the multidimensional state-space, which is created by magnetics and electronics as a function of offset position and vehicle operation points?" and "How can interoperability be verified?".

For compatibility of different manufacturers, the Society of Automotive Engineers (SAE) started the development of a technical standard for "Wireless Power Transfer for Light-Duty Plug-In/ Electric Vehicles and Alignment Methodology" (J2954) [3]. In their definition, interoperability is present if power can be transferred with an overall efficiency greater than 85% for target position and greater than 80% at offset positions. New designs, so called 'products', will be tested against a reference assembly. Unfortunately, this comes with two major drawbacks. First, a reference assembly consists of a defined coil geometry and specific electronics. This determination leaves no room for future development. Second, the overall efficiency alone is not a sufficient quantity for measurement. In the case of lower overall efficiency, the reason and the subsystem efficiencies remain unknown. A similar approach for low power applications exists in the CE. The AirFuel Alliance, former A4WP, uses a single impedance zone in their 'Baseline System Specification' for the reflected impedance, which limits the presented load to the primary

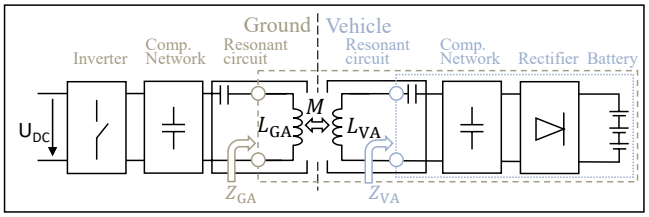

Fig. 2. Block diagram for an inductive charging system.

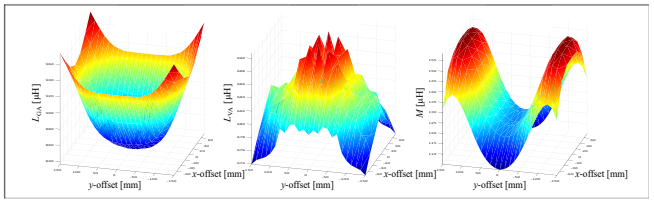

Fig. 3. Exemplary GA/VA inductance and their mutual coupling as a function of offset position (x, y) for circular coils.

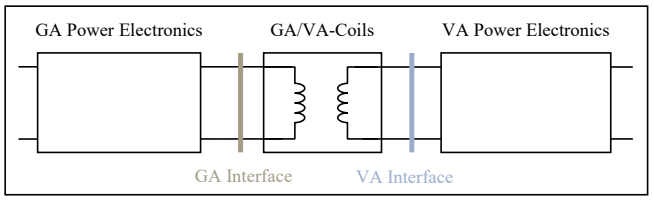

Fig. 4. Interfaces defined between power electronics and coils.

resonator [4]. In contrast to this, we use a different interface definition and add an additional impedance zone to qualify product GAs. Moreover, the applied power level differs by a factor $\sim 10^3$ and the frequency by $\sim 10^{-2}$ from CE to EV application.

In this paper, we propose a method for IPTS that uses an impedance-based approach for the interface description between vehicle and infrastructure. As a result, interoperability becomes describable and both subsystems can be developed independently. In this way flexibility in electronic and magnetic design is preserved by specifying the interface rather than specific electric circuits or coil topologies. In addition, a test bench is presented that can be applied for conformance testing.

II. Fundamentals

IPTS are based on electromagnetic induction. Alternating current inside the GA-coil generates an alternating magnetic field, which induces a voltage inside the VA-coil [5]. This transfers energy from GA to VA over typical airgaps of $10 - 25\,\mathrm{cm}$ to recharge the electric vehicle's battery. The basic setup of IPTS can be seen in Fig. 2. Magnetic and electric relevant components can be distinguished from each other.

A. Magnetics

The magnetic behavior of IPTS is determined by the geometric configuration of magnetic relevant coil components such as litz wire, ferrite, aluminum shielding, etc. The interesting electric parameters for circuit design and system behavior, $L_{\mathrm{GA}}, L_{\mathrm{VA}}$ and M, can be obtained by the use of FEM simulation or via measurements and the equation for the mutual inductance

$$M = k\sqrt{L_{\mathrm{GA}} L_{\mathrm{VA}}}\,, \tag{1}$$

where k is the coupling coefficient [7]. The parameters change with the relative position of vehicle and ground coil, the so called 'offset position'. Fig. 3 shows their characteristic dependence on offset position for a circular coil topology yield by FEM-simulation. The correlation of VA- and GA-coil also applies if someone exchanges the VA-coil with a new product. Hence, the magnetic behavior differs and the parameters $L_{\mathrm{GA}}, L_{\mathrm{VA}}$ and k change as well. In compliance with SAE J2954, the offset position may vary by $\pm 75\,\mathrm{mm}$ in the X-direction (front/rear) and $\pm 100\,\mathrm{mm}$ in the Y-direction (left/right). In addition, the z-distance may vary over a range of $10 - 25\,\mathrm{cm}$. This interdependence is one of the biggest challenges for interoperability. It is one of the reasons why the interface is not defined between ground and vehicle assembly where it physically exists, but rather next to the coils.

B. Electronics

The GA electronics generally consist of a PFC connected to a power supply, followed by an inverter, a compensation network and a resonant circuit. The VA electronics is comprised of a resonance circuit followed by a compensation network and a rectifier with filters and wiring to the EV's battery.

Electronics from current reference proposals of the SAE J2954 use resonant coupling, also referred to as strong resonant coupling, to transfer power with reasonable efficiency over air [6]. Thereby, the resonance frequency of the GA resonant circuit and VA resonant circuit are matched at $85\,\mathrm{kHz}$. However, for systems using frequency tuning to compensate for different offset and EV operation points, the operating frequency may vary within the frequency band from $81.38 - 90\,\mathrm{kHz}$. Besides frequency, other quantities may also vary. The battery voltage of EVs can change between $280 - 420\,\mathrm{V}$. The requested power can vary as defined by the specific wireless power transfer (WPT) class. The offset position (x, y, z), which sets the transformer values $(L_{\mathrm{GA}}, L_{\mathrm{VA}}, M)$, can differ. In addition, some concepts foresee active components for compensation, which adds another degree of freedom.

The behavior of the VA electronics can be characterized by the impedance Z_{VA}, which summarizes different network topologies including active components and different EV operation points, as depicted in Fig. 2. Impedance Z_{GA} describes the presented load to GA electronics and hence each operating point. If the GA electronics can drive the presented impedance Z_{GA}, the requested power can be delivered to the EV's battery.

III. Impedance Interface

To describe the multidimensional state space, we establish an interface between the coil parameters, which are design and

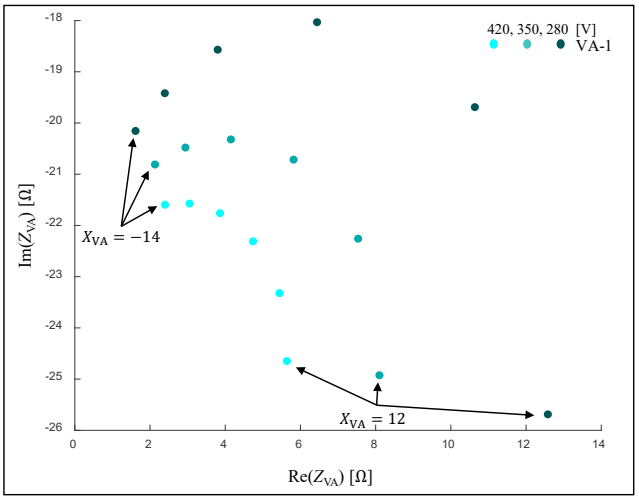

Fig. 5. VA impedance Z_{VA} for power $P = 6660\,\mathrm{W}$, battery voltages $U_{\mathrm{Bat}} = [280, 350, 420]\,\mathrm{V}$ and different X_{VA}-values.

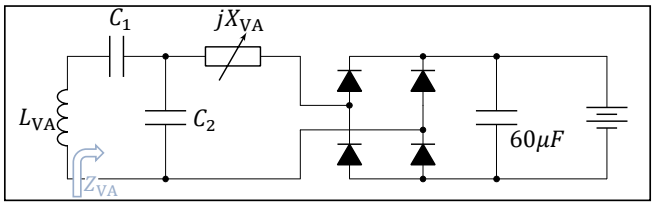

Fig. 6. Schematics of a reference proposal, denoted as 'VA-1' [3]. $C_1 = 140\,\mathrm{nF}$, $C_2 = 170\,\mathrm{nF}$ and $X_{\mathrm{VA}} \in [-14, 12]\,\Omega$.

offset dependent, and the power electronics, i.e., as close to the physical interface as possible. This separates the system into three parts as illustrated in Fig. 4:

- GA power electronics
- GA- and VA-coil (magnetics)
- VA power electronics

We define an impedance zone at both interfaces. The GA-impedance zone, between GA electronics and GA- and VA-coil, has to be met by the GA power electronics and by the presented VA impedance. It will be used for the qualification of product VAs. Analogously, product GAs will be tested at the VA-impedance zone. The transformation from VA impedance to GA impedance is mathematically described by

$$Z_{\mathrm{GA}} = j\omega L_{\mathrm{GA}} + \frac{\omega^2 M^2}{j\omega L_{\mathrm{VA}} + Z_{\mathrm{VA}}}\,, \tag{2}$$

with ω being the angular frequency. Applying this equation for all offset positions and EV operation points, yields an impedance zone representing all operation points that can be presented to the power electronics of the GA for that frequency. Hence, it can be used to design the GA power electronics respectively.

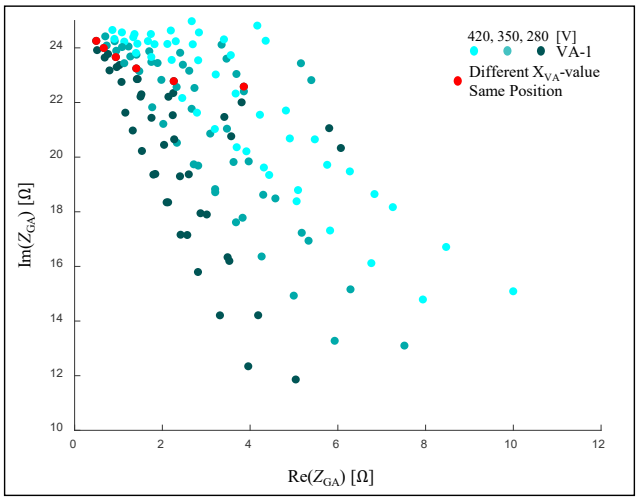

Fig. 7. Transformed VA impedances at the GA impedance interface for power $P = 6660\,\mathrm{W}$ and battery voltages $U_{\mathrm{Bat}} = [280, 350, 420]\,\mathrm{V}$. The red points represent different jX_{VA}-values.

TABLE I
PARAMETER VALUES FOR DIFFERENT OFFSET POSITION.[1]

offset					
x [mm]	y [mm]	z [mm]	k	L_{GA} [μH]	L_{VA} [μH]
0	0	100	0.24	35.5	42.8
75	0	100	0.18	40.0	42.7
0	100	100	0.26	37.7	42.7
75	100	100	0.20	41.1	42.6
0	0	150	0.16	42.8	39.0
75	0	150	0.12	44.4	39.1
0	100	150	0.15	44.0	39.0
75	100	150	0.12	45.1	38.9

IV. IMPEDANCE EXAMPLES

To illustrate the abstract concept of an impedance based interface, existing circuit topologies will be characterized by means of their Z_{GA} and Z_{VA} impedance.

A. System with one VA

Fig. 6 shows the schematic of a WPT2 ($P \leq 7.7\,\mathrm{kW}$) reference proposal with an active component for impedance matching described by a variable impedance jX_{VA}, referred to as tunable matching network (TMN). The electrical behavior of the VA power electronics can be approximately described by the VA impedance

$$Z_{\mathrm{VA}} = \frac{1}{j\omega C_1} + \frac{\frac{1}{j\omega C_2}(jX_{\mathrm{VA}} + R_{\mathrm{Bat}})}{\frac{1}{j\omega C_2} + jX_{\mathrm{VA}} + R_{\mathrm{Bat}}}\,, \tag{3}$$

[1]The data was obtained by FEM simulation of the GA-VA configuration described in Appendix H1m and D1m [3].

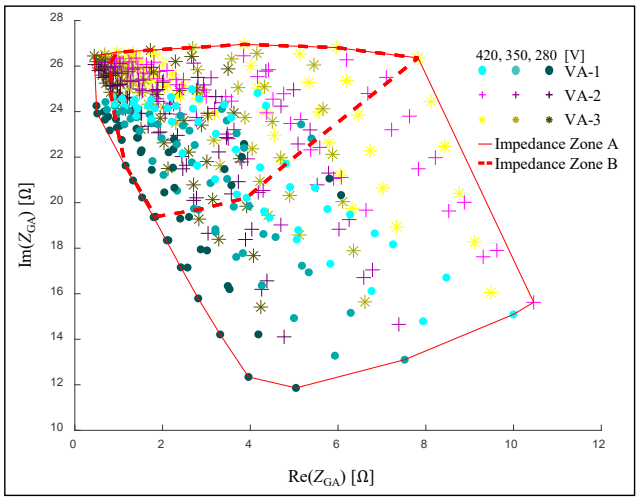

Fig. 8. Z_{GA} for different VAs at power $P = 6660\,\mathrm{W}$ and battery voltages $U_{\mathrm{Bat}} = [280, 350, 420]\,\mathrm{V}$. Impedance Zone A comprises all possible VA settings. Impedance Zone B shows a refined zone with constrained X_{VA} settings.

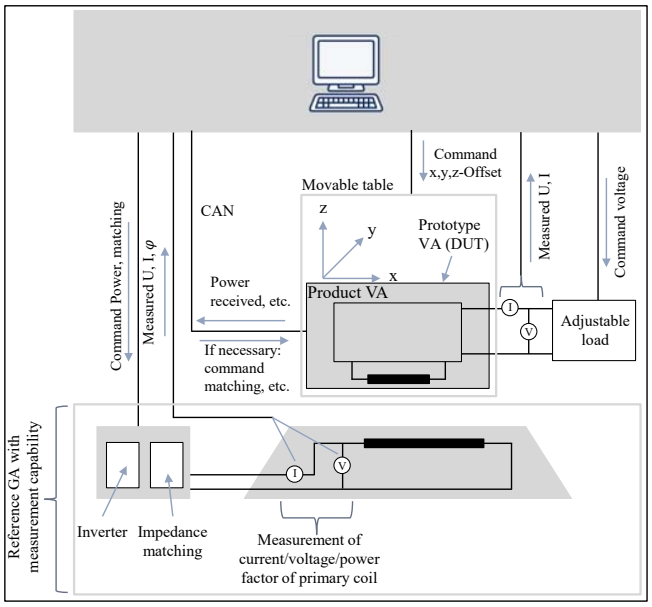

Fig. 9. Product VA test setup for IPTS.

with the AC equivalent resistance

$$R_{\mathrm{Bat}} = \frac{8}{\pi^2}\frac{U_{\mathrm{Bat}}^2}{P}\,, \tag{4}$$

as described by [8]. The VA impedance Z_{VA} is illustrated in Fig. 5 at full power for different battery voltages $U_{\mathrm{Bat}} = [280, 350, 420]\,\mathrm{V}$ and different TMN values $X_{\mathrm{VA}} \in [-14, 12]\,\Omega$. The TMN values are linearly spaced in steps of $5.2\,\Omega$ to demonstrate the matching capability. Within SAE J2954, it is not stated which TMN value has to be applied for a certain EV operation point. Depending on the operation strategy, for example, the TMN value could be set to minimize the VA-coil current for heat reduction or to shorten the charging time. Therefore, we have to assume that multiple TMN settings are possible. The transformed VA impedance can be obtained by substituting (3) into (2). Applying all VA impedances and parameters from Table I, which describes the electrical behavior of both coils depending on offset position, gives the GA impedances depicted in Fig. 7. The red marked data points display different TMN settings for the same offset position and battery voltage. The primary electronics need to be capable of driving only one of these values to ensure power transfer for that offset and EV operation point. Hence, a GA capability comprised of a subset of GA impedances with one X_{VA} for each offset and EV operation point would be sufficient.

B. System with multiple VAs

Requirements of a GA, capable of driving multiple VAs, can be derived by repeating the procedure for other VAs. This can be seen in Fig. 8, which shows the GA impedances for VA-1, VA-2 and VA-3[2]. A GA supporting all presented impedances, would be required to provide a GA-coil current I_{GA} in the range of $25.2 - 122.6\,\mathrm{A}$ to transfer $P = 6660\,\mathrm{W}$. Practically, the current range could be narrowed by constraining the allowed X_{VA} settings (cf. Fig 5) without power degradation. This can be seen in the refined 'Impedance Zone B' in Fig. 8, which comprises all EV operation points for all offset positions. The required current range can be narrowed to $29.2 - 90.4\,\mathrm{A}$ with this. Further narrowing the impedance zone will result in operation points that cannot reach full power transfer. In case of constraints, the applied VA impedances, which map inside the impedance zone and reach full power with respect to offset position, shall be applied for product GA testing.

The distribution of the presented Z_{GA}-data only differs slightly from VA-1 to VA-3, due to their similarity in electric and magnetic design.

V. Product VA Test

The requirements for product VAs at the Z_{GA}-interface can be tested with the test stand depicted in Fig. 9. It can be used during the development of new products to tune magnetic and electric design and to test the interoperability requirements. Compatibility between product VA and test stand GA is present when the measured Z_{GA} impedance falls within the GA capability, which means the requested power can be transferred. The test procedure is as follows:
The product VA, device under test (DUT), is inserted into the movable test bench and connected to a computer-controlled adjustable load. The DUT includes the mock-up of the underfloor structure and materials. The computer emulates the communication of the vehicle and the GA and steps through all necessary EV operation points for each offset position. It measures and records the DUT output $U_{\mathrm{DC}}, I_{\mathrm{DC}}$ and the GA-

[2]'VA-2' and 'VA-3' denote the VA reference proposals described in Appendix E1e and F1e, respectively [3].

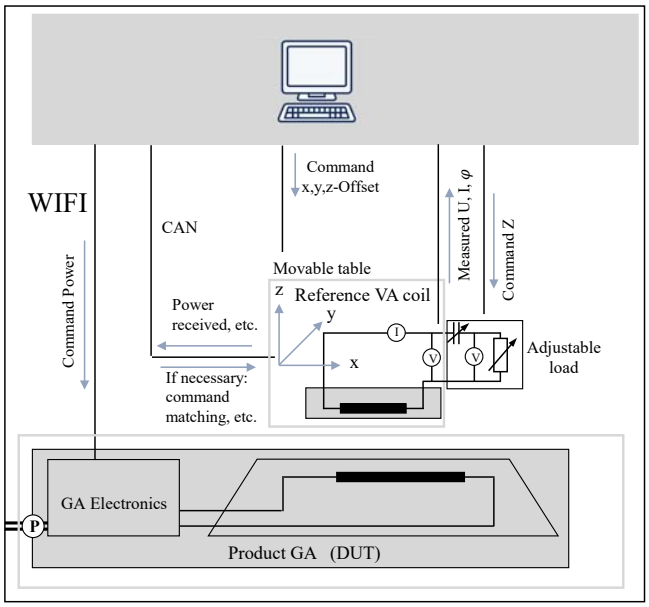

Fig. 10. Product GA test setup for IPTS.

coil input $U_{\mathrm{GA}}, I_{\mathrm{GA}}, \varphi_{\mathrm{GA}}$. The required Z_{GA} impedances can be calculated from the recorded data. In addition, it is also possible to measure the efficiency. The test has succeeded if the measured impedance falls inside the defined impedance zone for all operation points.

VI. Product GA Test

The requirements for product GAs at the Z_{VA}-interface can be tested with the test stand depicted in Fig. 10. It can also be used during the development of new products to tune magnetic and electric design and to test the interoperability requirements. Compatibility between product GA and test stand VAs is present when the GA is capable of driving the set VA impedances, which means the requested power can be transferred. The test procedure is as follows:

The product GA (DUT) is connected to the power supply and controlled via WiFi access by a test-bench computer. The reference VAs can be embedded within mock-ups representing general underfloor structure and materials. The computer emulates the communication between vehicle and GA and steps through all necessary EV operation points for each offset position. It sets the defined VA impedances and measures whether the set impedance is reached. When the set impedance is reached, it measures the transferred power. The test has succeeded if the set impedances were reached and the delivered power to all reference VAs has achieved a certain efficiency, e.g. $\mu \geq 92\%$.

VII. Discussion

Interoperability among product GAs and VAs from different manufacturers requires a common impedance zone. This zone can be derived from existing proposals of the SAE J2954. However, to reduce the number of tests, it is desirable to have as few reference coils as possible, for the compliance tests, in which product VAs will be tested against the reference GA and product GAs against reference VAs, respectively. Product GAs and product VAs come together at the customers. To ensure interoperability among products, we foresee a tolerance factor that incorporates deviations in magnetics and electronics, e.g. by vehicle integration, mechanics, temperature, aging or manufacturing. Their impact will be investigated in future measurements and incorporated in the tolerance factor.

Interoperability is especially present if for all operation points the measured impedance, after section V, falls within the defined impedance zone, including tolerances.

In general, the procedure described in section IV-A can be applied to all existing IPTS and be used to determine a common impedance zone. However, by considering many arbitrary VAs, the GA impedance zone will become very large, which means the requirements for the GA electronics will increase significantly. Therefore standardization has to have a meaningful trade-off between GA requirements and compatibility with VA designs, which mostly were not intended to work with the reference GA. Once established, the impedance zones will be extremely helpful in designing interoperable products.

VIII. Conclusion

We proposed an innovative methodology of how interoperability can be described and how it can be measured at high power applications. The introduced impedance-based interfaces for inductive power transfer systems will enable the independent development of ground and vehicle components. Once defined, the impedance zones will serve as a base guideline for future designs. This will preserve all freedom in magnetic and electronic designing. To illustrate the abstract concept of impedance zones, we characterized an IPTS by means of its VA and GA impedance. This showed that the electronic requirements could be reduced, while retaining the power transfer capability for all EV operation points. Moreover, the presented setups can also be applied for conformance testing.

References

[1] "Global Wireless Power Revenue Is Expected to Reach $17.9 Billion in 2024," *Navigant Research*, [Online]. Available: https://www.navigantresearch.com/. [Accessed 02-November-2017].

[2] IEC Standard, "Interoperability specifications of common external power supply (EPS) for use with data-enabled mobile telephones," *IEC 62684:2011*, 2011.

[3] SAE Standard, "Wireless Power Transfer for Light-Duty Plug-In/ Electric Vehicles and Alignment Methodology," *SAE J2954 TIR*, 2016.

[4] A4WP, "A4WP Wireless Power Transfer System Baseline System Specification (BSS)," *Alliance for Wireless Power*, 2014.

[5] M. Faraday, *Experimental researches in electricity*, Read Books Ltd, 2016.

[6] A. Kurs, A. Karalis, R. Moffatt, J.D. Joannopoulos, P. Fisher and M. Soljacic, "Wireless power transfer via strongly coupled magnetic resonances," *Science*, vol. 317, no. 5834, pp. 83-86, 2007.

[7] P. Steffen, P. Reinhold, *Grundlagen der Elektrotechnik und Elektronik 2*, Springer Berlin Heidelberg, 2012.

[8] R.L. Steigerwald, "A comparison of half-bridge resonant converter topologies," *IEEE Transactions on Power Electronics*, 3(2), pp. 174-182, 1988.

The Effect of Rotatory Coil Misalignment on Transfer Parameters of Inductive Power Transfer Systems

Florian Niedermeier[1,2], Marius Hassler[1,3], Josef Krammer[1], Benedikt Schmuelling[2]

[1]BMW Group, 80788 Munich, Germany

[2]University of Wuppertal, Rainer-Gruenter-Str. 21, 42119 Wuppertal, Germany

[3]Technical University of Munich, Arcisstr. 21, 80333 Munich, Germany

The characteristic transfer parameters of inductive power transfer systems highly depend on the relative position of the coils to each other. While translational offset has been investigated in the past, the effect of rotatory offset on the transfer parameters is widely unclear. This paper contains simulation results of an inductive power transfer system with rotatory offset in three axes and shows the possible improvements in the coupling coefficient. As a result, rotation angles can be used as control parameters and thereby increase the system efficiency. Alternatively, the allowed misalignment area of the secondary coil can be increased while maintaining the functionality and same dimensions.

Corresponding author: Florian Niedermeier; email: F.Niedermeier@me.com; phone: +49 151 601 95722

I INTRODUCTION

Over the last decade the research interest in inductive power transfer (IPT) has highly increased due to a wide range of possible applications. In the daily usage of mobile phones, medical implants or electric vehicles (EV), charging the device is an inevitable task that can benefit from IPT. The contactless charging of EVs comes with many advantages, such as user convenience, insusceptibility to weather and prevention of vandalism. [1–9]

The transfer of electrical energy in inductive charging systems is proceeding via an alternating magnetic field between two coils, using the principle of resonant electromagnetic coupling via induction. This way, power can be transferred from the grid to the car through an air gap to charge the battery. Nevertheless, inductive charging results in more complex systems in comparison to conductive charging systems. [3, 6, 7]

Using IPT for charging EVs, a major challenge is to design systems that work within a large area of coil positioning, due to parking inaccuracy and various ground clearances. Translatory and rotational misalignment of the coils results in a change of characteristic parameters, so it is important to be able to analyse wireless charging systems in all operating points. [10–12] Only if the characteristic transfer parameters of the electromagnetic coupler are known in all considered misalignments, a simulation of the

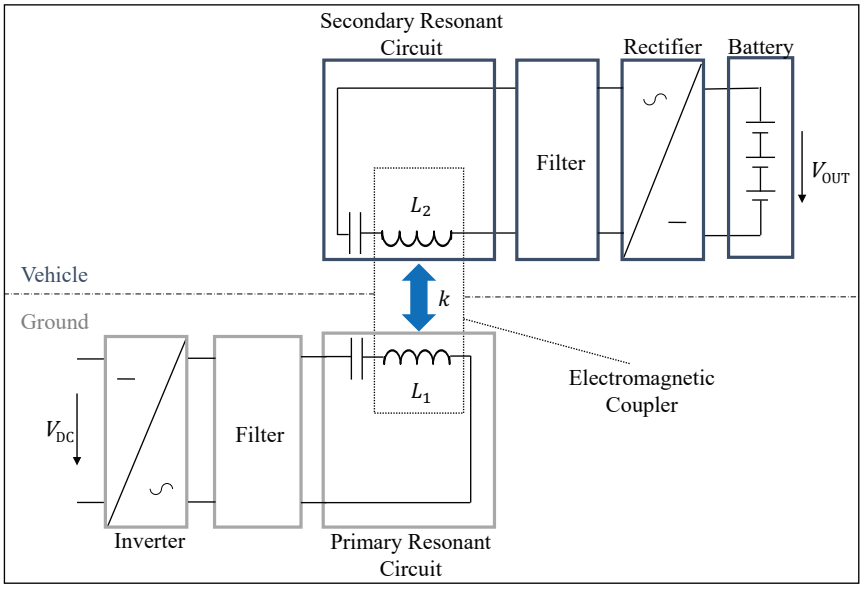

Figure 1: Block diagram of an exemplary IPTS.

system including electronic circuitry can be performed.
In this paper, we analyze the behavior of an inductive power transfer system (IPTS) when the secondary coil has rotational offset towards the primary coil. The effect of rotational misalignment on the characteristic transfer parameters of the IPTS is evaluated and thereby a new optimal position of coils is detected. Using the three rotational angles as additional control parameters, the system can reach new operating points with high magnetic coupling and avoid operating points with low magnetic coupling.

II FUNDAMENTALS

The block diagram in Fig. 1 shows the functional principle of an exemplary IPTS. The most elementary part for inductive power transfer is the electromagnetic coupler, which combines two resonant circuits that are galvanically isolated by the air gap. Each resonant circuit consists of an inductor and a capacitor, operating in resonance at a certain frequency f. An inverter processes the DC voltage V_{DC} to get alternating voltage at the input side of the electromagnetic coupler, and the output voltage is rectified to charge the battery with DC voltage. As a result, alternating current resonates in the primary resonant circuit and generates an alternating magnetic field. The magnetic field induces voltage in the secondary side and thereby transfers power through an air gap by means of electromagnetic induction. [1, 5, 8, 9, 13–15]

A) Transfer Parameters

In a first approach, the electromagnetic coupler can be approximated by a transformer. The difference to a classic transformer is that the leakage inductances are much higher than the mutual inductance because there is an air gap between the coils. The

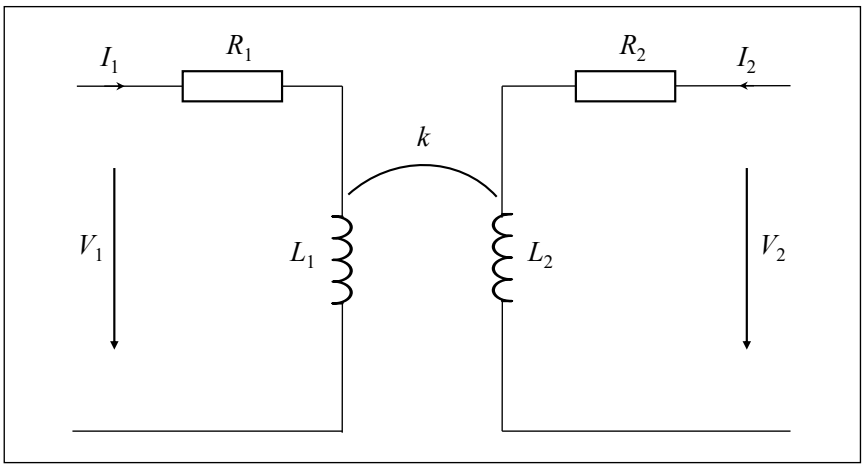

Figure 2: Equivalent circuit of the electromagnetic coupler.

established equivalent circuit of a transformer can be used to describe the electromagnetic coupler with five characteristic transfer parameters: [1, 9, 16, 17]

- mutual coupling k
- primary inductance L_1
- secondary inductance L_2
- primary resistance R_1
- secondary resistance R_2

Fig. 2 illustrates that the physical connectedness of the transfer parameters can be described by

$$V_1 = j\omega L_1 I_1 + R_1 I_1 + j\omega M I_2 \tag{1}$$
$$V_2 = j\omega L_2 I_2 + R_2 I_2 + j\omega M I_1 \tag{2}$$

with angular frequency $\omega = 2\pi f$ and mutual inductance $M = k\sqrt{L_1 L_2}$. [9, 18]
The transfer parameters highly depend on the designed geometry of primary and secondary coil, on the electromagnetic properties of materials close to the coupler, and especially on the instantaneous relative position of the coils. The effect of translational misalignment has been widely investigated. [3, 19–22] In this paper, we focus on the investigation of the effect of rotatory misalignment on the transfer parameters.

B) Optimization Variable: Coupling Coefficient

The coupling coefficient is defined by the ratio of magnetic flux received in the secondary coil and magnetic flux generated in the primary coil. To ensure that the magnetic flux in the secondary coil is high enough to induce the defined voltage, the principle of electromagnetic resonance is used. Since the primary side is operated in resonance, a high amount of reactive power is resonating between the electric field of the capacitor and the

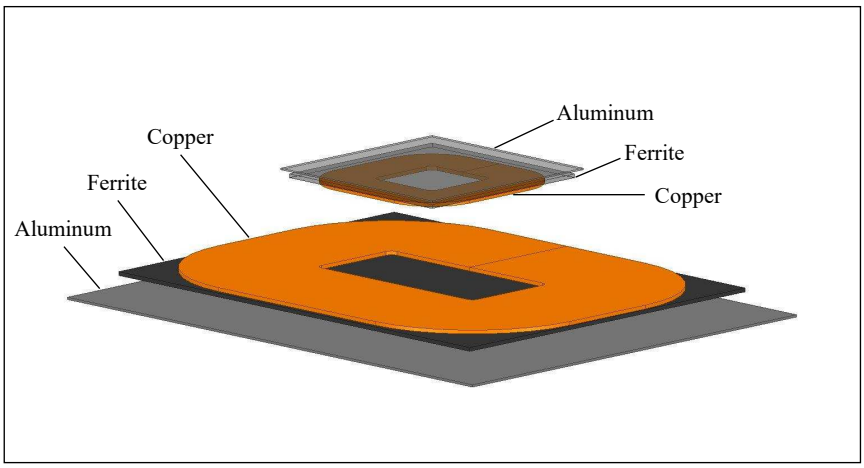

Figure 3: Simulation model of the electromagnetic coupler.

magnetic field of the inductor. This way, the induced secondary voltage is high enough to ensure power transfer, even if the coupling coefficient is low in loosely coupled systems. However, reactive power in real systems is always accompanied by power dissipation due to cable losses and eddy current losses. [23]
A high coupling coefficient on the other hand allows to minimize the reactive power in the system, thereby increasing the efficiency of power transfer. The development of an IPTS predominantly requires designing a coil system that offers high coupling coefficients in every allowed operating point with translational or rotatory coil offset. Thus, the coupling coefficient k is one of the most important optimization variables. This can also be seen in the equation for the optimum magnetic transformer efficiency

$$\eta_{\text{opt}} = \frac{\chi^2}{(1+\sqrt{1+\chi^2})^2}\,, \tag{3}$$

where the figure of merit $\chi = k\sqrt{Q_1 Q_2}$ comprises the coupling coefficient with the quality factors Q_1 and Q_2 of the primary and secondary coil [24].

III Method

There are two ways to get the transfer parameters of an electromagnetic coupler: measurement and simulation. In this paper, we choose simulation to be able to get the transfer parameters of the system in thousands of positions, for a more significant data set. The following sections explain the process of modelling and simulation.

A) Simulation with Finite Element Method (FEM)

A number of pertinent software applications is capable of calculating the required values by means of FEM. For this project *ANSYS Maxwell*, a high-performance software package that uses FEM to solve electromagnetic field problems, is chosen. By solving the Maxwell

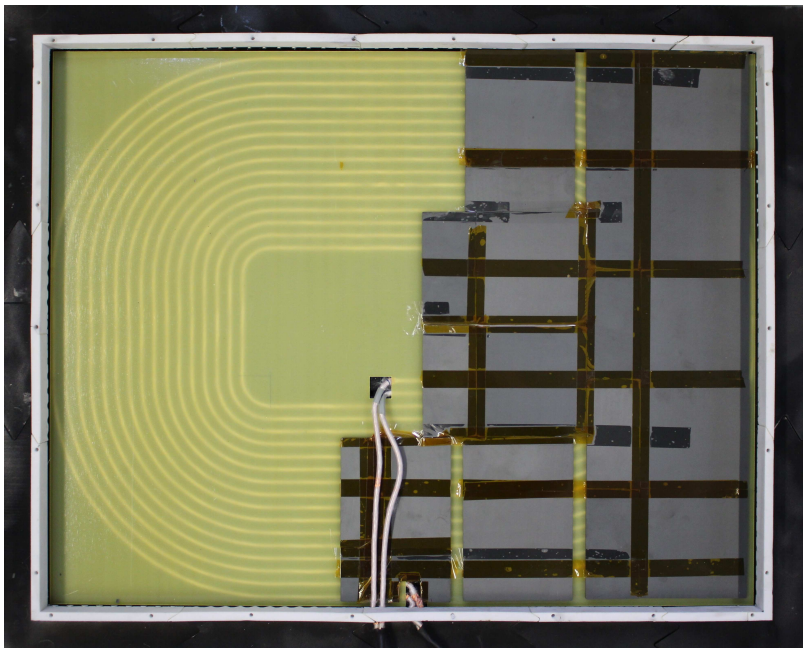

(a) Primary coil.

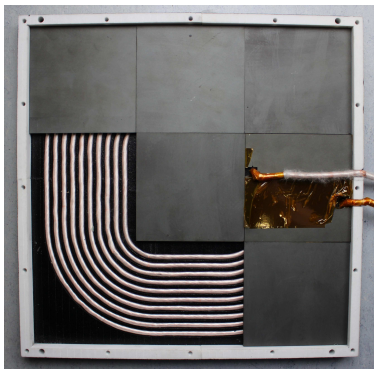

(b) Secondary coil.

Figure 4: Photograph of measuring object.

equations

$$\nabla \times \vec{E} = -\frac{\partial \vec{B}}{\partial t} \quad ; \quad \nabla \cdot \vec{D} = \rho \tag{4}$$

$$\nabla \times \vec{H} = \vec{J} + \frac{\partial \vec{D}}{\partial t} \quad ; \quad \nabla \cdot \vec{B} = 0 \tag{5}$$

in a finite region with boundary conditions, *ANSYS Maxwell* can obtain a unique solution of electromagnetic field problems of various kinds. The finite elements are defined as tetrahedrons and the field in each element is approximated with a quadratic polynomial of second order. All values are put together to one large, sparse matrix equation that is solved by applying the Sparse Gaussian Elimination. This way, the elementary transfer parameters k, L_1 and L_2 of diverse electromagnetic couplers can be calculated via simulation with high accuracy.

B) Modelling

In this paper we investigate the effect of rotation and tilt of the secondary module on the transfer parameters. Therefor we use the circular coil system that is proposed by the *Society of Automotive Engineers (SAE)* in its Information Report of standard *SAE J2954*. [25] The geometric modelling of the coil system can be restricted to materials that influence electromagnetic fields, so the created model only consists of aluminum, copper and ferrite. Additional material (i.e., plastic, air, filling material) is not significant for this investigation. To reduce complexity, two simplifications are made: the ferrite tiles are modelled as one solid ferrite plate, and the windings are approximated by one solid ring with homogeneous current density. The whole model can be seen in Fig. 3, illustrating two coils, two ferrite cores and two shielding plates.

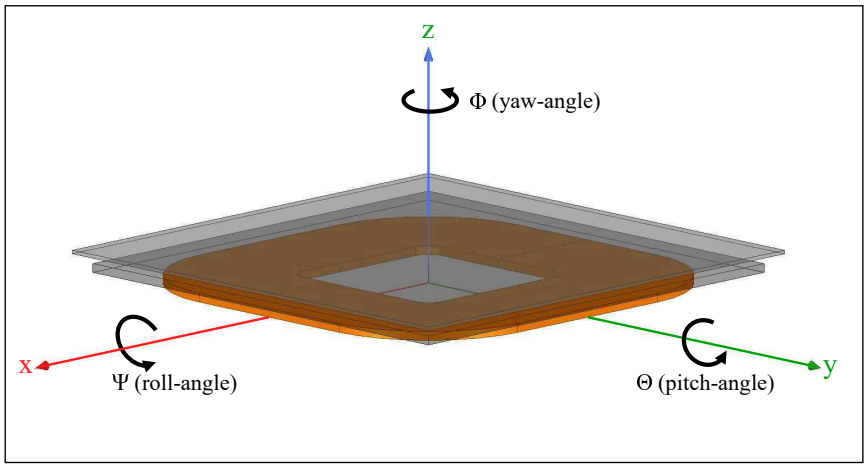

Figure 5: Three angles of rotation in relation to the secondary coil.

The transfer parameters of an electromagnetic coupler highly depend on the instantaneous relative position of the coils. The *SAE J2954* considers a mutual coil offset of $-75\ \text{mm} \leq x \leq 75\ \text{mm}$ in driving direction and $-100\ \text{mm} \leq y \leq 100\ \text{mm}$ in the transverse direction. For vertical displacement, it defines several z-classes specified by the respective ground clearances. The class z_1 is defined by a ground clearance range of $100\ \text{mm} \leq z_{\text{gc}} \leq 150\ \text{mm}$. Based on these data, the secondary coil is misaligned in x- and y-direction in the range of

$$-80\ \text{mm} \leq x \leq 80\ \text{mm} \tag{6}$$

$$-120\ \text{mm} \leq y \leq 120\ \text{mm} \tag{7}$$

with steps of 20 mm in both directions while the primary coil is fixed. The vertical distance of primary and secondary coil is set to a fixed coil-to-coil distance of $z_{\text{c2c}} = 75\ \text{mm}$, which corresponds roughly to the center of class z_1.

C) Measurements

A coil system has been built in accordance with the standard *SAE J2954* to verify the simulations and the modelling method. The coil system is able to transfer up to 3.6 kW over the lateral displacement range defined in equations (6) and (7). Fig. 4 shows pictures of the manufactured primary and secondary device.
For measuring the transfer parameters, low power measurements are conducted. A total of 7626 positions have been measured, equally distributed over the misalignment area depicted above. The coupling coefficient of every position is compared to the respective simulated value and the results show that the simulated coupling coefficient differs from the measured coupling coefficient only by 2.65 % in average. These results verify that the presented modelling method can be applied for further simulation and that the simulation results can serve as a verified base for drawing further conclusions.

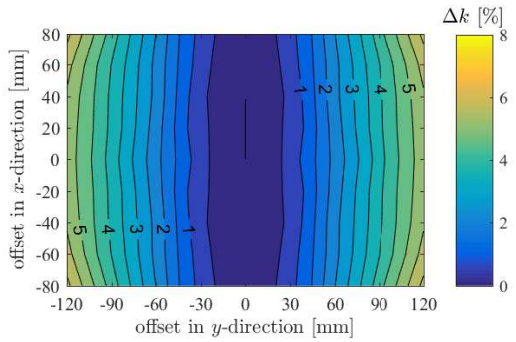

(a) Rotation in Ψ (around x-axis).

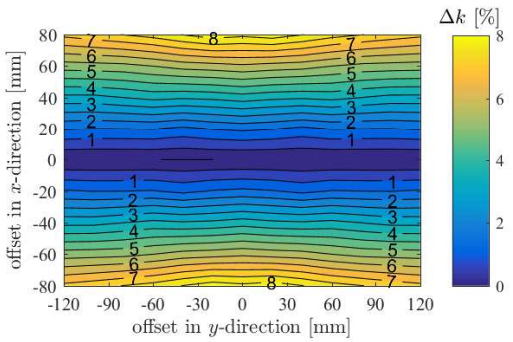

(b) Rotation in Θ (around y-axis).

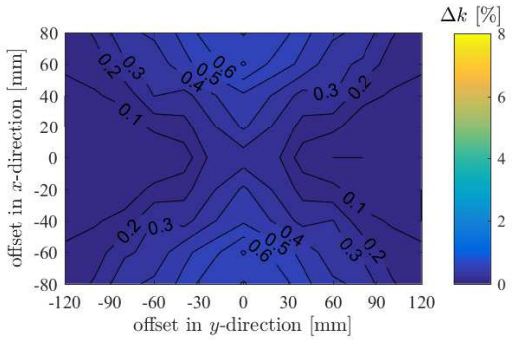

(c) Rotation in Φ (around z-axis).

Figure 6: Improvement of coupling coefficient Δk for mono-axial rotation.

D) Rotation and tilting of secondary coil

Apart from translational misalignment, the coil system can also have rotatory offset. To investigate the effect of rotatory offset, the secondary coil can be rotated in three axes: longitudinal x-axis (roll-angle: Ψ), lateral y-axis (pitch-angle: Θ) and vertical z-axis (yaw-angle: Φ). [25] Fig. 5 illustrates the three axes and the rotating direction. In this case, the origin of the coordinate system is set to the middle of the secondary coil, on the bottom of the copper.
To get a representative dataset, the coil system is simulated for

$$\begin{aligned} -6^\circ \leq \Psi \leq 6^\circ \\ -6^\circ \leq \Theta \leq 6^\circ \\ 0^\circ \leq \Phi \leq 90^\circ \end{aligned}$$

with steps of 2° in Ψ and Θ, and with steps of 15° in Φ. The range of $-90^\circ \leq \Phi < 0^\circ$ is redundant due to symmetries when the secondary coil is rotating. Summing up all translational and rotatory misalignments, the coil system is simulated in 40131 different positions.

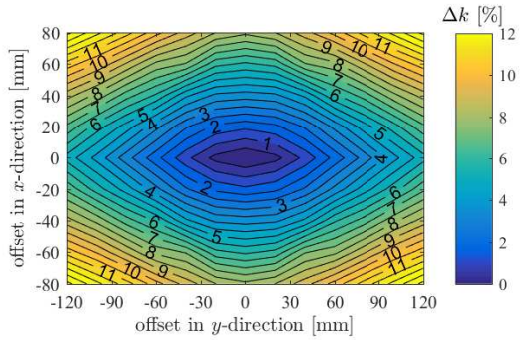

(a) Rotation in Ψ and Θ (around x,y-axes).

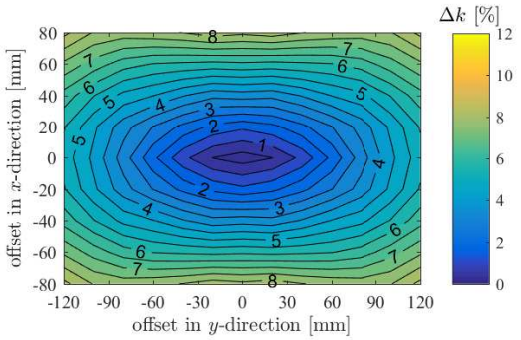

(b) Rotation in Θ and Φ (around y,z-axes).

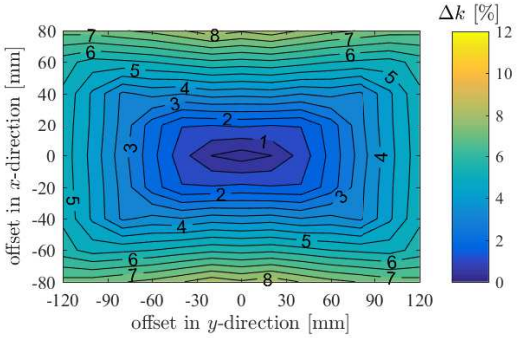

(c) Rotation in Ψ and Φ (around x,z-axes).

Figure 7: Improvement of coupling coefficient Δk for bi-axial rotation.

IV RESULTS AND DISCUSSION

Due to better visualization of differences that come along with rotation, the results are described as improvement potential Δk, which is defined as percentage change of the coupling coefficient with respect to the zero-rotation value. At each allowed offset position the secondary coil is rotated within its rotational range as stated in the previous section. First, the rotation along a single axis is studied to see the effects of each rotation direction individually. Then, results for combinations of different rotation directions are given.

A) Rotation around one axis

Fig. 6 shows the maximum possible improvement in the coupling coefficient that can be achieved at each position for rotation around one single axis. Fig. 6a illustrates that a rotation around the x-axis can improve the coupling coefficient up to $\Delta k_{\Psi}^{\max} = 6.1\,\%$. The mean value taken over all positions reveals an increase in coupling coefficient of $\overline{\Delta k_{\Psi}} = 2.5\,\%$. A rotation around the y-axis yields the highest improvement for mono-axial rotation. The maximum increase is given by $\Delta k_{\Theta}^{\max} = 8.3\,\%$ (see Fig. 6b). In addition to the highest improvement, it also achieves the highest mean value with an increase of $\overline{\Delta k_{\Psi}} = 3.7\,\%$. Fig. 6c shows that a single rotation around the z-axis can be neglected as it merely results in changes below one percent. The increase in coupling coefficient can be understood by consideration of the magnetic flux. The current inside the primary coil

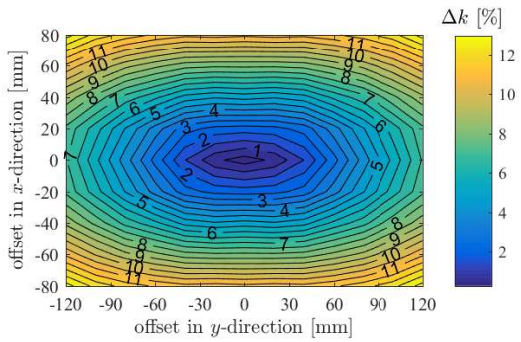

Figure 8: Improvement of coupling coefficient Δk for tri-axial rotation.

generates magnetic field lines, which have more horizontal components at higher offset from the origin. As only the field lines perpendicular to the receiving coil induce voltage, rotation can increase the coupling coefficient. The perpendicular flux through the receiving coil can be maximized at the outer positions in particular. The magnetic field in x-direction B_x increases with x-offset from the origin. Therefore, a rotation around the y-axis can increase the coupling coefficient. Analogously, at positions with y-offset the coupling coefficient can be maximized by rotating the secondary coil around the x-axis.

B) Rotation around two axes

The effect of rotating the receiving coil around two axes on the coupling coefficient of the system is depicted in Fig. 7. The benefits from mono-axial rotation can be combined to further exceed the improvements. Especially rotating around x- and y-axis can yield significant improvements. The highest improvement rates with $\Delta k_{\Psi\Theta}^{\max} = 13.2\,\%$ can be obtained for the outer offset positions. With offset in x- and y-direction, the magnetic field components B_x and B_y raise. These components can only be utilized to raise the induced voltage when the receiving coil is tilted in both directions. The mean value over the whole offset range of Fig. 7a calculates to $\overline{\Delta k_{\Psi\Theta}} = 6.1\,\%$. A combination with z-axis rotation (see 7b,c) severely influences the profile of the coupling coefficient x-offset for Ψ, Φ-rotation and y-offset for Θ, Φ-rotation, but cannot support to reach higher maximum values. Tab. 1 gives a comprehensive overview of the maximum and mean values for the different rotation angles, including the respective inductances. Note: when considering also $-90° \leq \Phi \leq 0°$ Fig. 7b and Fig. 7c become essentially identical.

C) Rotation around three axes

Fig. 8 illustrates the improvement of the coupling coefficient that can be achieved for a receiving coil with full rotational degree of freedom. Thereby, a maximum improvement of up to $\Delta k_{\Psi\Theta\Phi}^{\max} = 13.2\,\%$ can be achieved. The coupling coefficient can be increased at all positions. This is also represented in the mean value, which is raised to $\overline{\Delta k_{\Psi\Theta\Phi}} = 6.9\,\%$. For positions with high offset in x- and y-direction, the coupling coefficient can be raised with increasing yaw-angle until it reaches a maximum at $|\Phi| = 45°$. Therewith, Φ-rotation can improve the coupling coefficient with up to three percent.

Table 1: Overview of maximum change in transfer parameters.

rotation angle	$\Delta k^{\max}$	$\overline{\Delta k}$	$\Delta L_1^{\max}$	$\Delta L_2^{\max}$
Ψ	$6,1\%$	$2,5\%$	$1,5\%$	$0,3\%$
Θ	$8,3\%$	$3,7\%$	$1,2\%$	$0,3\%$
Φ	$0,7\%$	$0,3\%$	$0,7\%$	$0,2\%$
$\Psi + \Theta$	$13,2\%$	$6,1\%$	$2,6\%$	$0,5\%$
$\Theta + \Phi$	$8,6\%$	$4,5\%$	$1,9\%$	$0,4\%$
$\Psi + \Phi$	$8,3\%$	$4,9\%$	$1,8\%$	$0,3\%$
$\Psi + \Theta + \Phi$	$13,2\%$	$6,9\%$	$3,1\%$	$0,5\%$

D) Discussion

A summary of possible improvements of the coupling coefficient for different rotations in the studied offset range is given in Tab. 1. The highest percentage improvement can be realized when rotation around all axes is used. However, the results show that also the combined rotation around x- and y-axis is similarly potent. The study shows that the introduction of two new control parameters, roll-angle Ψ and pitch-angle Θ, can improve the coupling coefficient and therewith the system efficiency. High improvement rates of up to $13.2\,\%$ can be achieved in particular at the outer offset positions, where low coupling coefficients prevail. In Fig. 9 the absolute coupling values are compared. Fig. 9a shows the coupling coefficient values without rotation. In Fig. 9b the maximum coupling coefficient for all bi-axial rotations is depicted. It clearly shows that the absolute values are raised at all positions. In addition, it also shows that the position of the maximum values changes. Without rotation the maximum position is at $(x, y) = (0, \pm 60)\,\mathrm{mm}$ while the maximum position for the system with full rotational freedom shifts to $(x, y) = (0, \pm 80)\,\mathrm{mm}$. The control parameters for the new optimum are

$$\Psi = \pm 6^\circ \text{ and} \tag{8}$$

$$\Theta = 0^\circ\,. \tag{9}$$

Another advantage that comes with the introduction of the new control parameters Ψ and Θ is the extension of the working offset positions. The offset range is coupled to the lowest coupling coefficient, which is generally defined by maximum offset in all directions. The minimum of the coupling coefficient hence defines the possible offset range. Considering the *SAE J2954* offset range and vertical coil distance $z_{\mathrm{c2c}} = 75\,\mathrm{mm}$, the minimum coupling coefficient of the system without rotation is $k_{\min} = 19.2\,\%$ at $(x, y) = (\pm 75, \pm 100)\,\mathrm{mm}$. This offset range can be extended to $(x, y) = (\pm 90, \pm 120)\,\mathrm{mm}$ with the new control parameters. The applied angles of rotation are $\Psi = \Theta = \pm 6^\circ$. This way, the allowed offset range can be increased by $44\,\%$ while maintaining the functionality and same dimensions. Alternatively, this also allows to decrease the coil size while retaining the same functional offset range.
If it is not possible to set the rotation angles as control parameters but they come as random parameters, rotatory offset can also negatively affect k. In the worst case for the considered operating area the coupling coefficient even decreases up to $\Delta k^{\mathrm{wc}}_{\Psi\Theta\Phi} = -14.7\,\%$ at $(x, y) = (\pm 80, \pm 120)$. There, the coil is rotated by $\Psi = \Theta = \pm 6^\circ$ into the opposite

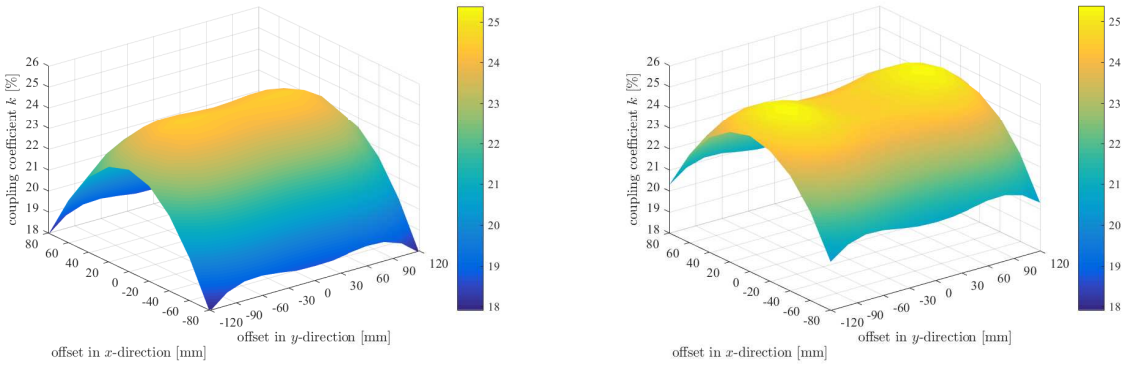

(a) Without rotation.

(b) With bi-axial rotation.

Figure 9: Comparison of absolute values of coupling coefficient k.

direction than for optimal improvement shown in the previous section. This rotation decreases the coupling coefficient, as the perpendicular flux through the receiving coil is reduced.

V CONCLUSION

In this study, we use FEM simulation to evaluate the effects of rotatory coil misalignment on transfer parameters of IPTS. The results show that the coupling coefficient can be increased with each rotation axis. Highest changes in coupling coefficient can be achieved for combination of all rotation axes. Rotation around x- and y-axis already achieves high improvements, whereas additional z-axis rotation further improves only slightly. This finding can be easily applied in EVs with air suspensions for stationary charging. The height of the air suspensions can be set individually to match the best coupling coefficient for efficient power transfer in this position. This way, two new control parameters can be utilized to extend the system performance.

REFERENCES

[1] Zahid, Z.; Dalala, Z.; Zheng, C.: Modeling and Control of Series-Series Compensated Inductive Power Transfer System. IEEE Journal of Emerging and Selected Topics in Power Electronics, **3** 1 (2014), 111-123.

[2] Raju, S.; Wu, R.; Chan, M.: Modeling of Mutual Coupling Between Planar Inductors in Wireless Power Applications. IEEE Trans. Power Electron., **29** 1 (2014), 481-490.

[3] Niedermeier, F.; Krammer, J.; Schmuelling, B.: A Linear Regression Based Method for Estimating Magnetic Parameters of Inductive Power Transfer Systems, IEEE PELS Workshop on Emerging Technologies: Wireless Power, Knoxville (USA), 2016.

[4] Imura, T.; Hori, Y.: Maximizing Air Gap and Efficiency of Magnetic Resonant

Coupling for Wireless Power Transfer Using Equivalent Circuit and Neumann Formula. IEEE Trans. Ind. Electron., **58** 10 (2011), 4746-4752.

[5] Kim, J.; Kong, S.; Kim, H.: Coil Design and Shielding Methods for a Magnetic Resonant Wireless Power Transfer System. Proc. of the IEEE, **101** 6 (2013), 1332-1342.

[6] Wu, H.; Gilchrist, A.; Sealy, K.: A High Efficiency 5kW Inductive Charger for EVs Using Dual Side Control. IEEE Trans. Ind. Inf., **8** 3 (2012), 585-595.

[7] Budhia, M.; Covic, G.; Boys, J.: Design and Optimization of Circular Magnetic Structures for Lumped Inductive Power Transfer Systems. IEEE Trans. Power Electron., **26** 11 (2011), 3096-3108.

[8] Covic, G.;Boys, J.: Inductive Power Transfer. Proc. of the IEEE, **101** 6 (2013), 1276-1289.

[9] Wang, C.; Stielau, O.; Covic, G.: Design Considerations for a Contactless Electric Vehicle Battery Charger. IEEE Trans. Ind. Electron., **52** 5 (2005), 1308-1314.

[10] Fotopoulou, K.; Flynn, B.: Wireless Power Transfer in Loosely Coupled Links. IEEE Trans. Magn., **47** 2 (2011), 416-430.

[11] Pinuela, M.; Yates, D.; Lucyszyn, S.; Mitcheson, P.: Maximizing DC-to-Load Efficiency for Inductive Power Transfer. IEEE Trans. Power Electron., **28** 5 (2013), 2437-2447.

[12] Sample, A.; Meyer, D.; Smith, J.: Analysis, Experimental Results, and Range Adaptation of Magnetically Coupled Resonators for Wireless Power Transfer. IEEE Trans. Ind. Electron., **58** 2 (2011), 544-554.

[13] Mur-Miranda, J.; Fanti, G.: Wireless Power Transfer Using Weakly Coupled Magnetostatic Resonators, IEEE Energy Conversion Congress and Exhibition (ECCE), Atlanta (USA), 2010.

[14] Mou, X.; Sun, H.: Wireless Power Transfer: Survey and Roadmap, IEEE Vehicular Technology Conference (VTC), Boston (USA), 2015.

[15] Niedermeier, F.; Hassler, M.; Krammer, J.; Schmuelling, B.: A Jacobi Based Method for Calculating the Steady State Characteristics of Non-Linear Circuit Elements, IEEE Vehicular Power and Propulsion Conference (VPPC), Belfort (France), 2017.

[16] Jiwariyavej, V.; Imura, T.; Hori, Y.: Coupling Coefficients Estimation of Wireless Power Transfer System via Magnetic Resonance Coupling Using Information from either Side of the System. IEEE Journal of Emerging and Selected Topics in Power Electronics, **3** 1 (2015), 191-200.

[17] Schuylenbergh, K.; Puers, R.: Inductive Powering - Basic Theory and Application to Biomedical Systems, Springer, 2009.

[18] Zhang, W.; Wong, S.; Tse, C.: Design for Efficiency Optimization and Voltage Controllability of SeriesSeries Compensated Inductive Power Transfer Systems. IEEE Trans. Power Electron., **29** 1 (2014), 191-200.

[19] Dang, Z.; Abu Qahouq, J.: Elimination method for the Transmission Efficiency Valley of Death in laterally misaligned wireless power transfer systems, IEEE Applied Power Electronics Conference (APEC), Charlotte (USA), 2015.

[20] Kurschner, D.; Rathge, C.; Jumar, U.: Design Methodology for High Efficient Inductive Power Transfer Systems With High Coil Positioning Flexibility. IEEE Trans. Ind. Electron., **60** 1 (2013), 372-381.

[21] Zhang, W.; White, J.; Abraham, A.; Mi, C.: Loosely Coupled Transformer Structure and Interoperability Study for EV Wireless Charging Systems. IEEE Trans. Power Electron., **30** 11 (2015), 6356-6367.

[22] Liu, F.; Yang, Y.; Jiang, D.; Ruan, X.; Chen, X.: Modeling and Optimization of Magnetically Coupled Resonant Wireless Power Transfer System With Varying Spatial Scales. IEEE Trans. Power Electron., **32** 4 (2017), 3240-3250.

[23] Abdolkhani, A.: Fundamentals of Inductively Coupled Wireless Power Transfer Systems, Coca, 2016.

[24] Vandevoorde, G.; Puers, R.: Wireless energy transfer for stand-alone systems. Sensors and Actuators A: Physical, **92** 1-3 (2001), 305-311.

[25] Wireless Power Transfer for Light-Duty Plug-In / Electric Vehicles and Alignment Methodology, SAE J2954 TIR, 2016.

Bibliographies

Florian Niedermeier received his B.Sc. in electrical engineering from the Technical University of Vienna, Austria, and his M.Sc. in electrical engineering from the Technical University of Munich, Germany. He is currently working on his Dr.-Ing. at University of Wuppertal, Germany, and works as research associate at BMW Group. His main research interests are simulation and analysis of inductive power transfer systems.

Marius Hassler received his B.Sc. and M.Sc. degree in physics with specialization in condensed matter from the Technical University of Munich, Germany. He is currently working toward the Dr.-Ing. degree in engineering with BMW Group, from the Technical University of Munich, Germany. His current research interests include circuit simulation and inductive charging.

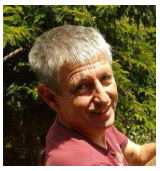

Josef Krammer received the Dipl.-Ing. degree in electrical engineering from the Department of Electrical and Computer Engineering at the Technical University of Munich, TUM, Germany. He worked as a researcher at the Institute of Circuit Theory and Signal Processing at the TUM where he received the degree of Dr.-Ing. Since 1991 he is working at BMW Group in different engineering positions for the development of electronics for conventional and electric vehicles.

Benedikt Schmuelling received the M.Sc. degree (Dipl.-Ing.) in electrical engineering from the Faculty of Electrical Engineering and Information Technology of Dortmund University, Germany, in 2005. From 2005 until 2010, he worked as a researcher at the Institute of Electrical Machines, RWTH Aachen University, Germany, where he also received his PhD in 2009. From 2010 until 2012 he was with Vahle Inc., Kamen, Germany, where he worked as an engineer on the development of wireless charging stations for electric vehicles. Since 2012 he is with the University of Wuppertal, Germany, where he is head of the Chair of Electric Mobility and Energy Storage Systems at the School of Electrical, Information and Media Engineering. His research fields include electric mobility, wireless power transfer, renewable energies, energy storage systems, and efficiency topics.

List of figures and tables

Impedance Measurement on Inductive Power Transfer Systems

Marius Hassler
BMW Group
80788 Munich, Germany
Marius.Hassler@bmw.de

Oguz Atasoy
WiTricity Corporation
MA 02472 Watertown, USA

Morris Kesler
WiTricity Corporation
MA 02472 Watertown, USA

Karl Twelker
WiTricity Corporation
MA 02472 Watertown, USA

Tobias Achatz
Zollner Elektronik AG
93499 Zandt, Germany

Markus Jetz
Zollner Elektronik AG
93499 Zandt, Germany

Josef Krammer
BMW Group
80788 Munich, Germany

***Abstract*—Inductive charging of electric vehicles requires that the vehicle and ground systems work together for power transfer from grid to the vehicle battery. In order to qualify if the vehicle system is compatible with the ground system, the presented impedance of the vehicle to the ground system can be used for characterization. However, there are no commercially available systems existing that are able to measure the impedance precisely while power transfer. For this reason, we developed a device that can be applied to characterize the presented impedance of vehicle systems. We will present first measurement results that were obtained with the device and discuss the main challenges in impedance measurements during power transfer.**

***Index Terms*—inductive power transfer, wireless charging, impedance measurement, interoperability, SAE J2954**

I. Introduction

Electric Vehicles (EVs) are on the rise. By 2025, 30% of all vehicle sales are projected to be electrified vehicles, including plug-in hybrids [1]. The increasing number of EVs will require more convenient charging than conventional plug-in charging. Wireless charging spares customers from the chore of connecting and disconnecting a charging cable—instead, charging begins automatically immediately after the vehicle is parked above a charging system. Customers who have a system at home will have no need to seek charging stations, as their regular needed range can be easily recharged overnight. This will make charging easier than refueling. And long distance travelers can recharge their vehicles at DC fast charging stations. In order to achieve that vision, it is essential that ground and vehicle system are compatible. The Society of Automotive Engineers (SAE) is elaborating a technical standard called "Wireless Power Transfer for Light-Duty Plug-In/ Electric Vehicles and Alignment Methodology" (J2954) [2]. They and [3] propose to use an impedance based interface to qualify if systems are compatible or not. The impedance can be retrieved either by simulation or by measurement. Simulation results can be achieved rather easily, but only account for variables and physical effects integrated into the simulation, whereas measurement shows you the reality. But measuring the impedance is rather difficult, especially with the prevailing close to 90° phase angle between voltage and current.

This research was partially funded by the Electric Power II program of the German Federal Ministry for Economic Affairs and Energy.

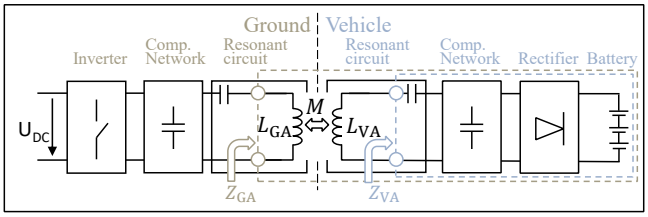

Fig. 1. Schematic setup of an inductive charging system.

Impedance measurements are usually performed for fuel cell or battery characterization, where the response of the system gives insights about the system state, called impedance spectroscopy [4]. In contrast to them, we do not want to use the impedance for insights of the system state, but to characterize the presented impedance of the vehicle inductive charging unit. The presented impedance is the combination of the primary coil inductance and the reflected vehicle system impedance. Based on it, we can judge whether the system can be operated. In general, the impedance is a function of the delivered power, the battery voltage, the operating frequency and the offset position. To our knowledge, there existed no other devices that are capable of measuring the impedance precisely at 85 kHz, 11 kW and phase angles close to 90°.

In this paper, we present a device for the impedance measurement of inductive charging systems that can be used for system characterization. We will present the first published impedance measurements of inductive charging systems during power transfer and give insight into the main measurement challenges. Further, we compare the measurement uncertainty of the direct voltage-current (UI) measurement with the proposed device. It is essential to reduce the measurement uncertainty as much as possible because the ground system must be designed to drive the full range of presented impedances

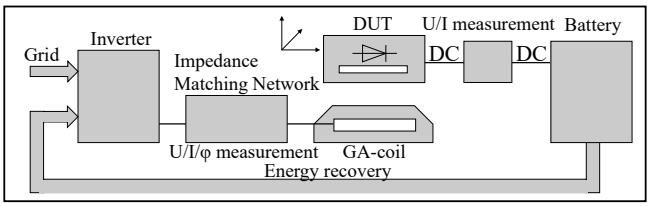

Fig. 2. Schematic impedance measurement setup.

including tolerances from measurement uncertainties.

II. Fundamentals

Inductive Power Transfer Systems (IPTS) rely on the principle of electromagnetic induction. An alternating magnetic field—produced by alternating current inside of the ground assembly coil—induces a voltage in the opposing coil, according to Faradays law of induction [5]. Therewith, energy can be transferred wireless over distances of tens of centimeters. The application of coils with high quality factors enables magnetic transfer efficiencies close to $100\,\%$. A basic setup is illustrated in Fig. 1.

The Ground Assembly (GA), comprises of a Power Factor Correction (PFC) stage (not shown in Fig. 1), an inverter, a compensation network and a resonant circuit that is connected with the primary coil, referred to as the GA coil. The counterpart is the Vehicle Assembly (VA), which includes the resonant circuit, consisting of a capacitor and the secondary coil, referred to as the VA coil, a compensation network, a rectifier with filters and connection to the EV's battery.

The positioning of magnetically active coil components, as ferrite, copper and the shielding material, determine the magnetic behavior of the GA and VA coil. The electric parameters describing the magnetic behavior, $L_{\mathrm{GA}}, L_{\mathrm{VA}}$ and M, are offset dependent and can either be acquired by measurement or simulation. In this paper offset denotes a three dimensional displacement (x, y, z) between GA coil center and VA coil center position. For clarity, we use the short forms $L_{\mathrm{GA}}, L_{\mathrm{VA}}$ and M instead of the detailed notation $L_{\mathrm{GA}}(x, y, z), L_{\mathrm{VA}}(x, y, z)$ and $M(x, y, z)$ indicating the offset dependency. The mutual inductance can be calculated by applying the coupling coefficient in the relation

$$M = k\sqrt{L_{\mathrm{GA}} L_{\mathrm{VA}}}\,, \tag{1}$$

as described by [6].

For all VA designs, behaviors of the VA electronics across battery voltages, differing power levels and frequencies, the VA impedance can be represented with Z_{VA}. The impedance Z_{GA}, defined at the GA coil terminals, incorporates the magnetic behavior of both coils. This can be seen in the equation for the GA impedance

$$Z_{\mathrm{GA}} = \mathrm{i}\omega L_{\mathrm{GA}} + \frac{\omega^2 M^2}{\mathrm{i}\omega L_{\mathrm{VA}} + Z_{\mathrm{VA}}}\,, \tag{2}$$

with the angular frequency ω. Hence, the complex impedance summarizes the electric and the magnetic behavior of the system in a single quantity. If the GA electronics can drive the presented impedance Z_{GA}, the requested power can be provided to the EV's battery. This motivates the use of impedance as a qualification metric for IPTS systems.

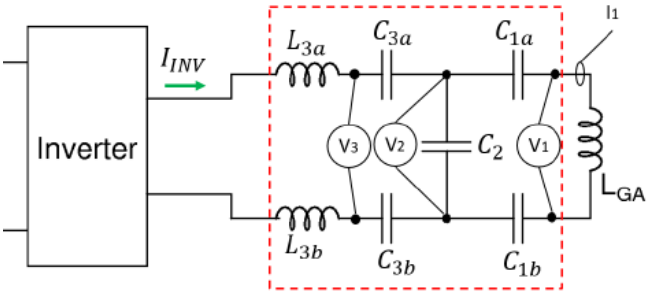

Fig. 3. IMN schematics with three voltage and one current measurement position.

TABLE I
Capacitor Values for Impedance Measurement Setup.

Capacitor	Capacitance [nF]
C_1	267.33
C_2	270.80
C_3	270.20

III. Measurement Setup

In [3], the authors also propose a measurement setup for product VA testing. Based on their proposal, the main components of our setup are shown in Figure 2. The measurement system is required to characterize a wide range of possible product VAs by means of their presented impedance at the GA coil terminals. For this experiment we employed a specialized laboratory inverter which can support a wide range of inductive loads. Although it is possible to measure the impedance directly by the UI-method, the close to $90°$ phase angle makes an accurate measurement nearly impossible. Small differences in phase have a large impact on the impedance calculation due to the behavior of the cosine function. E.g. a phase error of $\pm 1°$ at $85°$ impacts the cosine outcome by $150\,\%$ even though the relative error in the phase measurement is only $\sim 1\,\%$. A special measurement setup was designed to make precise measurements possible. Further, the measurement system supports a wide variety of different VA systems at different positions and different power levels, which makes the impedance matching network design more challenging.

The impedance matching network (IMN) is illustrated in Figure 3. The capacitors are arranged in a hybrid series-parallel resonator structure both to reduce the phase angle and to maximize the support range of presented impedances due to different power levels, positions, and VA systems. The capacitance values listed in Table I were

measured using an LCR meter with all inductors disconnected.

The device under test (DUT) can be integrated into a movable test bench robot, which ensures high precision in positioning and reproducibility. Its DC output is connected with a variable DC load to maintain a set battery voltage. Its internal energy feedback loop reuses the incoming energy to feed the DC source for energy conservation.

IV. Measurement Considerations

The measurements at the indicated positions of the passive impedance matching network (IMN) in Figure 3, can be used to calculate the impedance at the interface Z_{GA} in several ways. The measurement of voltage U_1, current I_1 and their phase difference $\varphi_{U_1 I_1}$ is the most direct way to calculate the impedance Z_{GA}. In order to evaluate this method, its uncertainty is derived for the exemplary parameter values and the estimated uncertainties given in Table II. The uncertainty for a single measurement is calculated by means of Gaussian error propagation for different phase values. Figure 4 shows the uncertainties $\Delta\,\mathrm{Re}(Z_{\mathrm{GA}}(U_1, I_1))$ and $\Delta\,\mathrm{Im}(Z_{\mathrm{GA}}(U_1, I_1))$. It can be seen that the uncertainty for the real part of the impedance is increasing with the phase angle up to $90°$ due to the cosine behavior, whereas the uncertainty of the imaginary part is decreasing due to its sine behavior. The main contribution to the error comes from the phase measurement. This also holds true when the phase uncertainty $\Delta\varphi_{U_1 I_1}$ would be reduced to 1%. To reduce the error resulting from cosine's natural behavior near $90°$ phase measurements, the phase needs to be reduced so that differences in phase contribute less. For this reason, the IMN has several voltage measurement positions with lower phase values. The measurands and the known capacitor values permit to calculate the impedance Z_{GA} in several ways:

$$Z_{\mathrm{GA}}(U_1, I_1) = \frac{U_1}{I_1} \mathrm{e}^{\mathrm{i}\varphi_{U_1 I_1}}\,, \tag{3}$$

$$Z_{\mathrm{GA}}(U_2, I_1) = \frac{U_2}{I_1} \mathrm{e}^{\mathrm{i}\varphi_{U_2 I_1}} - Z_{C_1}\,, \tag{4}$$

$$Z_{\mathrm{GA}}(U_1, U_2) = \frac{U_1}{U_2 \cdot \mathrm{e}^{\mathrm{i}\varphi_{U_1 U_2}} - U_1} Z_{C_1}\,, \tag{5}$$

$$Z_{\mathrm{GA}}(U_1, U_3) = \frac{-U_1 \alpha}{U_1 (Z_{C_2} + Z_{C_3}) - U_3 \cdot \mathrm{e}^{-\mathrm{i}\varphi_{U_1 U_3}} Z_{C_2}}\,, \tag{6}$$

$$Z_{\mathrm{GA}}(U_2, U_3) = \frac{-U_2 \alpha + U_3 \cdot \mathrm{e}^{-\varphi_{U_2 U_3}} Z_{C_1} Z_{C_2}}{U_2 (Z_{C_2} + Z_{C_3}) - U_3 \cdot \mathrm{e}^{-\mathrm{i}\varphi_{U_2 U_3}} Z_{C_2}}\,, \tag{7}$$

with $\alpha = Z_{C_1} Z_{C_2} + Z_{C_1} Z_{C_3} + Z_{C_2} Z_{C_3}$ and $Z_{C_i} = (\mathrm{i}\omega C_i)^{-1}$.

The error in impedance can be evaluated by comparing the calculated uncertainties of these impedance equations. The uncertainties are depicted in Fig. 5 for the parameter values from Table II. It can be seen that the proposed methods are clearly superior to the direct measurement. The respective phases are varied in the interval of $0° \leq \varphi \leq 90°$. However, the actual phase ranges depend on the to be measured setup and operation points and presented impedances. The uncertainty values also change with different parameter values. The method with lowest uncertainty could vary depending on the actual setup and parameters. The circular markers indicate the observed phase ranges from the measurements.

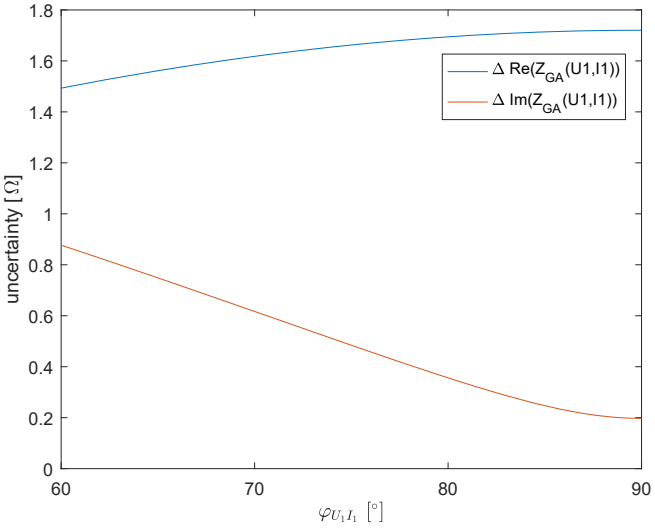

Fig. 4. Uncertainty in impedance measurement for different $\varphi_{U_1 I_1}$ phase values and absolute value $|Z_{\mathrm{GA}}(U_1, I_1)| = 19.713\,[\Omega]$.

TABLE II
Parameter Values for Uncertainty Calculation.

U_1 [V]	U_2 [V]	U_3 [V]	I_1 [A]	ΔU [%]	ΔI [%]	$\Delta\varphi$ [°]
1396.74	464.33	569.24	70.85	2	3	5

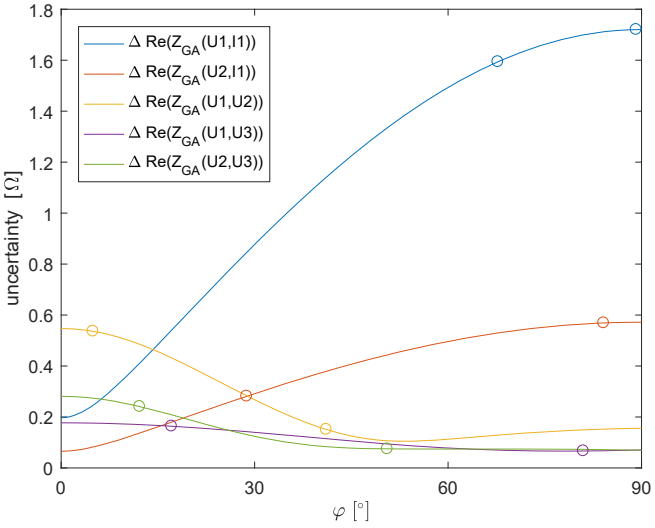

Fig. 5. Uncertainty in $\mathrm{Re}(Z_{\mathrm{GA}})$ measurements for different phase values.

The impedance measurements were performed with the WPT3 Z2 VA from [2] as DUT. Here, WPT3 delineates the power class of up to $11\,\mathrm{kW}$ and Z2 the height class in z-direction indicating compatibility within $14-21\,\mathrm{cm}$ offset. The electric circuit of the VA can be seen in Figure 6. The rectifier was designed to compensate for different battery voltages. Thus the impedance changes only very little with different

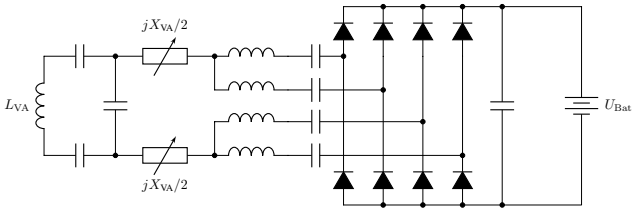

Fig. 6. VA schematics.

battery voltages. For this reason, we measured the battery voltages $U_{\mathrm{bat}} = \{280, 320, 380, 420\}\,\mathrm{V}$. The voltages were varied for each power level $P_{\mathrm{in}} = \{3.7, 7.7, 11\}\,\mathrm{kW}$. This procedure is repeated for each of the offset positions

$$(x, y) = (0, 0), (0, 100), (75, 0), (75, 100)\,[\mathrm{mm}], \tag{8}$$

at minimum and maximum z-height.

V. Results

First, we will present a single measurement result from the raw data for a single presented impedance of the different calculation approaches with their uncertainties. The deviation from the ideal measurement result will be discussed and a correction factor presented. After that the complete set of data across a range of VA positions, battery voltages, and power levels will be presented. We will then compare the required GA impedance zone with tolerance for the new method and for the direct UI-method.

In addition to the presented impedance equations, it is also possible to establish the phase values using the measured power delivered along with the voltage and current into the GA coil. The expressions for the phase differences can be derived from equating the real part of the given impedance equations to the ratio of expected real power and current. For brevity, we omit their derivations. The measured phases can be substituted by

$$\varphi_{U_1 I_1,\mathrm{s}} = \cos^{-1} \frac{\eta P_{\mathrm{out}}}{U_1 I_1}\,, \tag{9}$$

$$\varphi_{U_2 I_1,\mathrm{s}} = \cos^{-1} \frac{\eta P_{\mathrm{out}}}{U_2 I_1}\,, \tag{10}$$

$$\varphi_{U_1 U_2,\mathrm{s}} = 2\tan^{-1} \frac{\sqrt{X_{C_1}^2 + \beta^2 - \gamma^2} + X_{C_1}}{\beta + \gamma}\,, \tag{11}$$

where

$$\beta = 2\frac{\eta P_{\mathrm{out}}}{I_1^2}\,,\ \gamma = \frac{\beta(U_1^2 + U_2^2)}{2U_1 U_2}\,, \tag{12}$$

and η is the estimated or measured efficiency from the GA-interface to the battery. Figure 7 shows the different approaches to calculate the impedance Z_{GA} in a single measurement for the obtained parameter values: U_1, U_2, U_3, I_1 their respective phases and P_{out}, the output power at the battery. A perfect set of measurements would make them cluster on the exact same spot. However, real measurements include uncertainties, and the largest source of uncertainty in the impedance measurement is the measurement of phase

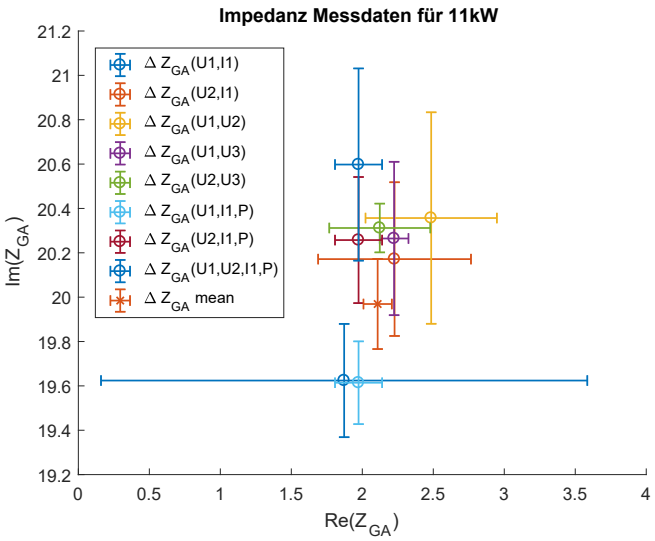

Fig. 7. Calculated impedances from a single measurement with their estimated uncertainties.

differences. It can be seen that the calculated impedances for $\Delta Z_{\mathrm{GA}}(U_1, U_2)$, $\Delta Z_{\mathrm{GA}}(U_1, U_3)$, $\Delta Z_{\mathrm{GA}}(U_2, U_3)$ differ, despite being measured using the same high differential voltage probes. This could be due to systematic errors of the voltage probes or to deskew errors of the oscilloscope channels. Besides the phase errors, the result suggests an additional systematic error in the current, which may be lower than measured. The current dependent impedance values show too small real parts and both U_1, I_1 dependent impedances have a too low imaginary part. We came to the conclusion that the current measurements were systematically high because the voltage probes were calibrated at $85\,\mathrm{kHz}$.

To compensate for the systematic errors, we apply an error calculation, in form of $a \cdot x$ for each measurand and in form of $x \pm b$ for the phases. Using this method, constant offsets can be canceled out. To not corrupt the data, we only allow small correction factors and and fit the correction factors across a large number of experiments. We assume that with a large number of measurements over different positions, power levels and battery voltages, statistical errors will average out and the correction factors can eliminate the systematic errors. The allowed correction factors are within the same range as the respective uncertainties. The a term is limited within 2% for voltage and capacitance, and $3\,\%$ for current values. The constant offset factor b has a $5°$ boundary for the voltage to current phase and a $3°$ boundary for the voltage to voltage phase.

The fit yields the correction factors given in Table III.

The resulting impedances are presented in Figure 8, with the differences between measurements reduced significantly. The different impedance values can be combined into a single

TABLE III
CORRECTION PARAMETERS.

a_{C_1}	a_{C_2}	a_{C_3}	a_{U_1}	a_{U_2}	a_{U_3}
0.980	0.993	1.007	0.990	0.980	0.991

a_{I_1}	$b_{\varphi_{U_1I_1}}$ [°]	$b_{\varphi_{U_2I_1}}$ [°]	$b_{\varphi_{U_1U_2}}$ [°]	$b_{\varphi_{U_1U_3}}$ [°]	$b_{\varphi_{U_2U_3}}$ [°]
0.970	1.102	-0.688	-1.788	-1.742	0.040

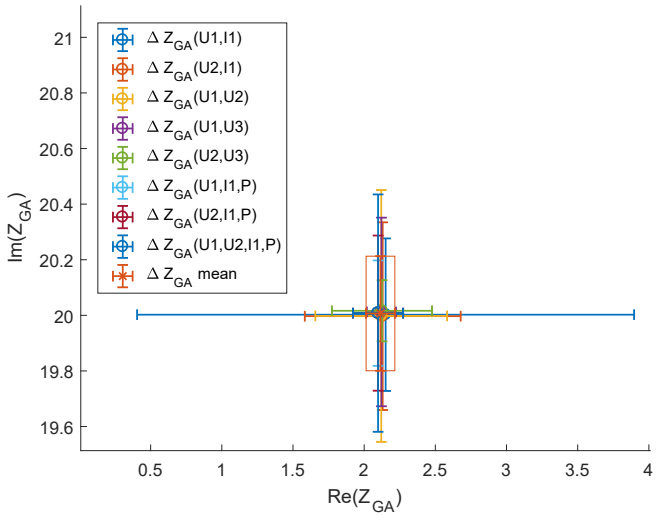

Fig. 8. Calculated impedances from a single measurement with applied correction factor.

result, by means of a weighted mean function

$$Z_{\mathrm{GA}_{\mathrm{mean}}} = \frac{\sum_{i=1}^{N} g_i \cdot Z_{\mathrm{GA},i}}{\sum_{i=1}^{N} g_i}, \tag{13}$$

where each function is weighted with its uncertainty $g_i = (\Delta Z_{\mathrm{GA},i})^{-2}$ after the Gaussian error propagation [7]. Therewith the influences of the shared measurands are accounted for. Note, this is not the same as treating it as a results from eight individual measurements.

The result in Figure 8 can be written as

$$Z_{\mathrm{GA}_{\mathrm{mean}}} = 2.115 \pm 0.101 + 20.007\mathrm{i} \pm 0.206\mathrm{i}\,\Omega, \tag{14}$$

and has a real part uncertainty which is approximately 17 times smaller than the direct UI-method has. Based on the data distribution, we judge the uncertainty in the real part well estimated. However, the uncertainty in the imaginary part looks a little overestimated after correcting for constant offsets. The correction parameters in Table III also indicate that the uncertainty in the phase measurements was initially overestimated.

Figure 9 shows the measured impedances for the different operation points. The mean uncertainties of the weighted mean impedance are incorporated in the red envelope, stating the GA electronic requirements. By taking into account the tuneable matching network on the VA side in Figure 6, the required

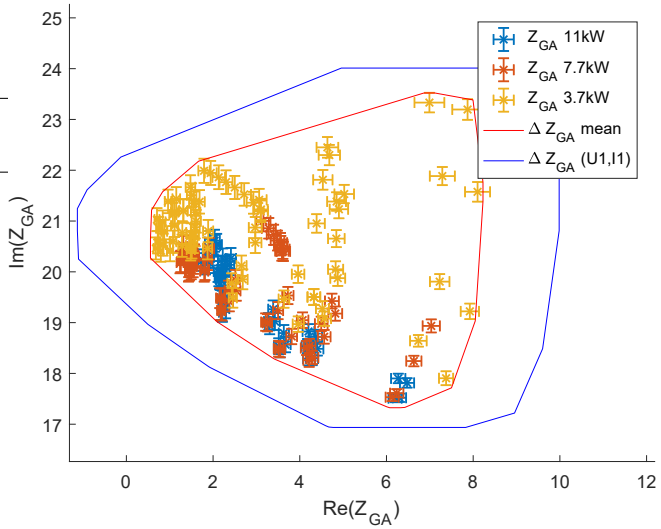

Fig. 9. Measured impedances for different power levels P_{in}, different battery voltages U_{bat} and offset positions (x, y, z) with required uncertainty tolerances for the UI-method $\Delta Z_{\mathrm{GA}}(U_1, I_1)$ (blue) and the proposed method ΔZ_{GA} mean (red).

GA space is smaller than shown in Figure 9, but this is not the scope of this work. Before this new measurement device was developed, the additional margin needed to account for unknown presented impedances is indicated with the blue envelope. Of course, the negative impedance region is meaningless, the lower limit is given from system point of view by the maximum coil current with the current probe tolerance. Table IV states the obtained uncertainties.

TABLE IV
UNCERTAINTY RESULTS.

	$\Delta\,\mathrm{Re}(Z_{\mathrm{GA}})$ [Ω]	$\Delta\,\mathrm{Im}(Z_{\mathrm{GA}})$ [Ω]
min	0.053	0.078
max	0.352	0.238
mean	0.125	0.189

VI. DISCUSSION AND OUTLOOK

Measurements with the presented setup yield astonishing results that exceed the uncertainty of the direct UI-method by high factors. The mean of $\mathrm{Re}(Z_{\mathrm{GA}})$ exhibits a 16 times lower uncertainty when measured and calculated with the presented methods. Although this system can make very precise measurements, it depends on careful calibration of the probes and measurement of circuit components. We tried to correct for systematic errors by applying correction factors within the uncertainty ranges that do not corrupt the data. A calibration tool with a well-known impedance could be the best solution to measure and correct for these systematic errors. We suggest a very simple VA, with precisely known components that has an AC resistor instead of a rectifier. The device positioning would be crucial and would need to be identical to where its magnetic

parameters were measured. Since the error in the real part of impedance of such a device depends on k^2, the positioning of the device would need to be very precise. Ideally, the coupling and inductance values would have little uncertainty over the positional tolerance of the device. An analogous error estimation yields a real part uncertainty of $0.09\,\Omega$ for $\Delta L_{\mathrm{GA}}, \Delta L_{\mathrm{VA}}, \Delta M$ and ΔZ_{VA} equal $0.5\,\%$ uncertainty.
For completeness, statistical error contributions are one order of magnitude smaller and are therefore neglected. In addition they can be further reduced by simply increasing the number of measurements, which is no problem at $85\,\mathrm{kHz}$.

VII. Conclusion

We proposed an innovative device and methodology to measure the presented VA impedances at high power. This device was designed to account for large measurement uncertainties resulting from impedance measurements with phases near $90°$. We presented the results from this system and performed error propagation that can be applied for result comparison. The comparison reveals that the proposed method to calculate the impedance improves upon the known direct UI-method by factors varying between 6 to 34 depending on the measurement parameters. With this new method the derived results are 16 times better than direct measurement. Decreasing the current measurement uncertainty by the use of wideband current transformer will improve the measurement result significantly. Further, the results show that an impedance measurement can be applied for characterizing the vehicle system. Thus, this system is suitable for qualifying VA designs, testing interoperability criteria as well as quality assurance testing of product VAs.

References

[1] "Driving into 2025: The Future of Electric Vehicles," *J.P. Morgan*, [Online]. Available: https://www.jpmorgan.com/global/research/electric-vehicles. [Accessed 24-January-2019].

[2] SAE Standard, "Wireless Power Transfer for Light-Duty Plug-In/ Electric Vehicles and Alignment Methodology," *SAE J2954 RP*, 2017.

[3] M. Hassler, F. Niedermeier, J. Krammer and K. Diepold, "A Method for Interoperable Interface Description of Inductive Power Transfer Systems," *2018 IEEE PELS Workshop on Emerging Technologies: Wireless Power Transfer (Wow)*, IEEE, 2018.

[4] E. Barsoukov and J.R. Macdonald, *Impedance spectroscopy: theory, experiment, and applications*, John Wiley & Sons, 2018.

[5] M. Faraday, *Experimental researches in electricity*, Read Books Ltd, 2016.

[6] P. Steffen, P. Reinhold, *Grundlagen der Elektrotechnik und Elektronik 2*, Springer Berlin Heidelberg, 2012.

[7] H. Holland, K. Scharnbacher, *Grundlagen der Statistik*, Gabler, 2003.

A Comparison on Simulated, Analytic and Measured Impedance Values for an Inductive Power Transfer System

Marius Hassler[1,3], Oguz Atasoy[2], Karl Twelker[2], Morris Kesler[2], Johannes Birkendahl[3], Josef Krammer[1]

[1]BMW Group, 80788 Munich, Germany

[2]WiTricity Corporation, MA 02472 Watertown, USA

[3]Technical University of Munich, Arcisstr. 21, 80333 Munich, Germany

Studies on Inductive Power Transfer (IPT) systems are most times either theoretical or experimental. In this paper, we want to bring theoretical models and experimental data together using the impedance based interface proposed in SAE J2954 [1]. This proposal characterizes the IPT system by impedances at both coil terminals. We show how the experimental data was retrieved at the interface and use it to validate an analytical model and a Simulink model described within this study. Such models can support the design and development process and therefore a comparison with reality is necessary.

Corresponding author: Marius Hassler; email: marius.hassler@bmw.de; phone: +49 151 601 56071

I INTRODUCTION

Recently, German car manufacturer Daimler, Porsche and VW announced that the fleet share of electrified vehicles is projected to be 50% in 2030 [2–4]. With every second car becoming electric, the rising number of electric vehicle (EV) users will ask for a more convenient way of charging than conventional wired charging, which requires them to plug in regularly. The chore of handling the charging cable, connecting to - and disconnecting from - the socket can be spared by wireless charging. A comfort charging solution that starts automatically when a vehicle is parked above a charging system to recharge the EV battery. The automatic recharging with a 11 kW system can reestablish around 440 km of range when charging for 8 hours during work or over night, assuming an EV driving consumption rate of 20 kWh per 100 km, covering the majority of regularly needed user ranges [5]. In order that customers with EVs from different OEMs can use the same infrastructure to recharge their vehicles, the SAE is elaborating a technical standard called "Wireless Power Transfer for Light-Duty Plug-In/ Electric Vehicles and Alignment Methodology" (J2954) [1]. The standard and [6] proposed to use an impedance based interface to characterize the system behavior due to the interdependency of vehicle assembly (VA) and ground assembly (GA) coils. Yet, there existed no measurement device that is capable to measure the impedance with acceptable precision. For this

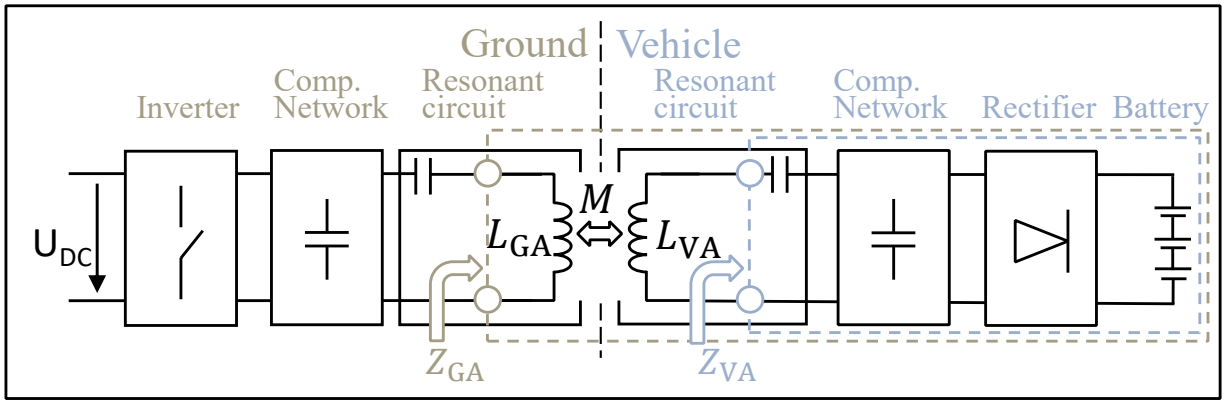

Figure 1: Block diagram of an inductive charging system [6].

reason, [7] developed a methodology consisting of current and voltage measurements in an impedance matching network and a calculation theory that make the precise impedance measurement during power transfer possible. Their results show impedance uncertainties reduced by factor $6 - 34$ from above $1\,\Omega$ to around $0.1\,\Omega$ in average, depending on the measurement parameters.
With real impedance measurement data available, the possibility to validate simulation models arose and provide an answer to the question "Do measurement and simulation agree?"
In this paper, we present an analytic model and a *Simulink* model. Both models will be compared with each other and with the measured impedance values. Such models can be applied to support the design and development of interoperable inductive charging systems. However, validation and comparison of a model with the reality is essential for further improvements. It is also an important step towards virtual validation of interoperability of inductive power transfer systems. In the paper, we'll also present how an impedance measurement can be integrated in a *Simulink* simulation and what a control loop may look like.

II Method

This section introduces two different simulation models, an analytical and a *Simulink* model, which will be compared within this study. The simulation models are used to simulate the impedance at the VA interface that is defined at the VA coil terminals as illustrated in Fig. 1. The electric parameters of the electromagnetic coupler L_{GA}, L_{VA} and M will be measured in the experimental setup by a Vector Network Analyzer (VNA) to achieve high precision [8–10]. Of course, these parameters could also be calculated by means of FEM simulation, but this would require many iterative steps to adapt the simulation model until it represents the real system with adequate agreement [11, 12]. The measurement is performed for each offset position, where offset denotes a vertical and horizontal displacement (x, y, z) between VA coil and GA coil centers. The relevant impedance at the GA interface Z_{GA} for VA characterization is then calculated with the obtained data from the simulation model (Z_{VA}) and the data from the VNA-measurement

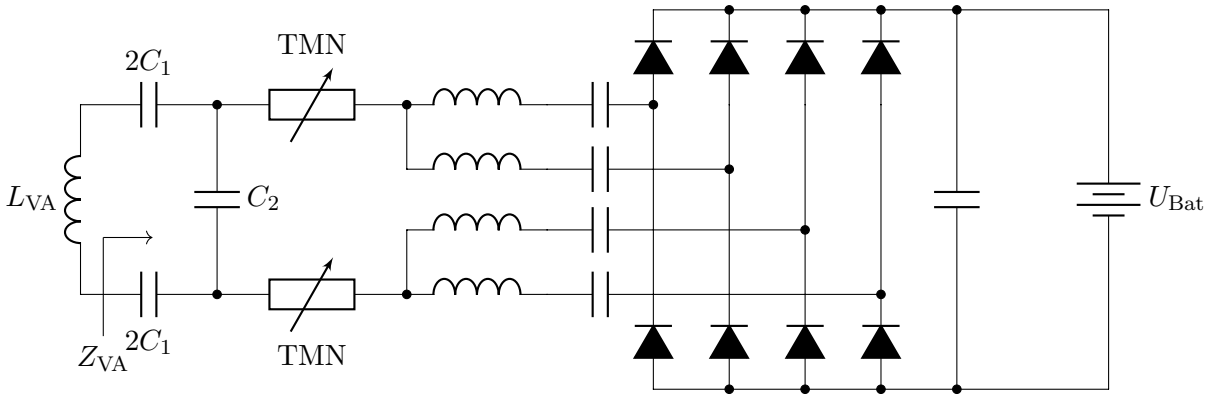

Figure 2: Example of a VA circuit from SAE J2954 [1].

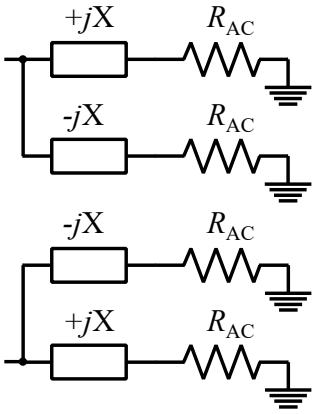

Figure 3: Equivalent circuit model of Fig 2 rectifier for analytic calculations.

using

$$Z_{\mathrm{GA}} = R_{\mathrm{GA}} + \mathrm{j}\omega L_{\mathrm{GA}} + \frac{\omega^2 M^2}{R_{\mathrm{VA}} + \mathrm{j}\omega L_{\mathrm{VA}} + Z_{\mathrm{VA}}}\,, \tag{1}$$

where ω is the angular frequency. R_{GA} and R_{VA} are the coil resistances. These resistances can be difficult to measure directly but can be determined from the quality factors of the coils using $R_{\mathrm{xA}} = \omega L_{x\mathrm{A}}/Q_{x\mathrm{A}}$. The quality factor is a function of relative coil position, and was not measured at all positions, so for this work we assume $Q_{x\mathrm{A}} = 400$.

A) Analytic Model

For a first approximation of the VA impedance of the circuit shown in 2, we use a simple analytic model that implements the functionality of the circuit and neglects any nonlinear behavior and phase changes. We assume the rectifier input current $I_{\mathrm{rect}}^{\mathrm{in}}$ in each branch to be sinusoidal and the rectified current I_{Bat} to be constant. Using the average of the rectified sine waves in the parallel branches, we can write

$$I_{\mathrm{Bat}} = \frac{4}{\pi} I_{\mathrm{rect}}^{\mathrm{in}}\,, \tag{2}$$

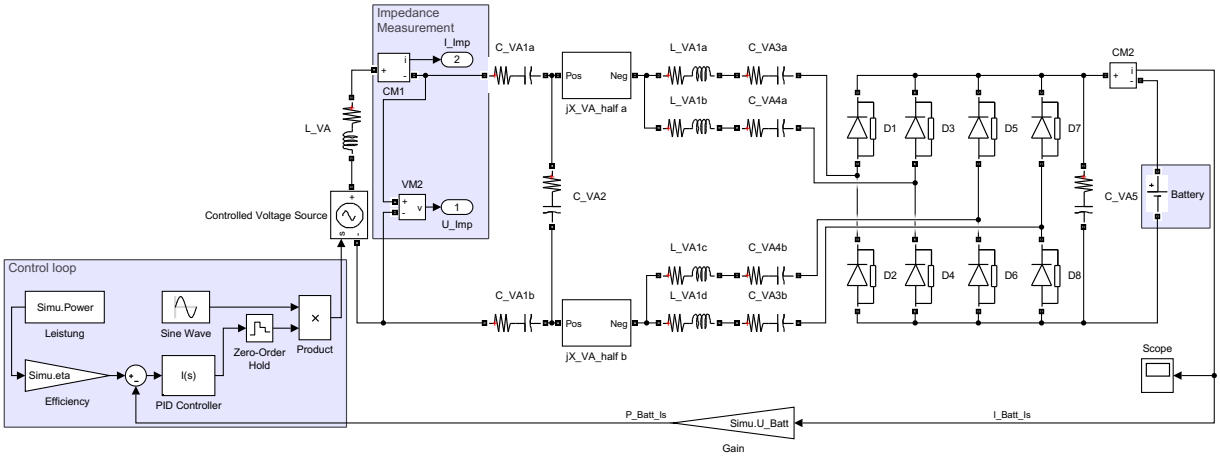

Figure 4: Simulink simulation model.

and introduce the simplified equivalent circuit model presented in Fig. 3, where X comprises the rectifier input filter inductance and capacitance.
The AC equivalent load resistance in each branch can be mathematically described using the Steigerwald approximation [13]

$$R_{\mathrm{AC}} = \frac{8}{\pi^2} \frac{U_{\mathrm{Bat}}^2}{P_{\mathrm{out}}} \,. \tag{3}$$

Subsequent, the rectifier input impedance can be summarized to

$$Z_{\mathrm{rect}} = \frac{X^2 + R_{\mathrm{AC}}^2}{R_{\mathrm{AC}}} \,, \tag{4}$$

a purely real impedance whose imaginary part cancels out.
The impedance at the VA coil terminals can be derived to

$$Z_{\mathrm{VA}} = \frac{1}{\mathrm{j}\omega C_1} + \frac{\frac{1}{\mathrm{j}\omega C_2} \cdot (Z_{\mathrm{TMN}} + Z_{\mathrm{rect}})}{\frac{1}{\mathrm{j}\omega C_2} + Z_{\mathrm{TMN}} + Z_{\mathrm{rect}}} \,, \tag{5}$$

with Z_{TMN} being the impedance of the tunable matching network that can be set to take any impedance value from $[0, -24]\,\mathrm{j}\Omega$.

B) Simulink Model

The characterization of a system across different states requires a sophisticated simulation model capable of handling different battery voltages, different power levels, frequencies and - if existing - different states of active circuit components. Therefore, a *Simulink* model is well suited. In *Simulink*, it is more convenient - compared to other simulation tools like *LTspice* - to implement a control loop that ensures that the same amount of power is transferred to the battery across different parameter sweeps, making automatization of the simulation model much easier.
The circuit illustrated in Fig. 2 is characterized by the impedance at the VA coil terminals, Z_{VA}. As the GA coil current is sinusoidal, we may reduce the simulation model

and omit the GA circuit, which has no effect on the impedance outcome. Instead, we apply a sinousoidal voltage source that represents the induced voltage into the VA circuit. The voltage source amplitude

$$U_{\mathrm{VA}}^{\mathrm{ind}} = \omega M I_{\mathrm{GA}}\,, \tag{6}$$

is steered by the control loop that ensures a certain amount of power at the battery. Sensors VM2 and CM1 (cf. Fig. 4) measure the voltage and current needed to calculate the impedance Z_{VA}.

1) Simulink Impedance Measurement

To retrieve the impedance from *Simulink* simulations, it is required to convert the direct observable time signal of current and voltage into a frequency dependent impedance value. Whenever the time signal deviates from a purely sinusoidal waveform, it contains harmonic contributions. To filter out these harmonic contents that do not contribute in the energy transfer, we apply a Fourier analysis. The impedance for the fundamental frequency averaged over one period can be calculated using the following identity [14]

$$\begin{aligned} a_n &= 2f_0 \int_0^T f(t) \cdot \cos(n\omega t)\,\mathrm{d}t\,, \\ b_n &= -2f_0 \int_0^T f(t) \cdot \sin(n\omega t)\,\mathrm{d}t\,. \end{aligned} \tag{7}$$

This divides the time signal into its cosine and sine components. Inserting $n = 1$ into eq. (7) yields the fundamental component.
The impedance is then given by

$$|Z| = \frac{\sqrt{a_{1,u}^2 + b_{1,u}^2}}{\sqrt{a_{1,i}^2 + b_{1,i}^2}}\,, \tag{8}$$

and the phase difference between voltage and current is

$$\varphi_{\mathrm{UI}} = \tan^{-1}\left(\frac{a_{1,u}}{b_{1,u}}\right) - \tan^{-1}\left(\frac{a_{1,i}}{b_{1,i}}\right). \tag{9}$$

III Measurement Setup

The measurement setup is based on the proposal of [1, 6]. First measurement results show that a significant improvement in comparison with the direct voltage-current (UI) method can be achieved [7]. The setup is illustrated in Fig. 5. Testing different VAs in different positions, different power levels and in different settings on the same setup requires the inverter and the impedance matching network to handle a wide range of impedances. We therefore utilize a special laboratory inverter[1] that can support a wide range of inductive loads and a special impedance matching network that maximizes the supported range of presented impedances at the GA coil terminals. The presented impedance comprises the primary coil impedance and the reflected vehicle system impedance, which are both offset dependent.

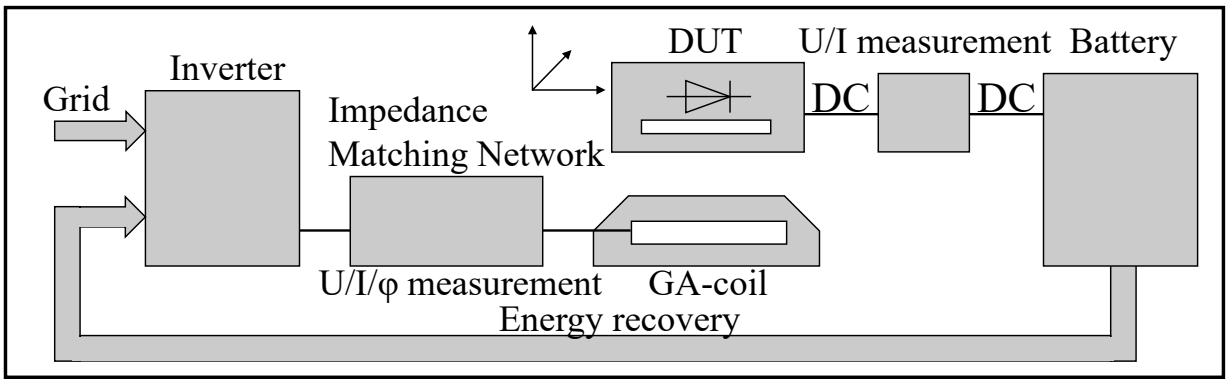

Figure 5: Schematic impedance measurement setup [7].

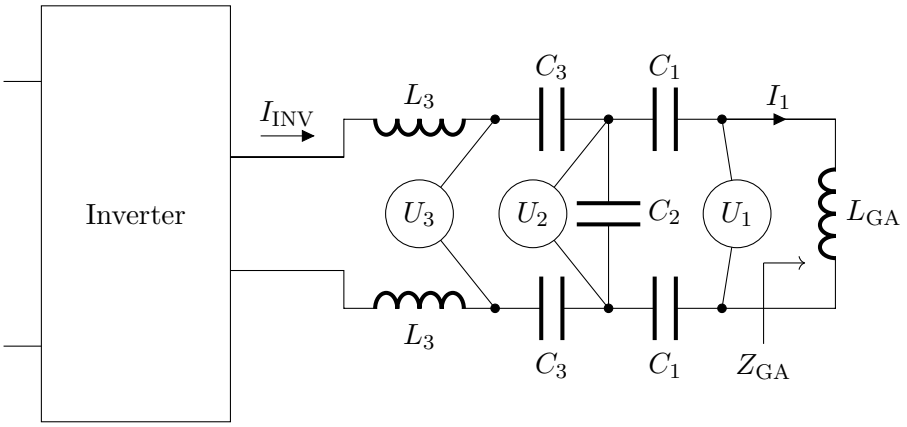

Figure 6: Schematics of impedance measurement device with three voltage and one current measurement position.

The schematics of the impedance matching network and the measurement ports are illustrated in Fig. 6. The device under test (DUT) is integrated in a test robot that ensures high positioning accuracy and reproducibility. Its DC output is connected with a controllable DC load that presents the set battery voltage. The received energy is recovered and reused for the DC source.
The measurands $U_1, U_2, U_3, I_1, P_{\mathrm{in}}, P_{\mathrm{out}}$ and their respective phases are used to calculate the impedance at the primary coil terminal in different ways ($Z_{\mathrm{GA},i}$). A perfect measurement set up would yield a cluster of points, each calculated differently, at the same Z_{GA} impedance. However, real world measurements are subject to measurement errors and thus deviate from perfect. To compensate for constant, systematic errors, we apply a fit in form of $a \cdot x$ for the measurands and in form of $b \pm x$ for the phases. The fit is applied across a large number of measurements and yields the correction parameters shown in Table 1 that minimize the measurement error. More details are presented in [7]. There, also the process of selecting the right correction parameters is given.

[1]Inverter details: $U_{\mathrm{DC}} = [100, 600]\,\mathrm{V}$, $I_{\mathrm{out,max}} = 100\,\mathrm{A}$, $\varphi = [0°, 70°]$, $f = [80, 90]\,\mathrm{kHz}$.

Table 1: Correction Parameters [7].

a_{C_1}	a_{C_2}	a_{C_3}	a_{U_1}	a_{U_2}	a_{U_3}
0.980	0.993	1.007	0.990	0.980	0.991

a_{I_1}	$b_{\varphi_{U_1I_1}}[^\circ]$	$b_{\varphi_{U_2I_1}}[^\circ]$	$b_{\varphi_{U_1U_2}}[^\circ]$	$b_{\varphi_{U_1U_3}}[^\circ]$	$b_{\varphi_{U_2U_3}}[^\circ]$
0.970	1.102	-0.688	-1.788	-1.742	0.040

The impedance Z_{GA} is calculated by means of a weighted mean function

$$Z_{\mathrm{GA_{mean}}} = \frac{\sum_{i=1}^{N} g_i \cdot Z_{\mathrm{GA},i}}{\sum_{i=1}^{N} g_i}, \tag{10}$$

which weighs each contributing function with its uncertainty $g_i = (\Delta Z_{\mathrm{GA},i})^{-2}$ according to Gaussian error propagation [15].

A) Coil Parameter Measurement

Measuring the coil parameters $L_{\mathrm{GA}}, L_{\mathrm{VA}}$ and k, can be straightforward during the development process. However, once a VA design is optimized towards automotive requirements and becomes more like a production ready product, it may no longer be possible to make such measurements directly, e.g. the capacitors may be integrated into the coil assembly and no longer be detachable - which would be required for a VNA measurement. For this reason, we measured the coil parameters before the final assembly with a VNA for different coil offset positions. These measurements were made using a custom-built computer-controlled positioning device, constructed from 80/20 aluminum extrusion. All aluminum extrusions supporting the VA assembly are positioned far from the power transfer coils to avoid affecting the measurements. These measurements use the same 1.1 m × 1.1 m aluminum plate used in the power transfer measurements. More details on the test setup can be found in [1].
However, those positions may not be identical to those used in the impedance measurement setup, and final assembly of the VA coil can result in some changes to coil properties. Consequently, there is some uncertainty in the coil parameter values that must be accounted for in addition to the measurement uncertainty originating from the VNA. To account for the possibly introduced offsets, we apply a fit for each position within the assumed uncertainty ranges depicted in Table 2. Numerous measurements were made at each position to help reduce uncertainty.

Table 2: Coil parameter uncertainty assumption.

ΔL_{GA} [%]	ΔL_{VA} [%]	Δk [%]
3	3	3

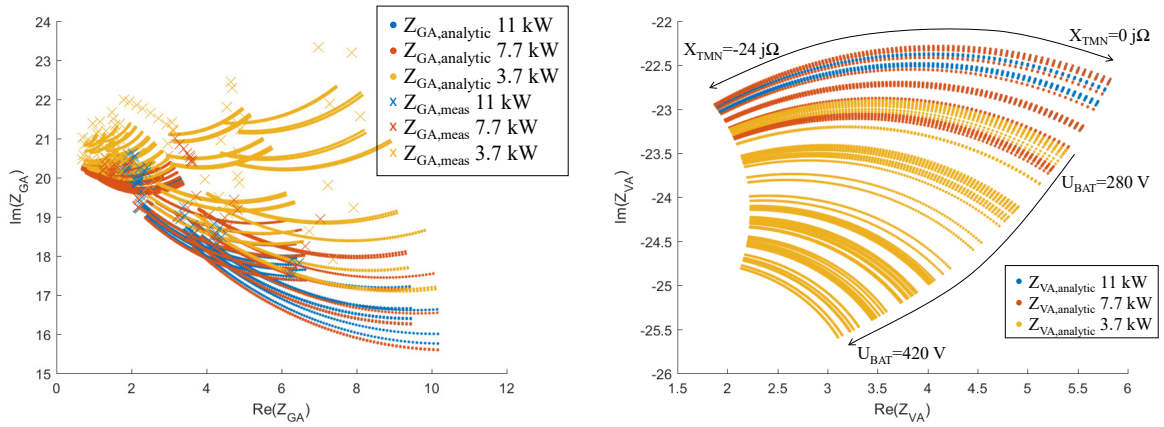

(a) GA impedance.

(b) VA impedance.

Figure 7: GA and VA impedance for WPT3 SAE J2954 Reference VA from [1] calculated with analytic model.

IV RESULTS AND DISCUSSION

First, the results for each method will be presented individually, then a comparison between each model and the real measurement data is drawn. To be able to compare the results, we use the measurement output data P_{out} and U_{Bat} as inputs for both models. The measurement was performed for the set of conditions

$$\begin{aligned} U_{\text{bat}} &= \{280, 320, 380, 420\}\,\text{V}\,, \\ P_{\text{in}} &= \{3.7, 7.7, 11\}\,\text{kW}\,, \\ (x, y) &= (0,0), (0,100), (75,0), (75,100)\,\text{mm}\,, \\ z &= 140, 210\,\text{mm}\,, \end{aligned} \tag{11}$$

and for different states of the active component in the VA circuit (c.f. Fig. 2), the so called tunable matching network (TMN).

A) Analytic Model Results

With Eq. (5) the impedance for the analytic model $Z_{\text{VA,analytic}}$ can be calculated. The TMN function is incorporated by a parameter sweep of Z_{TMN} that adds one dimension to the impedance vector Z_{VA}. The result is shown in Figure 7b. The GA impedance is calculated by inserting the VA impedance into Eq. (1). The result is shown in Figure 7a.

As seen in Fig. 7b, the TMN reactance provides a means to vary the VA impedance. During operation, due to different system constraints, for example, coil current limitations, voltage limits, etc., it may not be possible to achieve the desired power over the full TMN reactance range (nor would it be necessary). As a result, in the measurements reported here the TMN reactance values were limited to those at which the desired power could be reached. The TMN reactance value was adjusted from a control computer via a graphical user interface (GUI). The control value of the TMN setting in

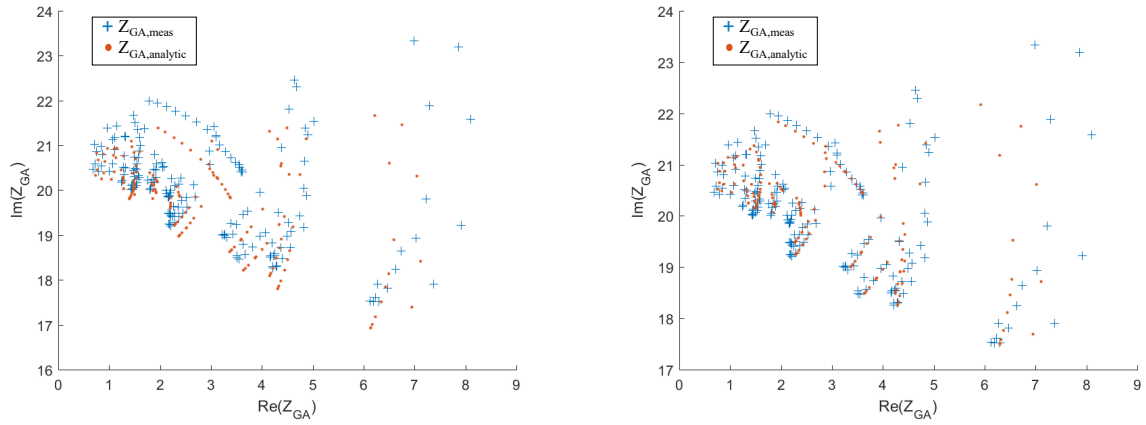

(a) GA impedance without offset correction.

(b) GA impedance with offset correction.

Figure 8: GA impedance before and after offset correction for analytic model.

the GUI is not directly the reactance of the element, and since the TMN was being used as a "black box", it was required to come up with a mapping for use in the analytical model. The mapping was developed using the constraints that the TMN value should be in the range $[0-24]\,\mathrm{j}\Omega$ and that the same TMN setting from any measurement must also show the same Z_{TMN} value. For the arbitrary mappings, the one Z_{TMN} value that yields the lowest overall deviation was chosen. The result of the mapping between TMN GUI setting and reactance value agrees well with our expectation.
In Figure 8a the results with the above described TMN selection process are shown. It can be directly seen that the analytically calculated $Z_{\mathrm{GA,analytic}}$ and the measured impedances $Z_{\mathrm{GA,mean}}$ share a similar shape and are in close proximity. However, we also see that there are deviations. These deviations could be the result of differences in L_{GA}, L_{VA} and M between the tested GA and VA coils and the VNA measurements made before final assembly as well as any differences in coil position between the same. This can be investigated by looking at different parameters of the electromagnetic coupler within the assumed uncertainty parameters depicted in Table 2. We therefore setup a fit that minimizes the euclidean distance ϵ between the measured and the respective analytically calculated impedances. We assume that the high number of measurements can be used to correct for any systematic errors in the positioning. Fig. 8b shows the result. For a better visualization we omitted the power dependent color coding. The applied correction parameters are given in Table 4.
It can be seen that the offsets could be clearly reduced through this correction process. This is also shown by the mean deviation $\bar{\epsilon}$ which could be reduced by more than a factor of two from $0.439\,\Omega$ to $0.190\,\Omega$. However, there are some points with high real part corresponding to 3.7 kW that differ from the measurement data. Looking at the deviation across different power levels , we see in Table 3 that the deviation for 3.7 kW is around 3

Table 3: Deviation between real data and analytic model for different power levels.

$\epsilon_{3.7\,\mathrm{kW}}\,[\Omega]$	$\epsilon_{7.7\,\mathrm{kW}}\,[\Omega]$	$\epsilon_{11\,\mathrm{kW}}\,[\Omega]$
0.294	0.107	0.132

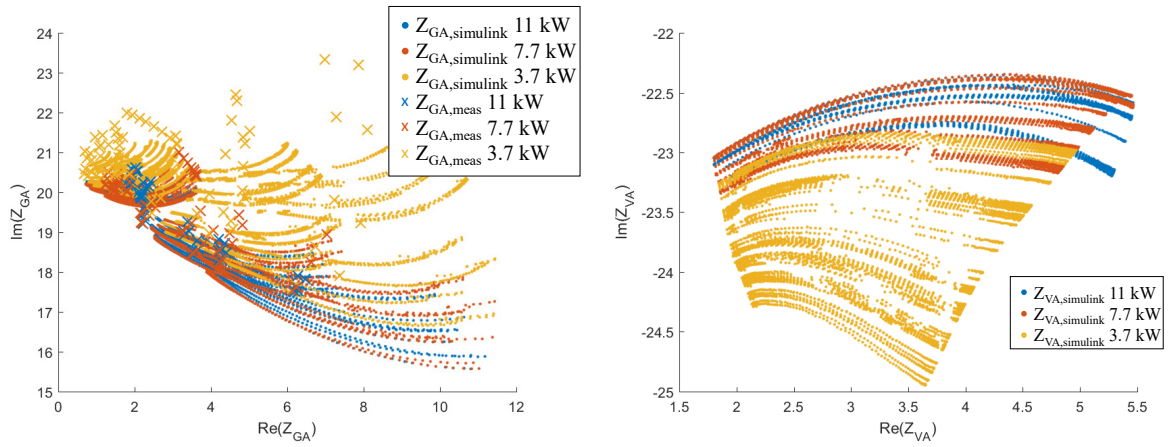

(a) GA impedance.

(b) VA impedance.

Figure 9: GA and VA impedance for WPT3 SAE J2954 Reference VA from [1] calculated with *Simulink* model.

times more than for higher power levels.

Table 4: Offset correction parameters for analytically calculated Z_{GA}.

x [mm]	y [mm]	z [mm]	L_{GA} [μH]	L_{VA} [μH]	k	$a_{L_{\mathrm{GA}}}$	$a_{L_{\mathrm{VA}}}$	a_k	$\epsilon_{(xyz)}$ [Ω]
75	100	140	36.6	44.0	0.170	1.01	0.993	0.993	0.196
0	100	140	35.8	44.1	0.210	1.02	0.993	0.993	0.284
75	0	140	36.1	44.0	0.175	1.01	0.993	0.979	0.209
0	0	140	35.1	44.1	0.221	1.01	0.999	0.993	0.354
75	100	210	37.9	43.1	0.089	1.01	0.994	1.02	0.090
0	100	210	37.7	43.1	0.108	1.01	0.997	0.992	0.104
75	0	210	37.8	43.1	0.097	1.01	1.00	0.985	0.099
0	0	210	37.5	43.2	0.118	1.02	0.993	1.03	0.165

B) Simulink Model Results

The impedance $Z_{\mathrm{VA,simulink}}$ was computed as indicated in Fig. 4 by applying the method presented in 1) to retrieve its impedance. The VA impedance is shown in Fig. 9b. For the mapping onto the GA interface, we also apply Eq. (1) and the measured coil parameters. Figure 9a shows the resulting calculated impedances $Z_{\mathrm{GA,simulink}}$. Similar to the analytic model, the VA and GA impedance also includes a parameter sweep of the TMN. For this reason, we apply the same selection process as used for the analytic model. Subsequent, we correct for systematic errors in the positioning by means of a fit that minimizes the euclidean distance between the measured and the respective simulated impedances. The result is shown in Fig. 10. The applied correction factors are given in Table 5. The mean deviation $\bar{\epsilon}$ between measured and simulated impedances can approximately be halved from 0.619 Ω to 0.304 Ω with the correction process. The deviation across different power levels is given in Table 6. It also shows a better agreement for 11 kW and 7.7 kW and

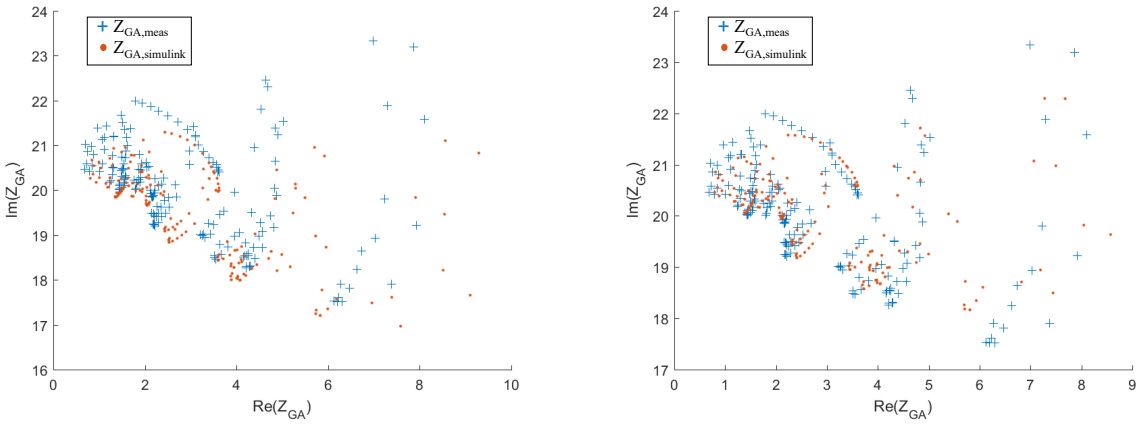

(a) GA impedance without offset correction.

(b) GA impedance with offset correction.

Figure 10: GA impedance before and after offset correction for *Simulink* model.

worse for 3.7 kW case. This could be from temperature dependent resistance effects of the SiC-diodes at higher power levels that were not implemented in the *Simulink* model but might meet the assumed resistance values better.

Table 5: Offset correction parameters for simulated Z_{GA}.

x [mm]	y [mm]	z [mm]	L_{GA} [μH]	L_{VA} [μH]	k	$a_{L_{\mathrm{GA}}}$	$a_{L_{\mathrm{VA}}}$	a_k	$\epsilon_{(xyz)}$ [Ω]
75	100	140	36.6	44.0	0.170	1.01	0.984	0.970	0.351
0	100	140	35.8	44.1	0.210	1.01	0.984	0.970	0.513
75	0	140	36.1	44.0	0.175	1.01	0.982	0.970	0.372
0	0	140	35.1	44.1	0.221	1.01	0.980	0.970	0.403
75	100	210	37.9	43.1	0.089	1.01	0.996	0.989	0.151
0	100	210	37.7	43.1	0.108	1.01	0.995	0.972	0.193
75	0	210	37.8	43.1	0.097	1.01	0.991	0.970	0.170
0	0	210	37.5	43.2	0.118	1.01	0.990	1.01	0.235

Table 6: Deviation between real data and *Simulink* model for different power levels.

$\epsilon_{3.7\,\mathrm{kW}}$ [Ω]	$\epsilon_{7.7\,\mathrm{kW}}$ [Ω]	$\epsilon_{11\,\mathrm{kW}}$ [Ω]
0.399	0.211	0.272

C) Discussion

At the beginning of this study, we had the expectation that the simple analytic model would deviate more from the measurements than the *Simulink* model. However, the results show the opposite finding. The analytic model - based on Steigerwalds' approximation - agrees well with the measurement results and the results obtained with the *Simulink* model do not. Of course, the reason is not the *Simulink* tool itself. Instead,

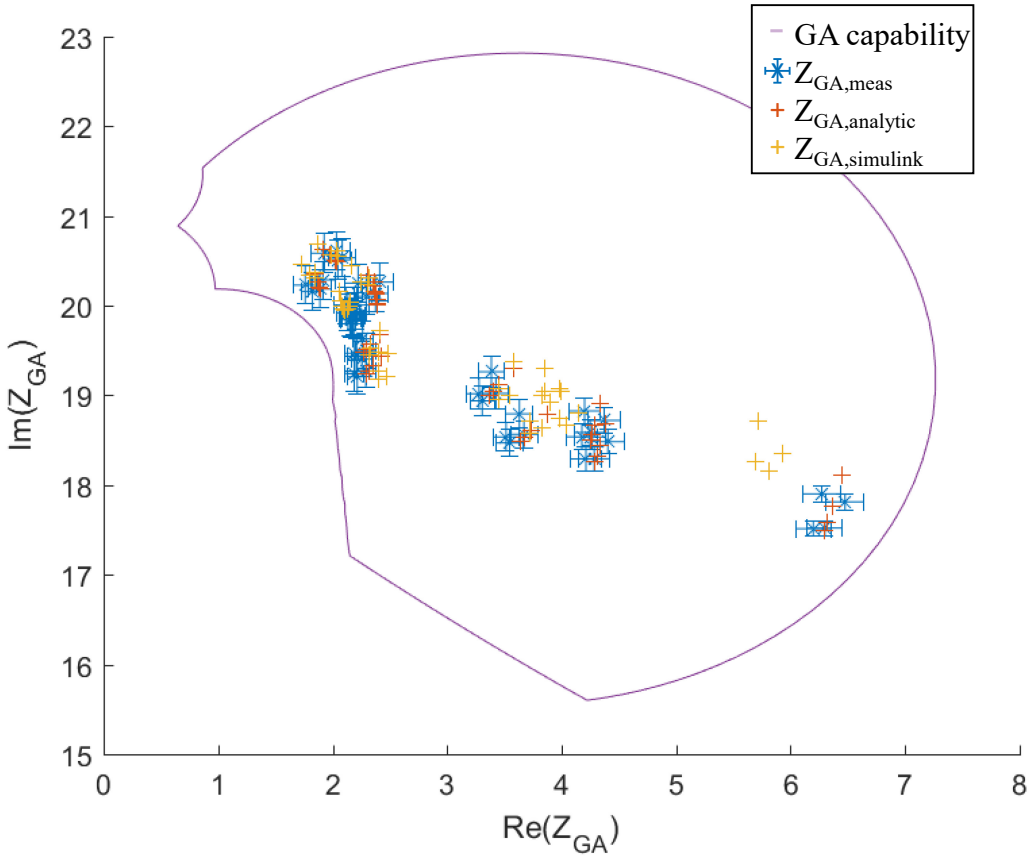

Figure 11: Calculated, simulated and measured impedance Z_{GA} with WPT3 reference GA electronics capability from [1]. All impedances within the purple envelope correspond to different EV operation points that can be powered with 11 kW.

there has to be a deviation between the simulated model and the actual VA. We traced the major difference back to the rectifier input impedance. The rectifier impedance contains no imaginary impedance in the analytic model. This is quite different in case of the *Simulink* model, based on a time-domain circuit simulation, where the rectifier impedance contains a capacitive reactance. This is due to nonlinear effects of the diodes that are not yet well understood and subject of future research. Further errors in the simulation model could be introduced by the unknown TMN, component deviations from specified values, or temperature effects. Further improvement in the agreement between simulation model and measurement data has not yet been successful and needs further investigation. Therefore, we recommend use of the analytical model for design purposes. However, for qualifying product VAs and ensuring standard conformity, impedance measurements are indispensable.

To determine if the circular WPT3 reference GA from SAE J2954 [1] is capable of driving the calculated and measured impedance values that characterize the WPT3 VA depicted in Fig. 2, we take the inverter assumptions given in Table 7 and calculate its impedance at the GA interface.

The result is shown in Fig. 11 with calculated, simulated and the measured impedance

values for the different operating points at 11 kW. The measured impedance values are also shown with their uncertainty. The mean uncertainty is $0.113\,\Omega + 0.176\,\mathrm{j}\Omega$. The GA electronics of the reference WPT3 GA from SAE J2954 can achieve 11 kW output power with all impedances inside the purple envelope. This shows that this method is well suited for the design development process indicating compatibility of VA and GA, or GA impedance and GA electronics. The feedback from impedance measurements can also be applied to improve the simulation models for better prediction capability.

Table 7: Inverter assumptions used to calculate GA electronic capability.

	I_{inv} [A]	U_{inv} [V]	φ_{inv} [°]	P_{GA} [kW]
Min	20	380	0	11
Max	40	500	45	

V CONCLUSION

In this paper, we presented two methods to analyze inductive power transfer systems. An analytic model and a *Simulink* model. We compared the theoretical values of both methods with the first impedance measurement results on IPT systems. On the way, we encountered a product challenge - differences in the coil parameters originating from the difference between the pre-assembly coil characterization and the impedance measurement positions. This problem could be solved by means of a fit that minimizes the error in each position. We assume that the systematic errors cancel out when having several different measurement settings for each position and does not corrupt the data. The results show that both models achieve a similar shape in close proximity to the measured values even before offset correction. However, the analytically calculated impedances $Z_{\mathrm{GA,analytic}}$ show a better agreement with the measurement results. In both cases, the agreement is better for 7.7 kW and 11 kW than for 3.7 kW. The proposed method to describe IPT systems is a way to specify and to test the compatibility of the energy transfer with few additional definitions and as a consequence, with little additional test machinery. One of the key features is to use the geometric definitions of standard coil systems as a reference. Hence the method is tied closely to the definition of the standard. Nevertheless, the technique and underlying calculations are challenging and additional VA systems need to be measured, simulated and compared for a better understanding.

REFERENCES

[1] Wireless Power Transfer for Light-Duty Plug-In / Electric Vehicles and Alignment Methodology, SAE J2954 RP, 2017.

[2] Preuss, S.: Daimler plant CO2-Wende: Bis 2030 soll jeder zweite Mercedes elektrisch sein, FAZ.NET, [Online]. Available at: https://www.faz.net/aktuell/wirtschaft/auto-verkehr/daimler-bis-2030-soll-jeder-zweite-mercedes-elektrisch-sein-16184951.html. [Accessed 14 Jun. 2019].

[3] Kreimeier, N.: Dr. Volks und Mr. Wagen, Capital.de, [Online]. Available at: https://www.capital.de/wirtschaft-politik/dr-volks-und-mr-wagen. [Accessed 12 Jun. 2019].

[4] Freitag, M.: Porsche plant mit Elektroanteil von 50 Prozent schon in sechs Jahren, manager magazin, [Online]. Available at: https://www.manager-magazin.de/unternehmen/autoindustrie/porsche-jedes-zweite-fahrzeug-soll-bald-elektroauto-sein-a-1153417.html. [Accessed 12 Jun. 2019].

[5] U.S. Department of Transportation: 2009 National Household Travel Survey, 2009.

[6] Hassler, M.; Niedermeier, F.; Krammer, J.; Diepold, K.: A Method for Interoperable Interface Description of Inductive Power Transfer Systems, 2018 IEEE PELS Workshop on Emerging Technologies: Wireless Power Transfer (Wow), Montréal (Canada), 2018.

[7] Hassler, M.; Atasoy, O.; Kesler, M.; Twelker, K.; Achatz, T.; Jetz, M.; Krammer, J.: Impedance Measurement on Inductive Power Transfer Systems, 2019 IEEE PELS Workshop on Emerging Technologies: Wireless Power Transfer (Wow), London (GB), 2019.

[8] Auvigne, C.B.: Electrical and Magnetical Modeling of Inductive Coupled Power Transfer Systems, EPFL, 2015.

[9] Cirimele, V.: Projet et intégration d'un système de transfert inductif pour les applications automobiles, 2017.

[10] Esteban, B.; Sid-Ahmed, M.; Kar,N. C.: A Comparative Study of Power Supply Architectures in Wireless EV Charging Systems. IEEE Transactions on Power Electronics, **30** 11 (2015), 6408–6422.

[11] Niedermeier, F.: Methoden zur Analyse von induktiven Ladesystemen für Elektro- und Hybridfahrzeuge, 2019.

[12] Kürschner, D.; Rathge, C.: Contactless energy transmission systems with improved coil positioning flexibility for high power applications, 2008 IEEE Power Electronics Specialists Conference, Rhodes (Greece), 2008.

[13] Steigerwald, R.L.: A comparison of half-bridge resonant converter topologies, IEEE Transactions on Power Electronics, **3** 2 (1988), 174–182.

[14] Unbehauen, R.: Grundlagen der Elektrotechnik - Allgemeine Grundlagen, Lineare Netzwerke, Stationäres Verhalten, Springer, 1994.

[15] Gupta, S. V.: Measurement Uncertainties: Physical Parameters and Calibration of Instruments, Springer Berlin Heidelberg, 2012.

Bibliographies


Marius Hassler received his B.Sc. and M.Sc. degree in physics with specialization in condensed matter from the Technical University of Munich, Germany. He is currently working toward the Dr.-Ing. degree in engineering with BMW Group, from the Technical University of Munich, Germany. His current research interests include circuit simulation and inductive charging.


Oguz Atasoy, PhD is working as a senior staff scientist at Witricity Corporation. His tasks include the design, development and improvement of wireless power solutions. His work at Witricity lead to patent applications as well as conference publications. He received his PhD from EPFL (Swiss Institute of Technology Lausanne) in Microsystems and Microelectronics, and his MSc and BSc in Electrical and Electronics Engineering from Bogazici University, Turkey.


Karl Twelker recieved his PhD in experimental neutrino physics from Stanford University in 2014. He joined WiTricity Corporation in 2015 to work on wireless power systems for automotive and consumer electronics applications. He is now at The Charles Stark Draper Laboratory, Inc.


Morris Kesler is the Chief Technology Officer at WiTricity Corporation where he is responsible for the research and development activities in the company. He joined WiTricity in 2007 and has served as Chief Engineer and vice president of research and development. Prior to joining WiTricity, he was a founder of Wide Net Technologies, Inc., which developed unique optical communication and sensing systems for both government and industry, and a Consulting Engineer at PhotonEx Corporation, which developed a 40 Gb/s long-haul optical transport system. Dr. Kesler spent ten years with the Georgia Tech Research Institute where he led research programs in electromagnetic scattering, antenna arrays, novel antenna structures and photonic band-gap structures. He holds over 100 patents and has published over 40 technical journal and conference papers. He holds a B.S., M.S., and Ph.D. from the Massachusetts Institute of Technology in Electrical Engineering and Computer Science.


Johannes Birkendahl received his B.Sc. and M.Sc. degree in electrical engineering from the Technical University of Munich, Germany, where the focus of his studies layed in energy storages. He is currently working as tester for the software development of the energy storages at BMW.


Josef Krammer received the Dipl.-Ing. degree in electrical engineering from the Department of Electrical and Computer Engineering at the Technical University of Munich, TUM, Germany. He worked as a researcher at the Institute of Circuit Theory and Signal Processing at the TUM where he received the degree of Dr.-Ing. Since 1991 he is working at BMW Group in different engineering positions for the development of electronics for conventional and electric vehicles.

List of figures and tables

Related publications

Related papers:

T. Mayr, F. Niedermeier, M. Hassler, “Application of composite materials in inductive charging systems for electric vehicles,” *Journal of Composite Materials*, 2019.

F. Niedermeier, M. Hassler, J. Krammer and B. Schmuelling, “A Jacobi Based Method for Calculating the Steady State Characteristics of Non-Linear Circuit Elements,” *2017 IEEE Vehicle Power and Propulsion Conference (VPPC)*, Belfort, pp. 1-5, 2017.

Authored standards:

SAE Standard, “Wireless Power Transfer for Light-Duty Plug-In/ Electric Vehicles and Alignment Methodology,” *SAE J2954 RP Annex G*, 2017.

IEC Standard, “Electric vehicle wireless power transfer (WPT) systems - Part 3,” *61980–3 Annex E*, 2019.

Related patents:

1 M. Hassler, J. Krammer, “Method for checking a primary or secondary unit of an inductive charging system,” *DE102017202025A1, WO2018145913A1*, 2017.

2 J. Krammer, M. Hassler, F. Niedermeier, “Primäreinheit für ein induktives Ladesystem, sowie Verfahren zum Betrieb einer Primäreinheit,” *DE102017218066A1, WO002019072576A1*, 2017.

3 J. Krammer, M. Hassler, V. Mahrla, F. Niedermeier, “Optimierte Litze für eine Spule zum induktiven Laden,” *DE102017206439A1*, 2017.

4 J. Krammer, M. Hassler, V. Mahrla, F. Niedermeier, “Spule mit einer Flachleitung,” *DE102017206440A1*, 2017.

5 J. Krammer, M. Hassler, “Spule und Verfahren zur Erhöhung des Kopplungsgrades eines induktiven Koppelsystems,” *DE102017215149A1*, 2017.

6 J. Krammer, M. Hassler, F. Niedermeier, “Verfahren zur Überprüfung einer Primär- oder Sekundäreinheit für induktives Laden,” *DE102017215469A1*, 2017.

7 M. Hassler, F. Niedermeier, J. Krammer, “Induktives Ladesystem und Verfahren zur Verbesserung des Kopplungsfaktors,” *DE102017218014A1*, 2017.

8 J. Krammer, M. Hassler, F. Niedermeier, “Primäreinheit für ein induktives Ladesystem, sowie Verfahren zum Betrieb einer Primäreinheit,” *DE102017218066A1*, 2017.

Bibliography

1. D. Mage, G. Ozolins, P. Peterson, A. Webster, R. Orthofer, V. Vandeweerd, and M. Gwynne, “Urban air pollution in megacities of the world,” *Atmospheric Environment*, vol. 30, no. 5, pp. 681–686, 1996.

2. B. R. Gurjar, A. Jain, A. Sharma, A. Agarwal, P. Gupta, A. S. Nagpure, and J. Lelieveld, “Human health risks in megacities due to air pollution,” *Atmospheric Environment*, vol. 44, no. 36, pp. 4606–4613, 2010.

3. N. Künzli, R. Kaiser, S. Medina, M. Studnicka, O. Chanel, P. Filliger, M. Herry, F. Horak, V. Puybonnieux-Texier, P. Quénel, J. Schneider, R. Seethaler, J.-C. Vergnaud, and H. Sommer, “Public-health impact of outdoor and traffic-related air pollution: a European assessment,” *The Lancet*, vol. 356, no. 9232, pp. 795–801, 2000.

4. T. Ketelaer, T. Kaschub, P. Jochem, and W. Fichtner, “The potential of carbon dioxide emission reductions in German commercial transport by electric vehicles,” *International Journal of Environmental Science and Technology*, vol. 11, no. 8, pp. 2169–2184, 2014.

5. L. Canals Casals, E. Martinez-Laserna, B. Amante García, and N. Nieto, “Sustainability analysis of the electric vehicle use in Europe for CO2 emissions reduction,” *Journal of Cleaner Production*, vol. 127, pp. 425–437, 2016.

6. U.S. Department of Energy, “Reducing pollution with electric vehicles,” [Online]. Available: https://www.energy.gov/eere/electricvehicles/reducing-pollution-electric-vehicles. [Accessed 04-January-2019].

7. C. Giffi, J. Vitale, M. Drew, Y. Kuboshima, and M. Sase, “Unplugged - electric vehicle realities versus consumer expectations,” 2011.

8. T. Franke, I. Neumann, F. Bühler, P. Cocron, and J. F. Krems, “Experiencing range in an electric vehicle: understanding psychological barriers,” *Applied Psychology*, vol. 61, no. 3, pp. 368–391, 2012.

9. J. S. Krupa, D. M. Rizzo, M. J. Eppstein, D. Brad Lanute, D. E. Gaalema, K. Lakkaraju, and C. E. Warrender, “Analysis of a consumer survey on plug-in hybrid electric vehicles,” *Transportation Research Part A: Policy and Practice*, vol. 64, pp. 14–31, 2014.

10. Bundesinstitut für Bau-, Stadt-, und Raumforschung, “Immer mehr Menschen pendeln zur Arbeit,” [Online]. Available: https://www.bbsr.bund.de/BBSR/DE/Home/Topthemen/2017-pendeln.html. [Accessed 21-July-2019].

11. SAE J1772, *Electric vehicle and plug in hybrid electric vehicle conductive charge coupler*. United States: SAE International, 2016.

12. T. D. Chen, K. M. Kockelman, and J. P. Hanna, “Operations of a shared, autonomous, electric vehicle fleet: implications of vehicle & charging infrastructure decisions,” *Transportation Research Part A: Policy and Practice*, vol. 94, pp. 243–254, 2016.

13. A. Aditya, H. Kersten, K. Philipp, and S. Emily, “Gauging the disruptive power of robo-taxis in autonomous driving,” 2017.

14. P. M. Bösch, F. Becker, H. Becker, and K. W. Axhausen, “Cost-based analysis of autonomous mobility services,” *Transport Policy*, vol. 64, pp. 76–91, 2018.

15. O. H. Hannisdahl, H. V. Malvik, and G. B. Wensaas, “The future is electric! The EV revolution in Norway—explanations and lessons learned,” in *World Electric Vehicle Symposium and Exhibition (EVS27)*. IEEE, 2013, pp. 1–13.

16. S. Lukic and Z. Pantic, “Cutting the cord: static and dynamic inductive wireless charging of electric vehicles,” *IEEE Electrification Magazine*, vol. 1, no. 1, pp. 57–64, 2013.

17. J. M. Miller, O. C. Onar, C. White, S. Campbell, C. Coomer, L. Seiber, R. Sepe, and A. Steyerl, “Demonstrating dynamic wireless charging of an electric vehicle: the benefit of electrochemical capacitor smoothing,” *IEEE Power Electronics Magazine*, vol. 1, no. 1, pp. 12–24, 2014.

18. G. R. Nagendra, G. A. Covic, and J. T. Boys, “Sizing of inductive power pads for dynamic charging of EVs on IPT highways,” *IEEE Transactions on Transportation Electrification*, vol. 3, no. 2, pp. 405–417, 2017.

19. B. Song, J. Shin, S. Lee, S. Shin, Y. Kim, S. Jeon, and G. Jung, “Design of a high power transfer pickup for on-line electric vehicle (OLEV),” in *IEEE International Electric Vehicle Conference*. IEEE, 2012, pp. 1–4.

20. F. Chen, *Sustainable implementation of electrified roads: structural and material analyses*, Ph.D. dissertation. Stockholm: KTH Royal Institute of Technology, 2016, vol. 143.

21. S. Ahn and J. Kim, “Magnetic field design for high efficient and low emf wireless power transfer in on-line electric vehicle,” in *Proceedings of the 5th European Conference on Antennas and Propagation (EUCAP)*. IEEE, 2011, pp. 3979–3982.

22. J. Shin, S. Shin, Y. Kim, S. Ahn, S. Lee, G. Jung, S.-J. Jeon, and D.-H. Cho, "Design and implementation of shaped magnetic-resonance-based wireless power transfer system for roadway-powered moving electric vehicles," *IEEE Transactions on Industrial Electronics*, vol. 61, no. 3, pp. 1179–1192, 2014.

23. N. P. Suh and D. H. Cho, "Wireless power transfer for electric vehicles," in *The On-line Electric Vehicle*, N. P. Suh and D. H. Cho, Eds. Springer International Publishing, 2017, vol. 1–2, pp. 17–34.

24. S. Jeong, Y. J. Jang, and D. Kum, "Economic analysis of the dynamic charging electric vehicle," *IEEE Transactions on Power Electronics*, vol. 30, no. 11, pp. 6368–6377, 2015.

25. A. Brooker, M. Thornton, and J. Rugh, "Technology improvement pathways to cost-effective vehicle electrification," in *Green Technologies and the Mobility Industry*. SAE, 2011, pp. 35-47.

26. H. Lund and W. Kempton, "Integration of renewable energy into the transport and electricity sectors through V2G," *Energy Policy*, vol. 36, no. 9, pp. 3578–3587, 2008.

27. W. Kempton and J. Tomić, "Vehicle-to-grid power fundamentals: calculating capacity and net revenue," *Journal of Power Sources*, vol. 144, no. 1, pp. 268–279, 2005.

28. J. Tomić and W. Kempton, "Using fleets of electric-drive vehicles for grid support," *Journal of Power Sources*, vol. 168, no. 2, pp. 459–468, 2007.

29. IEC 62196-3, *Plugs, socket-outlets, vehicle connectors and vehicle inlets - Conductive charging of electric vehicles - Part 3: Dimensional compatibility and interchangeability requirements for d.c. and a.c./d.c. pin and contact-tube vehicle couplers: Edition 1.0*, 2014.

30. IEC 61851-1, *Electric vehicle conductive charging system - Part 1: General requirements: Edition 3.0*, 2017.

31. C. Kalialakis and A. Georgiadis, "The regulatory framework for wireless power transfer systems," *Wireless Power Transfer*, vol. 1, no. 02, pp. 108–118, 2014.

32. SAE J2954 Technical Information Report, *Wireless power transfer for light-duty plug-in/ electric vehicles and alignment methodology*. United States: SAE International, 2016.

33. SAE J2954 Recommended Practice, *Wireless power transfer for light-duty plug-in/ electric vehicles and alignment methodology*. United States: SAE International, 2017.

34. M. Treffers, “History, current status and future of the Wireless Power Consortium and the Qi interface specification,” *IEEE Circuits and Systems Magazine*, vol. 15, no. 2, pp. 28–31, 2015.

35. R. Tseng, B. von Novak, S. Shevde, and K. A. Grajski, “Introduction to the Alliance for Wireless Power loosely-coupled wireless power transfer system specification version 1.0,” in *IEEE Wireless Power Transfer (WPT)*. IEEE, 2013, pp. 79-83.

36. Wireless Power Consortium, *The Qi wireless power transfer system power class 0 specification: parts 1 and 2: Interface Definitions*, 2016.

37. AirFuel Alliance, *AirFuel resonant wireless power transfer (WPT) system baseline system specification (BSS)*, 2017.

38. Alliance for Wireless Power, *A4WP wireless power transfer system baseline system specification (BSS): A4WP-S-0001 v1.3*, 2014.

39. IEC TS 61980-3, *Electric vehicle wireless power transfer (WPT) systems: Part 3 specific requirements for the magnetic field wireless power transfer systems: Edition 1.0*, 2018.

40. J. R. Macdonald, “Impedance spectroscopy,” *Annals of Biomedical Engineering*, vol. 20, no. 3, pp. 289–305, 1992.

41. X.-Z. Yuan, C. Song, H. Wang, and J. Zhang, *Electrochemical Impedance Spectroscopy in PEM Fuel Cells*. London: Springer London, 2010.

42. A. Cuadras and O. Kanoun, “SOC Li-ion battery monitoring with impedance spectroscopy,” in *2009 6th International Multi-Conference on Systems, Signals and Devices*. IEEE, 2009, pp. 1–5.

43. A. Christensen and A. Adebusuyi, “Using on-board electrochemical impedance spectroscopy in battery management systems,” *World Electric Vehicle Journal*, vol. 6, no. 3, pp. 793–799, 2013.

44. L. Callegaro, *Electrical impedance: principles, measurement, and applications*. Boca Raton: CRC Press, 2013.

45. M. Toshio, T. Isao, T. Ryohei, and T. Yoshinori, “Development of a real-time power and impedance sensor for WPTS,” in *IEEE Wireless Power Transfer Conference (WPTC)*. IEEE, 2015, pp. 1-3.

46. D. Kürschner, U. Jumar, and A. Lindemann, *Methodischer Entwurf toleranzbehafteter induktiver Energieübertragungssysteme*, Ph.D. dissertation. Aachen: Shaker, 2010.

47. F. Niedermeier, *Methoden zur Analyse von induktiven Ladesystemen für Elektro- und Hybridfahrzeuge*, Ph.D. dissertation. To be published, 2019.

48. A. Abdolkhani and A. P. Hu, "Magnetic coupling coefficient determination of IPT systems under operating conditions," *Wireless Power Transfer*, vol. 1, no. 2, pp. 83–86, 2014.

49. C. B. Auvigne, "Electrical and magnetical modeling of inductive coupled power transfer systems," Ph.D. dissertation, EPFL, 2015.

50. B. Esteban, M. Sid-Ahmed, and N. C. Kar, "A comparative study of power supply architectures in wireless EV charging systems," *IEEE Transactions on Power Electronics*, vol. 30, no. 11, pp. 6408–6422, 2015.

51. R. L. Steigerwald, "A comparison of half-bridge resonant converter topologies," *IEEE Transactions on Power Electronics*, vol. 3, no. 2, pp. 174–182, 1988.

52. M. Hassler, F. Niedermeier, J. Krammer, and K. Diepold, "A method for interoperable interface description of inductive power transfer systems," in *IEEE PELS Workshop on Emerging Technologies: Wireless Power Transfer (Wow)*. IEEE, 2018, pp. 1–5.

53. F. Niedermeier, M. Hassler, J. Krammer, and B. Schmuelling, "The effect of rotatory coil misalignment on transfer parameters of inductive power transfer systems," *Wireless Power Transfer*, vol. 6, no. 2, pp. 77–84, 2019.

54. M. Hassler, O. Atasoy, M. Kesler, K. Twelker, T. Achatz, M. Jetz, and J. Krammer, "Impedance measurement on inductive power transfer systems," in *IEEE PELS Workshop on Emerging Technologies: Wireless Power Transfer (Wow)*. IEEE, 2019, pp. 39–44.

55. M. Hassler, O. Atasoy, M. Kesler, K. Twelker, J. Birkendahl, and J. Krammer, "A comparison on simulated, analytic and measured impedance values for an inductive power transfer system," *Wireless Power Transfer*, vol. 7, no. 1, pp. 51–59, 2020.